NUREG/CR-1808

Countercurrent Air/Water and Steam/Water Flow above a Perforated Plate

Prepared by C. Hsieh, S. G. Bankoff, R. S. Tankin, M. C. Yuen

Department of Chemical Engineering
Northwestern University

Prepared for
U.S. Nuclear Regulatory
Commission

Available from

GPO Sales Program
Division of Technical Information and Document Control
U. S. Nuclear Regulatory Commission
Washington, D. C. 20555

Printed copy price: $5.50

and

National Technical Information Service
Springfield, Virginia 22161

NUREG/CR-1808
R1, R2, R4

Countercurrent Air/Water and Steam/Water Flow above a Perforated Plate

Manuscript Completed: October 1979
Date Published: November 1980

Prepared by
C. Hsieh, S. G. Bankoff, R. S. Tankin, M. C. Yuen

Department of Chemical Engineering
Northwestern University
Evanston, IL 60201

Prepared for
Division of Reactor Safety Research
Office of Nuclear Regulatory Research
U.S. Nuclear Regulatory Commission
Washington, D.C. 20555
NRC FIN No. B6188

ABSTRACT

The perforated plate weeping phenomena have been studied in both air/water and steam/cold water systems. The air/water experiment is designed to investigate the effect of geometric factors of the perforated plate on the rate of weeping. A new dimensionless flow rate in the form of H^* is suggested. The data obtained are successfully correlated by this H^* scaling in the conventional flooding equation.

The steam/cold water experiment is concentrated on locating the boundary between weeping and no weeping. The effects of water subcooling, water inlet flow rate, and position of water spray are investigated. Depending on the combination of these factors, several types of weeping were observed. The data obtained at high water spray position can be related to the air/water flooding correlation by replacing the steam flow rate to an effective steam flow rate, which is determined by the mixing efficiency above the plate.

TABLE OF CONTENTS

List of Figures Page

Figure

List of Tables Page

Table

NOMENCLATURE

A	area
C	coefficient in the conventional flooding equation.
C_o	orifice coefficient in equation (1).
D	diameter.
D^*	Bond Number defined in equation (27).
f	friction factor
F_p	correlation canstant in equation (41).
h	height(or head) of liquid.
h'	heat transfer coefficient.
H^*	dimensionless velocity defined in equation (55).
I^*	dimensionless velocity defined in equation (28).
j	superficial velocity through holes.
J^*	dimensionless velocity defined in equation (9).
k	wave number (= $t_p/2$).
k'	constant in Fair's weep point correlation.
L^*	Bond Number defined in equation (53).
m	coefficient in the conventional flooding equation.
$N_{Eö}$	Eotvos Number defined in equation (47).
p	pressure
R_T	thermodynamic boundary.
t_p	Thickness of the perforated plate.
U_{cr}	critical velocity.
w	characteristic length.
W	mass flow rate.
σ	surface tension
τ	shear stress
ρ	density

Subscripts

f	liquid phase
L	liquid phase
g	gas or vapor phase
h	hole
i	inside or interface
in	inlet
o	outside
s	steam
sat	saturated condition
w	wall

ACKNOWLEDGEMENTS

The Mechanical Engineering Staff is humbly thanked for all their marvellous skill in processing the purchasing and construction work. The secretaries: Lillian Kurtz, Brenda Wilson, Pat Dyess, and Larry Rockoff were particularly helpful and tolerant. The shop foreman and personnel: Robert Klaub, Mike Luczak, T. F Felton, and J. Torluemke proficiently constructed the apparatus used in this experiment.

The contributions from co-investigators can not be thanked too much. They are: Robert Jensen, David Cook, Fae Wang, and Sang Lim.

1. Introduction

The flooding phenomena of vertical counter-current two phase flow have been studied in various types of flow channels. Packed columns were the first to receive a systematic investigation. After forty years, the basic model proposed by Sherwood(1) and Lobo(2) is still widely accepted by chemical engineers in packed tower design(3, 4). Flooding inside circular tubes, which may be encountered in several types of process equipment(e.g., cyclone, liquid film evaporator, updraft condenser, etc.), has probably been given the most extensive studies in this field. Much basic research related to the flooding phenomenon is carried in this type of geometry(5). The understanding accumulated here also serve as a basic guide for the study on other shapes of flow channels.

Recently, due to concern about the refilling and reflooding process in the event of a loss-of-coolant-accident(LOCA) in nuclear reactor safety analysis, flooding phenomena in annuli(6) or outside the fuel rod bundles(7) have drawn attention. Owing to similar concerns the restrictive effect of ascending steam on water flowing downward through a perforated support plate is currently being studied.

Throughout this thesis, the term "dumping" is used to describe the condition where essentially all the inlet liquid falls down through the perforated plate, once the instability starts. Should there be only part of the inlet liquid falling through, it is called "weeping", and the starting point of weeping is called the weep point. Weeping is further divided into two categories: continuous weeping and oscillatory or intermittent weeping.

The objective of the present research is to investigate

weeping in perforated plates with different hole size and geometries with both air/water and steam/cold water system. Study of the air/water system, where the condensation-driven fluid motions have been totaly eliminated, can lead to some insight into the hydrodynamic aspects of the weeping phenomenon. The effect of plate geometry, along with several other factors, has been studied. Next, the experiments on the steam/cold water are to determine the effect of condensation on the initiation of weeping. The experimental parameters studied include: number of holes in the test plate, inlet steam mass flow rate, degree of steam superheat, effect of soft volume, inlet water mass flow rate, degree of subcooling of the inlet water, position of water injection, and liquid head above the perforated plate.

2. Air/Water Experiment

Basically, the weeping phenomenon, like any other counter-current flow limiting(CCFL) phenomenon, is a hydrodynamic process where the momentum and frictional drag of the ascending gas/vapor and descending liquid interact with each other.

The air/water experiments were performed in the same test channel with the same perforated plates(Figure 1) designed for the steam/cold water experiment. The following factors may be expected to be important: superficial gas velocity through the perforations j_{gh}, head of liquid pool above the perforated plate h_L, height of liquid inlet point above plate h_{in}, diameter of holes D_h, soft volume V_s, and perforation ratio A_h/A_T.

2.1 Technical Background

Since the early 50's, weeping has been studied by investigators interested in the performance of perforated plate in distillation towers or packed-bed chemical reactors. Operating with the air/water system, Mayfield(9), Arnold(10), and Zene(11) separately reported that the weep point is a function of j_{gh} and h_L(Figure 2). According to their observations, a higher j_{gh} is required to keep the plate from weeping as the head of liquid pool is increased

Supported by data from Hunt(12) and Van Winkle(13), Leibson (14) indicated that superficial gas velocity through the holes j_{gh} can be related to the pressure drop across the plate in the following way:

$$h_p \equiv \Delta p_{12}/(g\rho_f) = \rho_g j_{gh}^2/(gC_o^2\rho_f) \qquad (1)$$

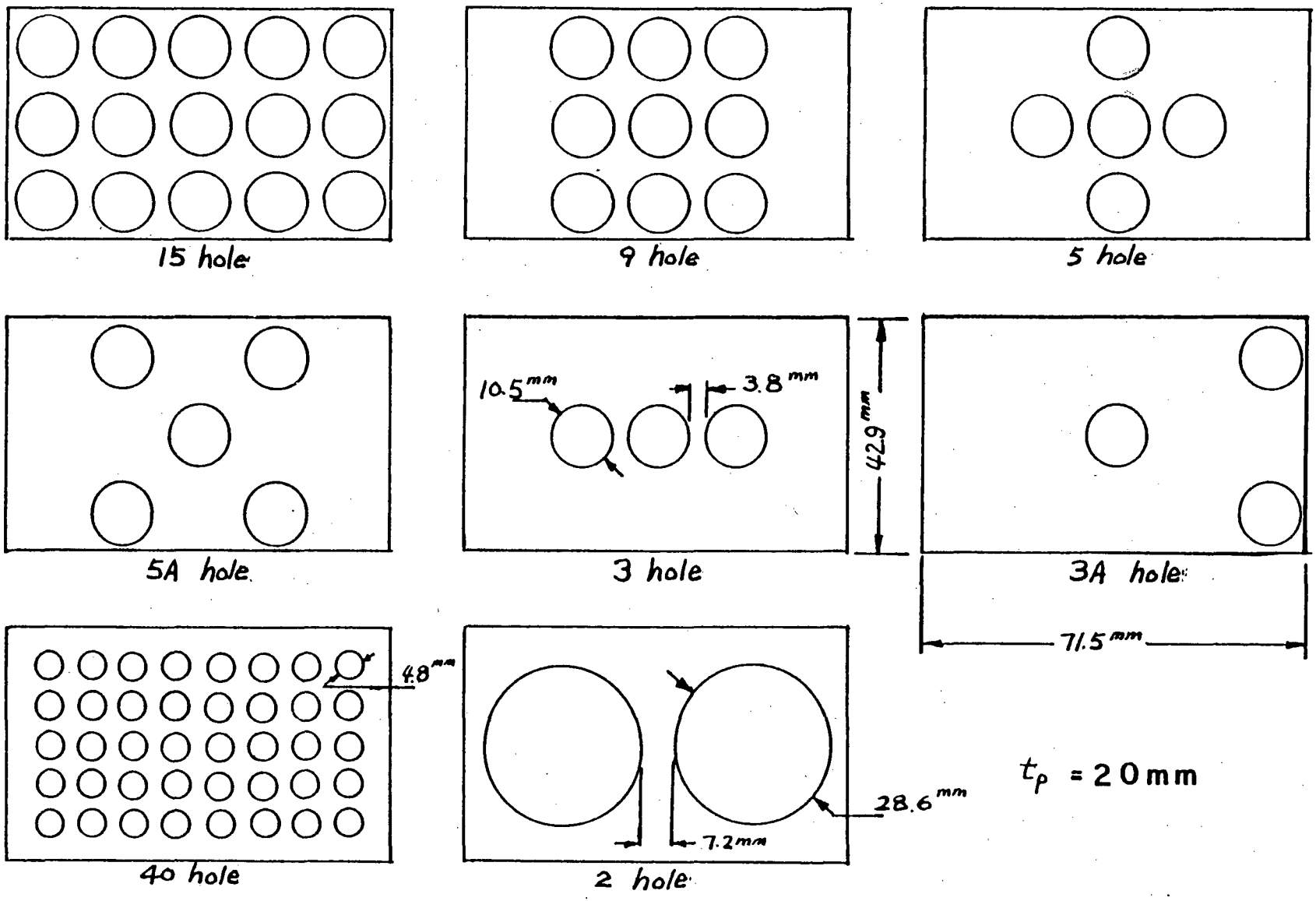

FIGURE 1. Geometries of the test perforated plate.

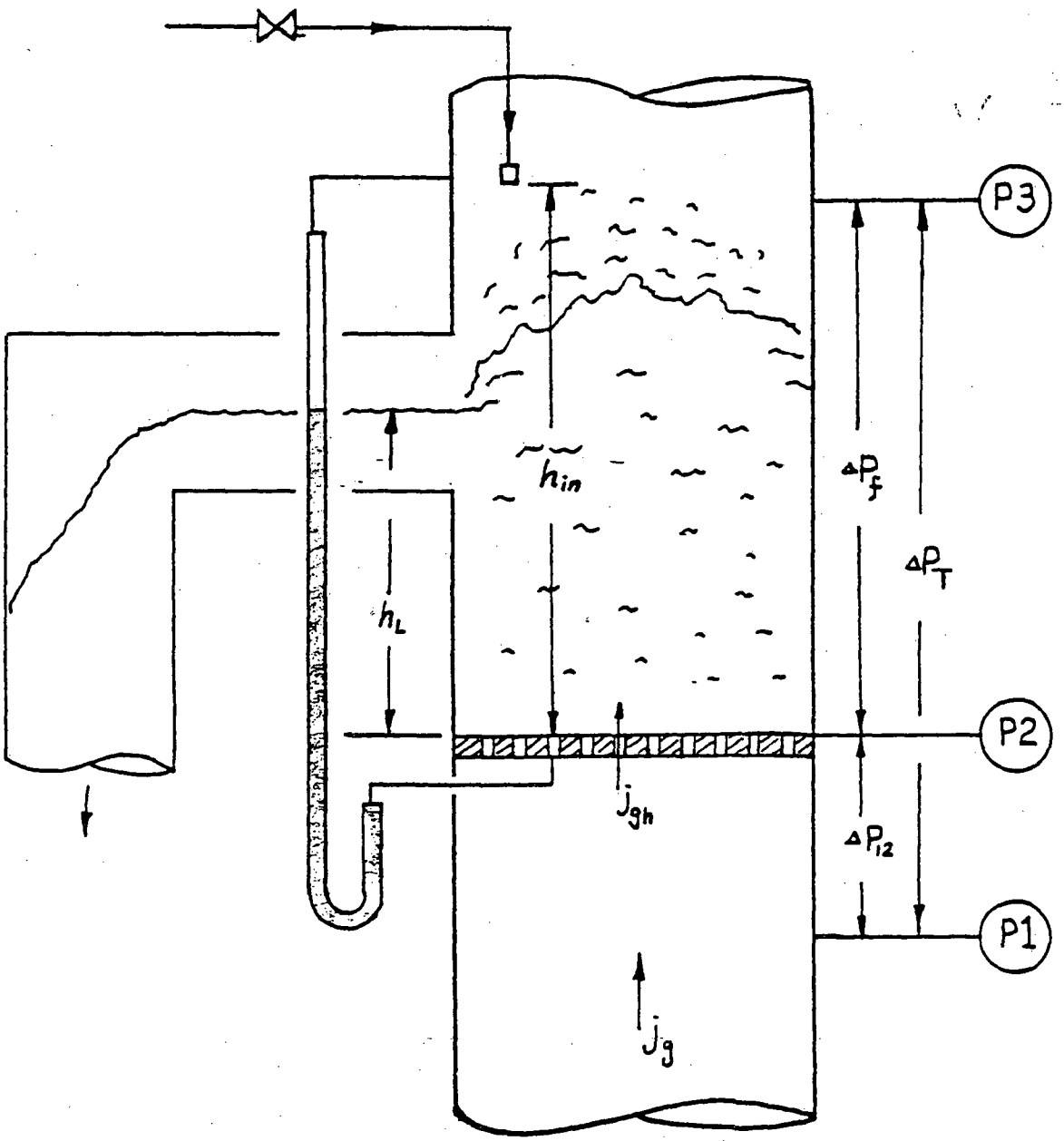

Figure 2. Perforated Plate Diagram

where C_o, the orifice coefficient, is a function of perforation ratio A_h/A_T, ratio of plate thickness to hole diameter t_p/D_h, and hole layout. Though this approach oversimplified the real physical situation where gas/liquid interaction effects are present, it has been convenient for design purposes. He further suggested that the weep point can then be correlated as a relation between h_L and h_p(Figure 3).

Essentially, based on a steady-state force balance across a particular hole in the perforated plate, weeping will occur if and only if the following relation is satisfied(Figure 2):

$$p_2 > p_1 + p_{el} \tag{2}$$

where p_{el} is the excess pressure required to overcome the resistance to liquid flow through the holes. It is assumed here that p_1, p_2, and p_{el} are all time independent variables.

By subtracting p_3 from both side of equation (2), this criterion of weep point becomes

$$\Delta p_f > \Delta p_T + p_{el} \tag{3}$$

Further defining

$$\Delta p_f = \overline{\Delta p}_f + p_{fv} \tag{4}$$

$$\overline{\Delta p_{12}} = \Delta p_T - \overline{\Delta p}_f \tag{5}$$

where $\overline{\Delta p}_f$ means the time average value of Δp_f, etc., equation (3) can then be expressed as

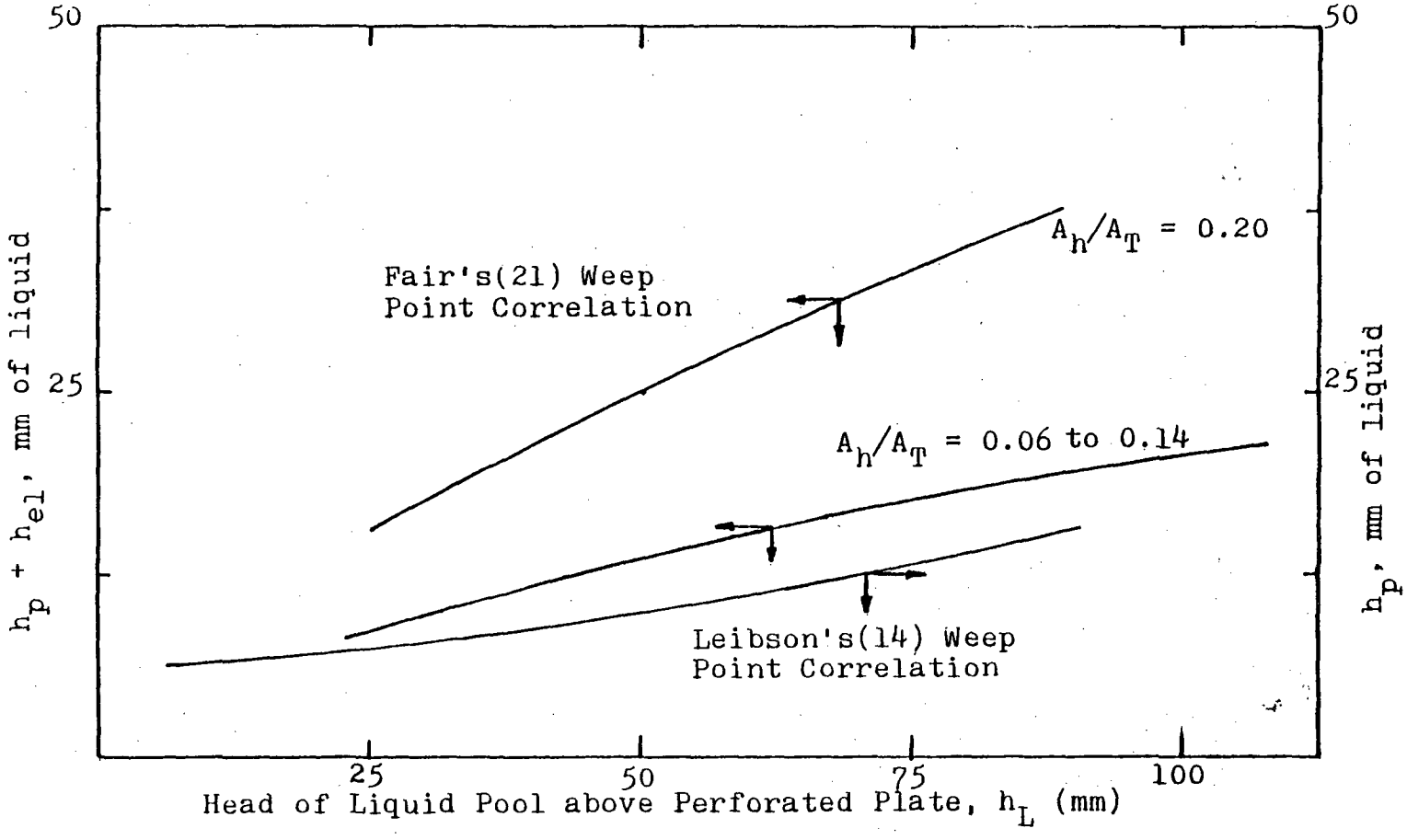

Figure 3. Perforated Plate Weep Point Correlations

$$p_{fv} > \Delta p_{12} + p_{el} \qquad (6)$$

where p_{fv} is the fluctuating component of p_v. Causes of this fluctuation are many. Should the liquid above the plate be subcooled, condensation(15) can cause the pressure fluctuation. Two types of oscillation have also been observed when the system is operating at pressures below atmospheric(16). In the first type, full-wave oscillation, a standing wave is generated in the gas/liquid free surface, with the nodes at the walls(Figure 4-I). With further increase in the vapor velocity to a critical point half-wave oscillation is reached where there is a violent slashing from side to side across the direction of liquid flow(Figure 4-II). If there is no condensation or oscillation, Zanelli and Bianco(17) showed that p_{fv} is a function of head of liquid pool h_L only. This may explain why Leibson successfully correlated his weep point data in a h_L vs. h_p curve.

This simple model for weep point prediction has been followed by most of the perforated plate designers(17-20). Up to now, the weep point correlation curves suggested by Fair(21), where p_{el} is equal to $k'(\sigma/D_h)$, is still recommended by Chemical Engineers' Handbook(22) as the standard weep point prediction method.

However, since almost all of these experiments are simulating the operating conditions of the distillation tower, the highest liquid head h_L studied is less than 105 mm, perforation ratio never exceeds 25%, and plate thickness t_p is usually less than 5 mm. Of course, the condensation-driven fluid motion has never been mentioned. Therefore, their results would not be applicable for the weep point prediction on the geometries and operating condition similar to the tie plate of a nuclear fuel assembly in the LOCA condition.

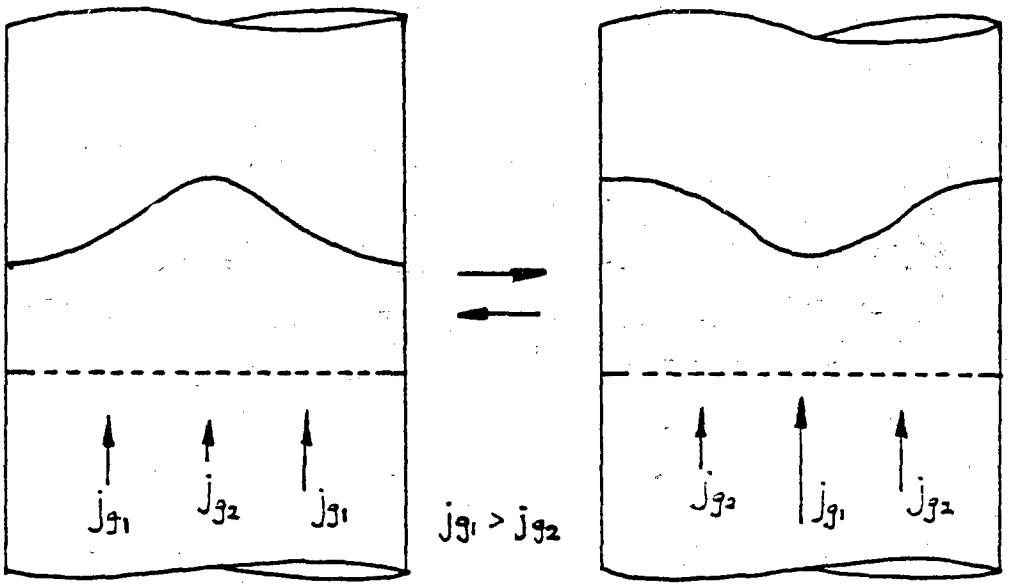

I. Full-Wave Oscillation

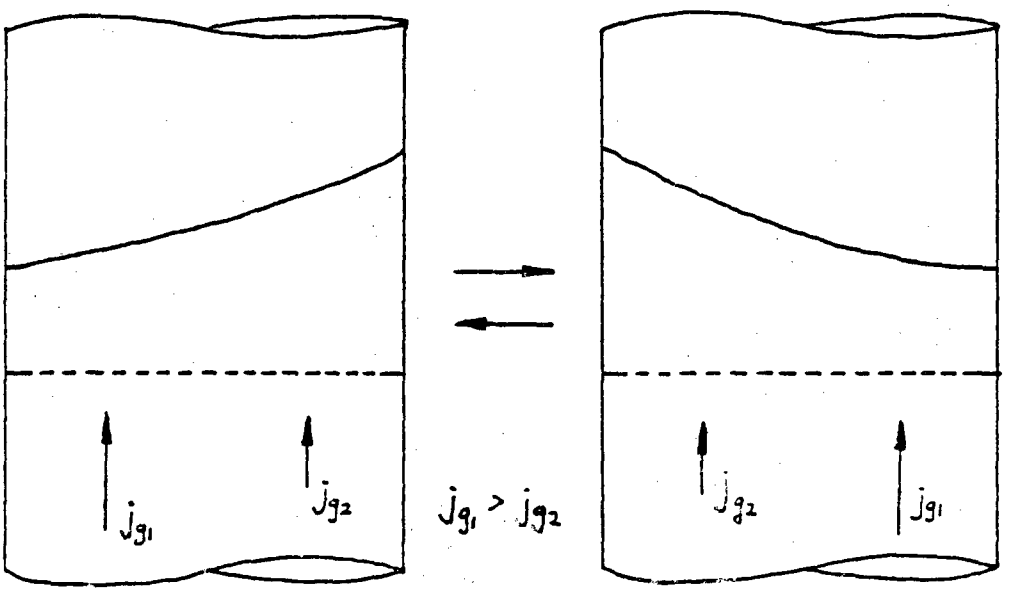

II. Half-Wave Oscillation

Figure 4. Oscillation Behavior of Perforated Plate

McCann and Prince(23) initiated theoretical investigations on the rate of weeping. By using potential flow analysis, the rate of weeping in a single orifice was studied. According to their report, weeping of liquid happens after every bubble detachment in a cyclic way as a result of the pressure behind the rising bubble becoming greater that the chamber pressure(Figure 5A). The agreement between their experimental and predicted values is fairly good; nonetheless, this model does not fit the observation of those experiments on a perforated plate where many holes operate all together. Instead, the model suggested by Shoukry and Kolar is closer to the real situation for a perforated plate(24).

In this model(Figure 5B), the total cross-section area of the plate can be divided into three areas which are instantaneously changing value and position such that:

$$A_T = A_g + A_f + A_b \qquad (7)$$

As the liquid flows down in the weeping area A_f, and gas flows up in the gas area A_g, there is no fluid flow in the blocked area A_b. However, no data on the rate of weeping were reported in their research.

Wallis'(25) flooding equation and/or its modifications(26). which has long been used to correlate the flooding data in vertical tubes and annuli, has been again adapted here by many investigators to correlate the data on weeping rate from perforated plates(8, 27).

Using a separated cylinder model with the assumption of a constant mixing length in each cylinder, Wallis proved that, in the absence of viscous and surface tension effects, the flooding equation in a vertical two-phase counter-current flow system is

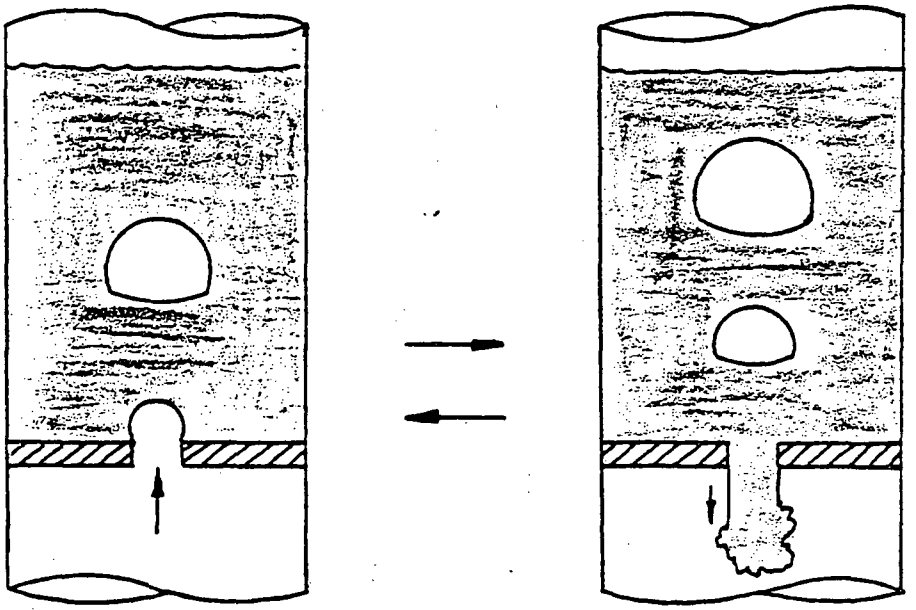

A. Intermittent Weeping

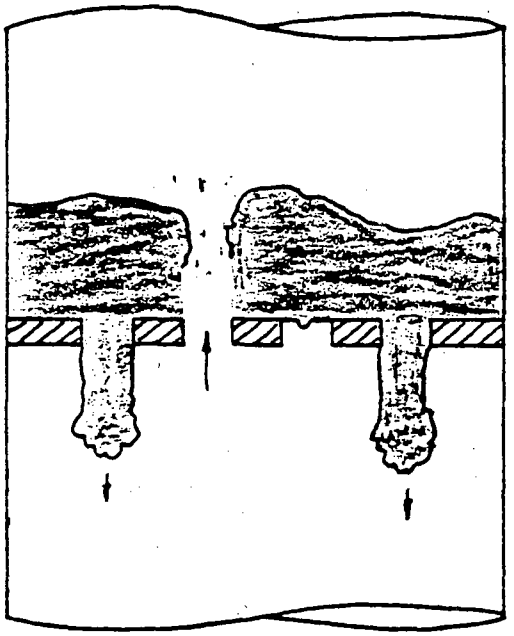

B. Alternative Weeping

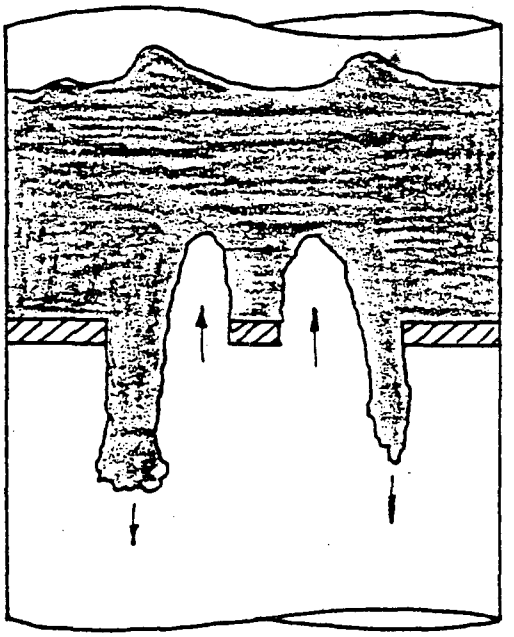

C. Counter-current Weeping

Figure 5. Perforated Plate Weeping Models

of the form:

$$J_g^{*2/(n+1)} + J_f^{*2/(n+1)} = 1 \qquad (8)$$

where $J^*_{g,f} = [\rho_{g,f}/gw(\rho_f - \rho_g)]^{1/2} j_{g,f}$ (9)

and w is a characteristic dimension of the duct cross section. The value of n is equal to 3.5 or 2.5, depending upon whether the mixing length l_f and l_g are scaled by the dimensions of each cylinder or by the overall pipe diameter. Let n take on the intermediate value of 3, equation (8) then becomes

$$J_g^{*1/2} + J_f^{*1/2} = 1 \qquad (10)$$

This equation is empirically further modified to:

$$J_g^{*1/2} + m\, J_f^{*1/2} = C \qquad (11)$$

For flooding inside a single vertical tubes, the characteristic dimension w, as suggested by Wallis, is equal to the diameter of the tube.

Based on the survey held by Tien and Liu(5), the value of C depends mainly on the tube inlet and exit geometries, ranges from 0.7 to 1.0, while m has a value of 0.8 to 1.0. For fully turbulent flow the value of m is equal to 1. The curves of both Lobo(2) and Sherwood(1) for flooding in a packed column can also be fitted by this equation as:

$$J_g^{*1/2} + J_f^{*1/2} = 0.775 \qquad (12)$$

The Wallis equation has also been adapted to correlate the flooding data in annular geometries. Shires and Pickering(30)

suggested four different types of characteristic dimensions for this type of flow channel:

$$w_1 = D_o \tag{13}$$

$$w_2 = (D_o - D_i)/2 \tag{14}$$

$$w_3 = D_i \tag{15}$$

or $$w_4 = (D_o^2 - D_i^2)/D_i \tag{16}$$

Though their experiments did not provide enough information to decide the appropriate dimension, the mean hydraulic diameter calculated by equation (16) best brought their annulus data together. Using w_4 as the characteristic length, their air/water flooding data were correlated as:

$$J_g^{*1/2} + J_f^{*1/2} = 0.71 \tag{17}$$

Ueda and Suzuki(7) used as their form of characteristic dimension for the annular geometry:

$$w_5 = (D_o^2 - D_i^2)/(D_o + D_i) = 2\, w_2 \tag{18}$$

Using this characteristic dimension, their data can be expressed as

$$J_g^{*1/2} + J_f^{*1/2} = 0.80 \tag{19}$$

while using w_4, the same data can be correlated as

$$J_g^{*1/2} + J_f^{*1/2} = 0.64 \tag{20}$$

Flooding phenomena in annular geometries with gap size of

the annulus(w_2) between 6.4 mm and 50.8 mm have been investigated by Creare Incorporated and Battelle Coumbus Laboratories(31, 32 33, 34). The data obtained can not be correlated by the use of gap size w_2 as the characteristic length. Since scale effects and L/D effects have not been sufficiently studied, a definitive choice of a characteristic length for the annulus is not possible at present. The average circumference of annulus has been conditionally accepted by Creare Incorporated(6, 35), Battelle Columbus Laboratories(36) and Dartmouth College(37) in their data correlations. This characteristic length can be formulated as

$$w_6 = \pi(D_i + D_o)/2 = \pi(D_i + w_2) \qquad (21)$$

$$\left(\quad D_i \quad \text{if } D_i \gg w_2 \right)$$

Rothe(35) gave a thorough review of the data obtained from these laboratories. By using w_6 as the characteristic length, all the data can be correlated by equation (11) with m ranging between 0.7 and 0.8, and C between 0.34 and 0.42. Since D_i is five to ten times larger than w_2 in the annuli studied, correlating the data with w_6 as the characteristic length essentially means that the flooding condition is relatively independent of the gap size. Further investigation in larger annulus is necessary to verify the proper characteristic l ength for equation (11).

Pushkina and Sorokin(26) suggested another form of characteristic length:

$$w_7 = [\sigma/(g(\rho_f - \rho_g))]^{1/2} \qquad (22)$$

This characteristic length is similar to the horizontal wave length used in Taylor instability. Introducting this wave length into equation (11) will result in:

$$K_g^{*1/2} + m\, K_f^{*1/2} = C \qquad (23)$$

where K^*, the Kutateladze number, is

$$K^*_{f,\,g} = \rho_{f,g}^{1/2}\, j_{f,g} / [g\,\sigma(\rho_f - \rho_g)]^{1/4} \qquad (24)$$

Their experiments shows that the breakdown of liquid film downflow(the zero liquid penetration point) can be expressed as

$$K_g^* = 3.2 \qquad (25)$$

Essentially, K^* can be rewritten in the following form:

$$K^* = J^*\, D^{*1/2} \qquad (26)$$

where D^* is a dimensionless characteristic length

$$D^* = D\,[g(\rho_f - \rho_g)/\sigma]^{1/2} \qquad (27)$$

D^* is the square root of the Eötvös number, or equivalently one half of the square root of the Bond number(38), and is a ratio of buoyancy and surface tension force. Wallis and Makkenchery(39) found that J^* correlated the data over a limited range of D^* from 3 to 20, while the criterion $K^* = 3.2$ was more appropriate for D^* larger than 30. Recent work by both Battelle Columbus Laboratories(36) and Dartmouth College(37) indicated that neither parameter K^* nor parameter J^* with circumference as the characteristic length can satisfactorily correlate the data over a wide range of scale.

Based on the Helmholtz instability concept for annular geometries, a new dimensionless flow rate scaling I^* is now under development(40, 48). This I^* scaling is expressed as

$$J_g^{*1/2} + (\rho_g/\rho_f)^{1/2} J_f^{*1/2} =$$

$$= [\sigma k\, B(k, R_o, R_i)/(g(\rho_f-\rho_g)D)]^{1/4} \qquad (28)$$

where $B(k, R_o, R_i) = [I_1(kR_o)K_1(kR_i)-K_1(kR_o)I_1(kR_i)]/$
$[I_1(kR_o)K_o(kR_i)-K_1(kR_o)I_o(kR_i)]$ (29)

I, K are the modified Bessel functions, and k is a critical wavelength. The characteristic length is suggested to be either w_3 or w_6. However, one sees that in the limit as $R_o \to \infty$, $R_i \to \infty$, with $R_o - R_i$ fixed, $B \to 0$, which does not agree with equation (11)(as it should). In order to generalize equation (28), they suggested that $B(k, R_i, R_o)$ be replaced by D^{α}, leading to

$$J_g^{*1/2} + J_f^{*1/2} = [\sigma k\, D^{\alpha-1}/(g(\rho_f-\rho_g))]^{1/4} \qquad (30)$$

It is suggested that when $\alpha=1$, equation (30) is reduced to J^* scaling, for $\alpha=0$, it goes to K^* scaling, and for $0 < \alpha < 1$, equation (30) represents an intermediate I^* scaling. However, one should notice that while all the terms in the left hand side of equation (30) are dimensionless, the right hand side of this equation is not a dimensionless term, which may cause some problems in the data analysis.

By the use of the momentum equation, Wallis(29) obtained another form of the flooding equation:

Ignoring compressibility effects and variations of liquid film thickness, a momentum balance on the gas core of an annulur two-phase flows yields:

$$(dp/dz) + \rho_g g + 4\tau_i/D\sqrt{\alpha} = 0 \qquad (31)$$

where τ_i is the interfacial shear stress, which may be related to the interfacial friction factor f_i as

$$f_i = 2\tau_i \alpha^2 / \rho_g j_g^2 \qquad (32)$$

By considering the force balance for the entire cross-section of the tube, one can have

$$(dp/dz) + \rho_g g + (1-\alpha)(\rho_f - \rho_g) = 4\tau_w / D \qquad (33)$$

And the relation between the wall shear stress τ_w and the wall friction factor f_w is given as

$$f_w = 2\tau_w (1-\alpha)^2 / \rho_f j_f^2 \qquad (34)$$

By combining equations (31) and (33), the gas and liquid flow rate can be related as

$$2f_i J_g^{*2} / \alpha^{5/2} + 2f_w J_f^{*2} / (1-\alpha)^2 = (1-\alpha) \qquad (35)$$

Provided the friction factors f_i and f_w are known, the limiting J_f^* and J_g^* can be obtained as an envelope of curves generated with $(1-\alpha)$ as a parameter. This envelope will lie above the flooding curve given by equation (12) in the J_g^* vs J_f^* plane.

Sun(49) suggested that in addition to equation (35), the equation of continuity should also be considered:

$$(1/\alpha) J_g^* + (\rho_f/\rho_g)^{1/2} J_f^* / (1-\alpha) = U_{cr} (\rho_f / gD(\rho_f - \rho_g))^{1/2} \qquad (36)$$

where U_{cr} is the critical relative velocity between the phases.

The flooding limitation is, then, to find the intersection

of equation (35) and equation (36), along with the proper expressions for f_i and f_w, at various values of the void fraction α. The flooding curve obtained is a convex line in the $J_g^{*1/2}$ vs $J_f^{*1/2}$ plane. Therefore, the suitability of these flooding models for any particular channel geometry can easily be verified by the data distribution in a $J_g^{*1/2}$ vs $J_f^{*1/2}$ plane.

Tobin's steam/water flooding data on a 7x7 BWR fuel bundle sleaves(41) shows a straight line in the $K_g^{*1/2}$ vs $K_f^{*1/2}$ plane, which means the conventional flooding relation expressed as equation (12) or (23) is more suitable for this case. These data are correlated as

$$K_g^{*1/2} + K_f^{*1/2} = 1.79 \pm 2\% \qquad (37)$$

Jones' data(8) for 8x8 BWR fuel bundle upper tie plate is correlated as:

$$K_g^{*1/2} + K_f^{*1/2} = 2.07 \pm 8\% \qquad (38)$$

Naitoh's data(42) for BWR 8x8 upper tie plate is

$$K_g^{*1/2} + K_f^{*1/2} = 2.06 \pm 6\% \qquad (39)$$

Mohr and Jacoby(43) reported their air/water flooding data obtained with a full size model of the upper core and upper regions corresponding to a single pressurized water reactor(PWR) fuel bundle of both Westinghouse Electric Corporation and German Kraftwerk Union(KWU) designs. Their data can also be correlated by straight lines in the form of

$$K_g^{*1/2} + m\, K_f^{*1/2} = C \qquad (40)$$

Depending on the particular geometry studied, the value of m varied between 0.7 and 2.2, and C between 1.31 and 2.04. Therefore, one can conclude that the flooding phenomena for this case are heavily geometry dependent.

2.2 Experimental Apparatus

2.2.1 Test Channel

Figure 6 shows the schematic diagram of the experimental apparatus. A detail drawing of the test channel is shown in Figure 7. The channel frame, which includes the side, top and bottom plates, is made of 12.7 mm thick brass. In order to provide visual observation during the experiment, the front and back wall of the channel are made of transparent Lexan. After covering the contact surfaces between Lexan and brass with silicone adhesive, the Lexan plates are clamped to the brass frame by tie rods. This method effectively prevented any leakage from the Lexan-brass contact surfaces.

The plate geometries that have been tested in air/water system have been labeled(Figure 1): 15 hole, 9 hole, 5 hole, 5A hole, 3 hole, 3A hole, 40 hole and 2 hole. The hole diameter(D_h) in the 2 hole plate is 28.6 mm, and in the 40 hole plate is 4.8 mm. D_h in all other test plates is fixed at 10.5 mm, which is same as the lower tie plate of the German KWU PWR fuel assembly. The dimension of all the plates is 72 mm x 43 mm. The thickness of the plates, which is also simulating the KWU geometry, is 20 mm.

The perforation ratio, the ratio of total hole area to channel cross-section area , has been varied between 42.3% and 8.5%. The 15 hole plate, with the perforation ratio of 42.3%, has a geometry similar to that of the KWU lower tie plate.

2.2.2 Water Line

Tap water from building 1-1/4 inch water supply line is

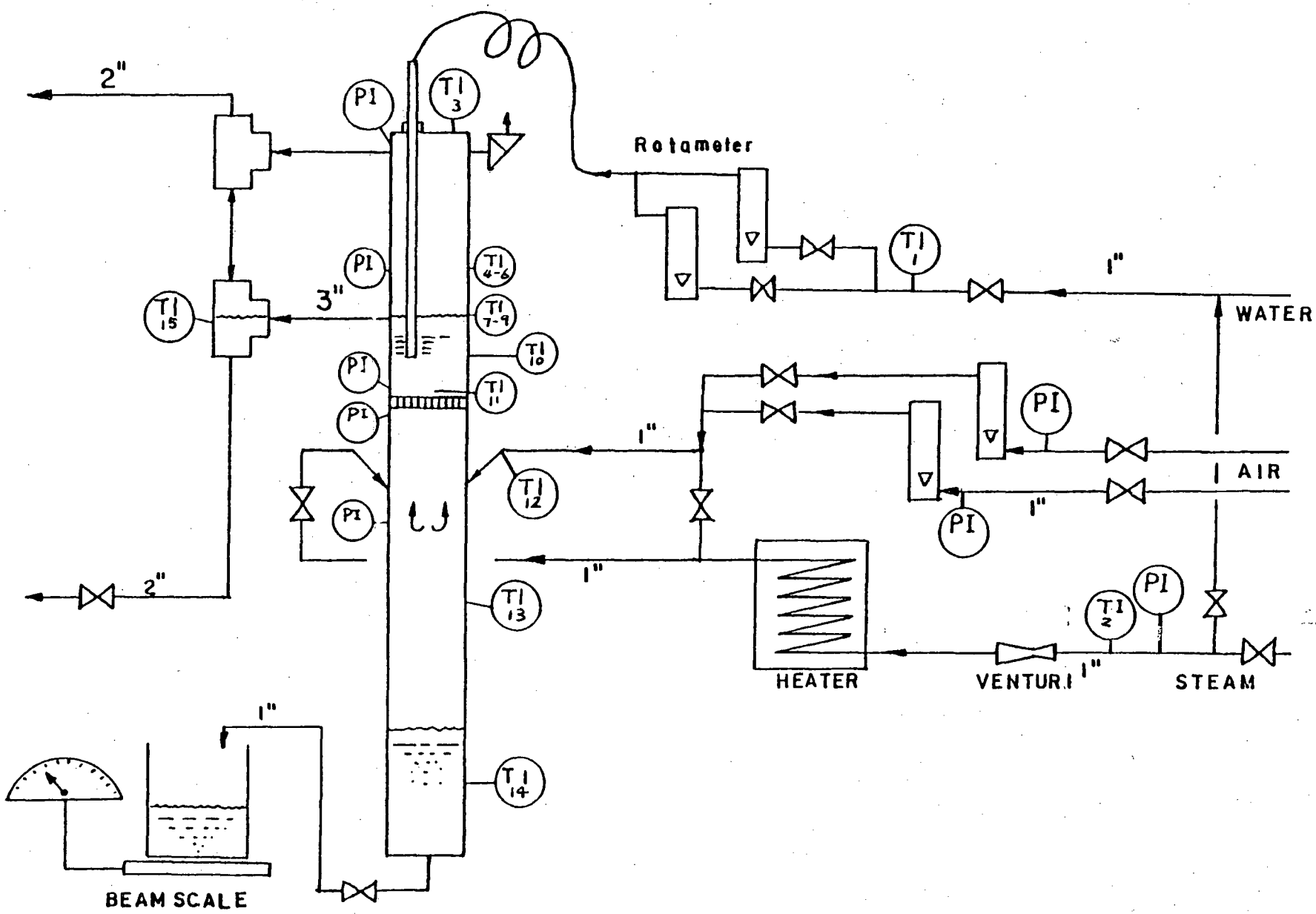

FIGURE 6. Schematic diagram of experimental apparatus.

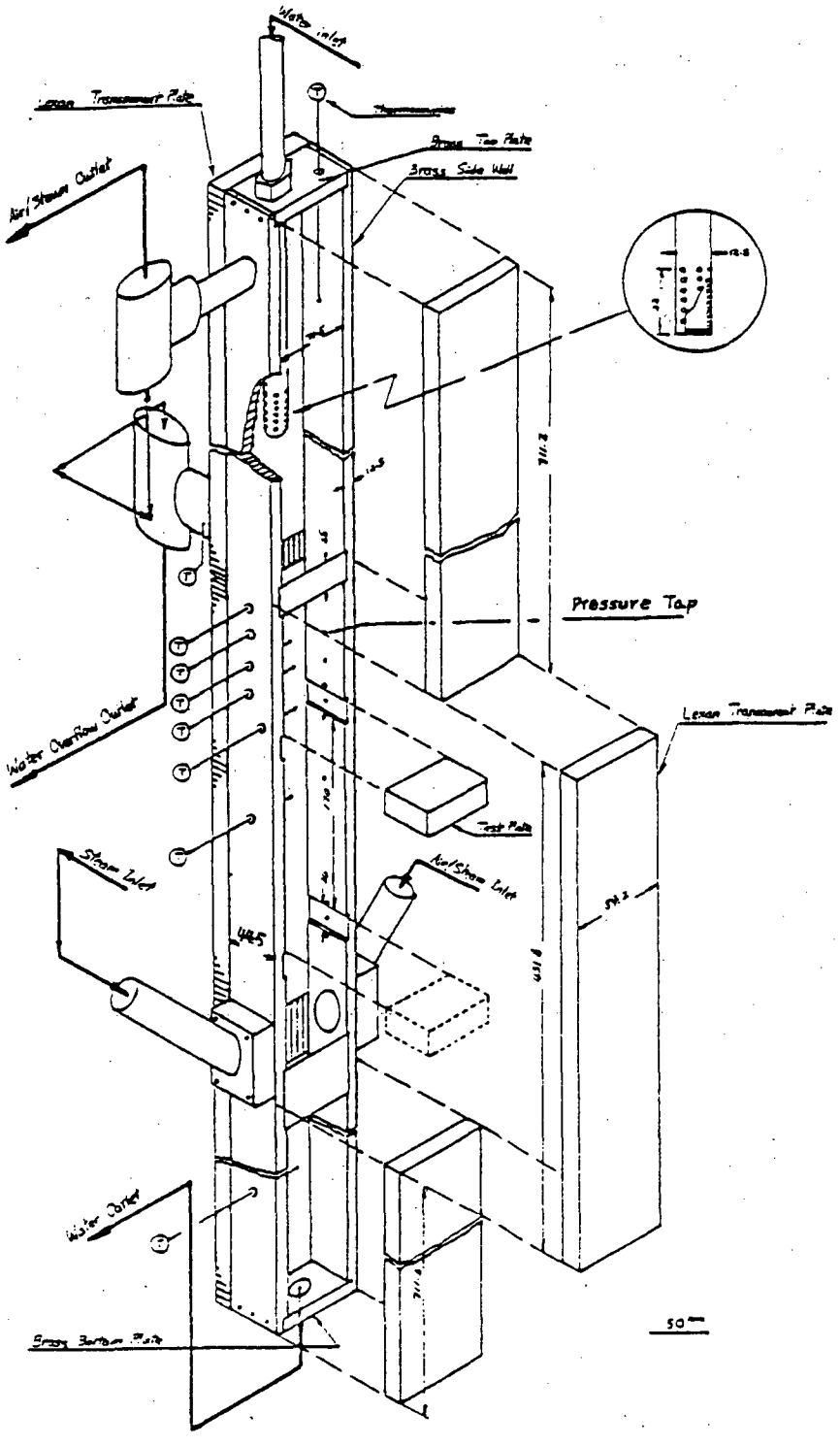

Figure 7. Isometric Diagram of the Test Channel

brought to the test channel by a 1 inch brass pipe line. During the whole period of experiment, the tap water temperature varied from 276 K(winter) to 288 K(summer). Water is fed into the channel through a 1/2 inch flexible hose connected from the water line to a water inlet spray device. This device is made of a 1.5 m long 1/2 inch O. D. brass tube. At the bottom end of this tube, the whole cross-section area is sealed by welding, while 5 rows of 3 mm diameter holes, 6 holes in each row, are drilled along the wall of the tube.

Water to the channel flows out horizontally through these holes, so that the downward direction momentum flux of the feed water can then be minimized. The distance between the test plate and the bottom tip of the spray tube, h_{in}, can be adjusted. After h_{in} is adjusted, the spray tube is fixed to the top plate of the channel by tightening a swagelock fitting at the top of the channel.

A 50 mm I.D. water overflow port is attached on the Lexan back wall of the channel. By changing the position of the test perforated plate, the distance between the centerline of the port and the top of the plate can be adjusted to either 267 mm or 445 mm. It is assumed that this distance is equal to the head of clear liquid above the plate, h_L(Figure 3). Excess water that can not weep downward will flow out the channel through this port, passing a 50 mm I.D. pyrex glass tee, and then flowing down to the water sump. This pyrex glass tee, with its main function as a gas-liquid separator, facilitates a visual observation of the onset of water overflowing.

Water weeping down through the perforated plate will flow out through a 1 inch nozzle at the bottom plate of the channel. A 1-1/4 inch I.D. flexible hose connected to this nozzle can lead the water either to the water sump or to the beam scale measurement to determine the rate of weeping. By adjusting the high point

of the hose the liquid level in the lower section of the channel, and hence the soft volume, can be altered.

2.2.3 Air Lines

Two independent air supply lines have been connected to the test channel. A 1 inch brass line can supply air from the departmental air compressor at 800 kPa with a maximum flow rate of 1.18 x 10^{-2} m^3/s. Another 3/8 inch air line connected from building air supply facility can supply air at 300 kPa with its maximum flow rate equal to 1.17 x $10^{-3} m^3/s$.

Air and/or steam will flow into the channel through two 1 inch nozzles built into the side wall of the channel. Pointing downward, these nozzles make a 45 degree angle to the side wall of the channel, in order to minimize the entrance effect of the inlet gas momentum.

After passing through the perforated plate, air/steam can flow out either with water through the water overflow port mentioned above or through a 1 inch nozzle on the side wall right beneath the top plate of the channel. Both of these gas streams then combine into a 3 inch flexible hose and flow out of the window. Pressure drop along along this gas outlet pipe line is very small; hence, operating pressure of the channel in all test runs is very near to atmospheric pressure.

2.2.4 Instrumentation

The water flow rate is measured by two rotameters installed in parallel along the water line, with range: 0.0227 kg/s to 0.273 kg/s and 0.0379 kg/s to 0.417 kg/s. The maximum water flow rate, scaled to the KWU experiment, exceeds 0.038 kg/s/hole for the test plates with 10.5 mm diameter holes. Therefore, the water flow rate must be greater than 0.57 kg/s to run the 15 hole test plate. The flow rate through these rotameters can be controlled separately by adjusting two 1 inch brass globe valves. The rate of weeping is measured by a beam scale and a watch. Detailed measurement procedures are described in section 2.2.6 of this thesis. No measurement was made of the rate of water overflow.

The air flow rate is measured by two rotameters connected to the two air lines mentioned in section 2.2.3. The scales on these rotameters are 2 to 25 SCFM and 0.15 to 2.47 SCFM. Both the rotameter readings and the pressure at the rotameter inlet are required to calculate the air mass flow rate. A pressure gauge is, therefore, installed at the entrance of each rotameter. The air flow rate can be controlled by adjusting the globe valves both up and down stream of the rotameter. Opening the upstream globe valve will increase both the rotameter reading and pressure gauge reading, while opening the downstream valve will increase the rotameter reading but decrease the pressure gauge reading.

The temperature of the inlet water is measured by thermocouple T1(Figure 6). installed upstream of the water rotameters. The temperature of the inlet air is measured by thermocouples T4 and T5. These measurements show that the water temperature was 285$\pm$ 3 K. Readings of the remaining thermocouples were not recorded.

Two Validyne DP103 Extra Low Range Differential Pressure

Transducers were installed for pressure measurement. The range of these transducers is from 0.15 kPa to 3.6 kPa. Figure 8 shows the piping of these transducers. Along the sidewall of the channel, pressure taps have been installed. The pressure drop between any two of them can be measured by connecting them to the pressure transducer via a Swagelock quick-connect assembly. The absolute pressure at any pressure tap point can also be measured by connecting the positive end of the pressure transducer to the tap while leaving the negative end open to the atmosphere.

2.2.5 Computer Program

A computer program has written in FORTRAN IV to carry out the calculation and data plotting tasks. All the important variable names in the Program is given in Appendix I. Input of the Program includes rate of liquid weeping W_f(lbs/s), air rotameter reading W_g(SCFM), and pressure gauge reading P_g(psig). Superficial gas and liquid velocity through the holes are calculated by:

$$F_p = \exp(-0.05088459721+0.02841336269 \times \ln(P_g) - 0.05218174597 \times \ln(P_g)^2) \quad (41)$$

$$j_{gh} = W_g/(60.0 \times F_p \times A_h), \text{ ft/s} \quad (42)$$

These equations are obtained from Fischer&Porter Catalog 10A1022. Superficial liquid velocity is calculated by equation (43):

$$j_{fh} = W_f/(\rho_f \times A_h) \quad (43)$$

The conventional flooding equation in the form of equation (12) or equation (23) with several types of characteristic length were

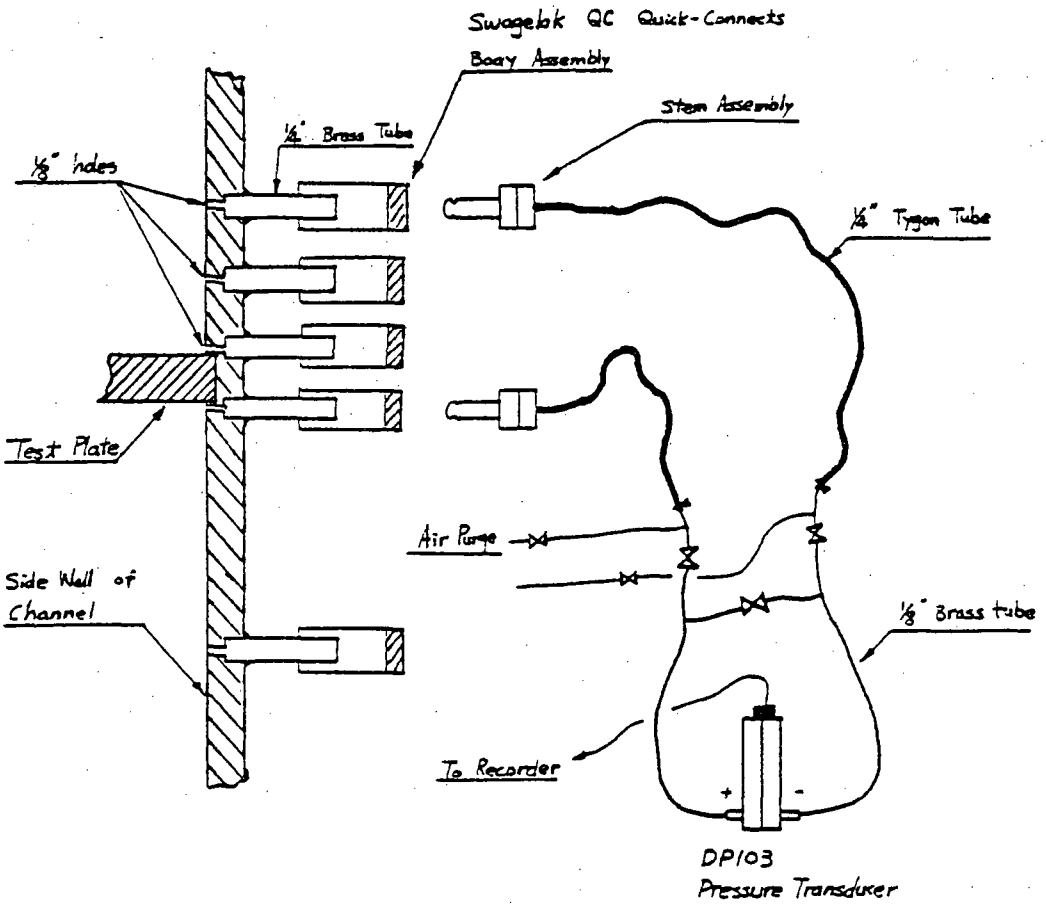

Figure 8. Piping of Pressure Measurement Device

tried to correlate the data. Physical properties of the fluid, which includes density of air and water, and surface tension of water, are all assumed constant. Results of these correlations are discussed in Chapter 3.

2.3 Experimental Procedure

The standard experimental procedure can be listed as follows:

1. Select a test perforated plate. Fix it into its position in the channel.

2. Fix the height of water inlet nozzle.

3. Fix the water inlet flow rate at the pre-selected rotameter reading.

4. Measure the rate of weeping by beam scale and stop watch through the following steps:

   4.1 Leave the empty water container on the beam scale. Balance the scale with a weight.

   4.2 Measure the time(sec.) required for a pre-set amount of water(lbs.) to flow into the container. Calculate the water flow rate in lbs/sec.

   4.3 Repeat step 4.2 at least twice for different amount of water accumulated.

   4.4 Take the average value obtained in step 4.2 to 4.3 as the

rate of weeping. Without water overflowing, this value should be equal to the rotameter reading obtained in step 3.

5. Turn on the air inlet control valves. Record the rotameter reading and pressure gauge reading.

6. Measure the rate of weeping at this air flow rate by following steps 4.1 to 4.4.

7. Increase the air flow rate to a new reading. Record the air air rotameter reading and the pressure gauge reading.

8. Repeat step 6 to 7 at a different air flow rates, and measure the rate of water weeping.

8. After enough data points have been collected through step 6 to 8, further increase the air flow rate to the weep point, which is determined by visual observation. Record the air flow at the weep point.

10. Repeat step 3 to 9 at different water flow rates to verify the influence of inlet water rate, if any, on the rate of weeping.

11. (Option) Repeat step 2 to 10 at different heights of water inlet, h_{in}, to study the influence of water inlet position on therate of weeping.

12. (Option) Repeat step 1 to 10 at different heads of water above the plate, h_L, to study its influence on the rate of weeping.

3. Air/Water Experiment Data Analysis

Altogether, the data of 195 test runs have been collected in the air/water experiments. The parameters studied in these experiments include: height of liquid pool above the plate h_L, liquid inlet position h_{in}, liquid inlet flow rate, and soft volume. The data matrix is given in Table 1.

The flooding model in the form of equation (12) or equation (23) is adopted for analysis of the data obtained. This analysis will involve the selection of a proper characteristic length w for the flooding equation, and the correlation of coefficient m and C in the equation.

3.1 Visual Observations

In the 40 hole, 15 hole and 9 hole experiments, the ascending air and descending water flowed separately through different holes. Most of the holes near the channel wall were occupied by the descending water, while the air usually flowed through the holes near the middle of the plate, and there was essentially no counter-current flow at any particular hole. As the air flow rate increased, the number of holes which were filled with descending water was decreased. The weep point is then defined as the operating condition where no further weeping occurred, as in Shoukry and Kolář's model(24). (Figure 5B)

For the 5(5A) hole, and especially the 3 hole experiments, the mode of liquid delivery changed to intermittent weeping(Figure 5A). We can see bubble detachment in the pool, followed by a falling stream of liquid.

Table 1. Data Matrix of Air/Water Experiment

	h_L(mm)	h_{in}(mm)	W_{Lin}(Kg/s)	No. of Data Point
15 Holes	267	305	0.165	6
	267	5	0.165	18
	267	305	0.243	6
	267	305	0.474	5
	445	305	0.248	11
	445	100	0.475	10
9 Holes	267	305	0.182	12
	267	305	0.282	10
5 Holes	267	5	0.318	6
	267	305	0.318	6
	267	5	0.248	6
	267	305	0.248	9
5A Holes	267	305	0.147	11
	267	305	0.118	10
3 Holes	267	305	0.292	6
	267	305	0.099	9
	267	305	0.168	7
40 Holes	267	305	0.248	18
2 Holes	267	305	0.273	11
	267	305	0.335	11
	267	305	0.216	7

As for the 2 hole experiment, counter-current weeping occurred in each hole. Though 3 different types of weeping have been observed, they will all be analyzed by the flooding equation in the form of equation (12) or equation (23).

3.2 Correlation for Coefficient m

As a first trial, the data were plotted with $J_g^{*1/2}$ against $J_f^{*1/2}$ in Figure 9. The data of each plate can be fitted by a straight line which means the relation of

$$J_g^{*1/2} + m\, J_f^{*1/2} = C \qquad (44)$$

holds here. The negative value of the slope of these lines is equal to m. As shown, all the lines, except the one for 40 hole data, can be correlated to m = 1. Data obtained in BWR or PWR tie plate geometries by Jones(8), Naitoh(42) and Mohr(52) also confirmed that m = 1.

The data of the 40 hole experiment can be correlated as

$$J_g^{*1/2} + 1.44\, J_f^{*1/2} = 1.9 \qquad (45)$$

with the coefficient of determination equal to

$$r^2 = 0.9958 \qquad (46)$$

This higher value of m is possibly caused by the surface tension effect. As mentioned by Wallis(38), surface tension will dominate in the two-phase flow system when the following equation is satisfied:

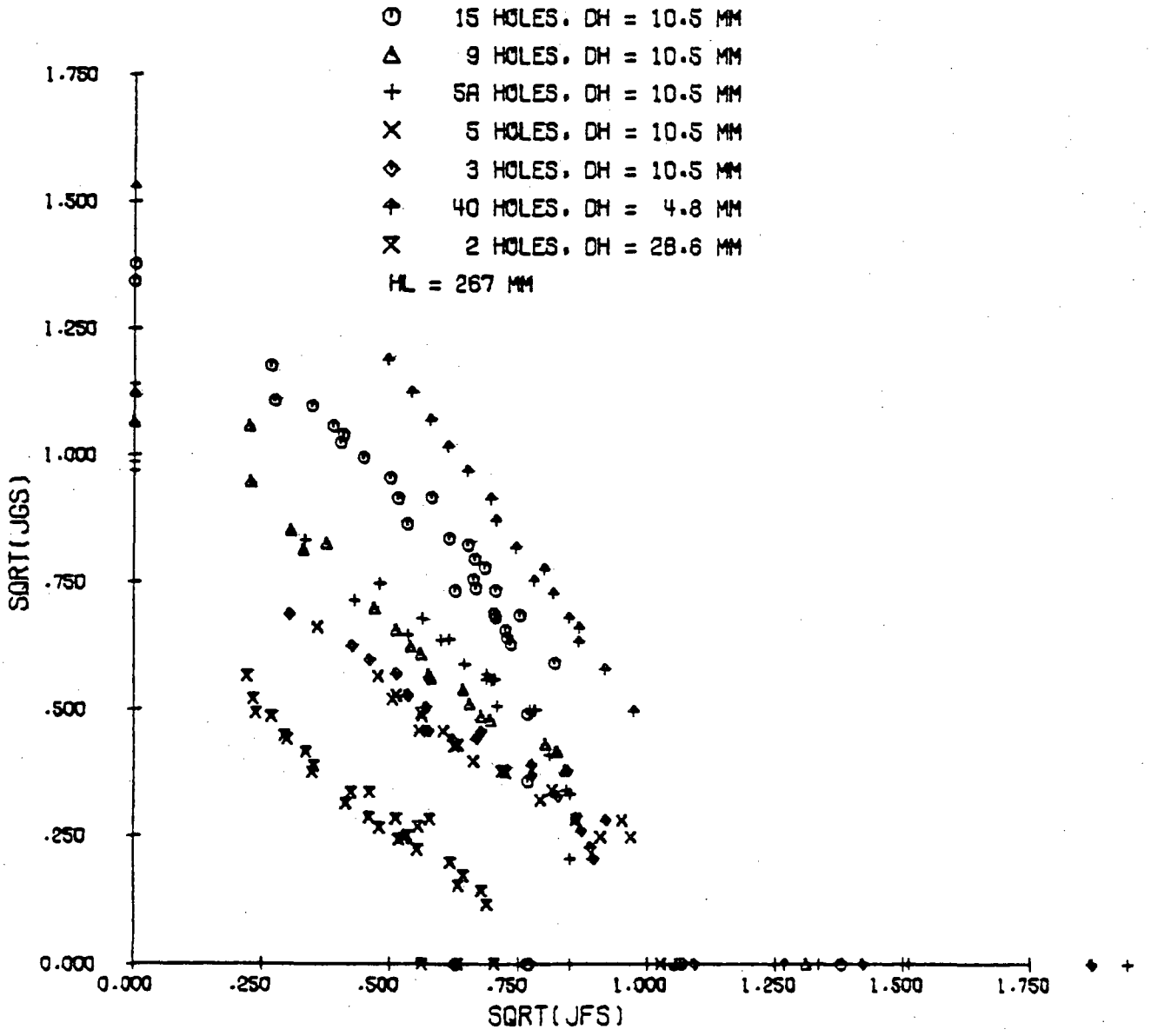

Figure 9. Data Correlation with Equation (12), w = D_h.

$$N_{E\ddot{o}} = [gD^2(\rho_f - \rho_g)/\sigma] < 3.37 \qquad (47)$$

For 40 hole plate, D_h = 4.76 mm, and its Eötvös number is

$$N_{E\ddot{o}} = 3.03 < 3.37 \qquad (48)$$

Therefore, in the low air flow rate region, surface tension could reduce the rate of water delivery, resulting a higher value of m.

3.3 Correlation of Coefficient C

As shown on Figure 9, the dependence of coefficient C on the geometry of the perforated plate can not be properly eliminated by using diameter of hole as the characteristic dimension. In other words, the coefficient C obtained in this way in a perticular perforated plate will not be applicable for other perforated plates. Sun(28) has made the same conclusion in his flooding correlation for BWR bundle side-entry orifices.

Equation (23) was then tried in order to correlate the data. The result is plotted as $K_g^{*1/2}$ vs. $K_f^{*1/2}$ in Figure 10. It shows that the coefficient C is still influenced by some geometric factors of the perforated plate.

Based on a hanging film model, Wallis(36, 37) indicated that the Kutateladze number, i.e., equation (23), is more suitable for the flooding correlation of large tubes($D^* > 30$), while equation (12) can be used in the range of $3 < D^* < 20$. Hence, a new dimenless flow rate is suggested as:

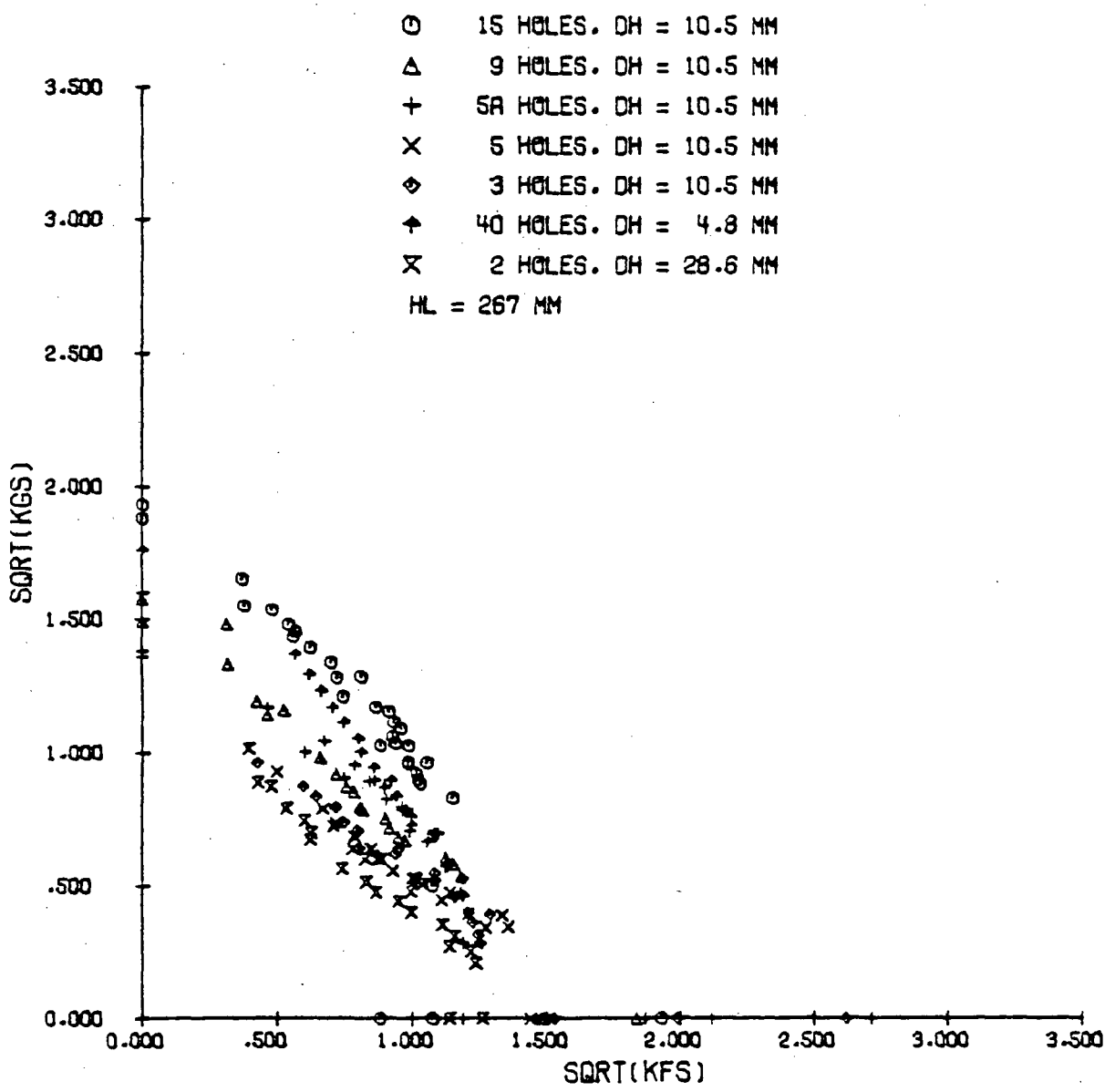

Figure 10. Data Correlation with Equation (23).

$$H_g^{*1/2} + H_f^{*1/2} = C \tag{49}$$

where $$H^*_{f,g} = [\rho_{f,g}/gw_8(\rho_f - \rho_g)]^{1/2} j_{f,g} \tag{50}$$

$$w_8 = D_h^{(1-\alpha)}[\sigma/g(\rho_f - \rho_g)]^{\alpha/2} \tag{51}$$

The value of α lies in the interval between zero and one. when α is equal to zero, w_8 is just equal to D_h and equation (49) reduces to the form of equation (12) with J^* as the appropriate scaling form. For α equal to one, $w_8 = w_7$ ($= [\sigma/g(\rho_f - \rho_g)]^{1/2}$), and thus K^* scaling results. For α between zero and one, equation (49) represents the H^* scaling. Therefore, H^* scaling is essentially a smooth transitional scaling between J^* and K^* scaling.

The α is defined as a hyperbolic tangential function of kD_h and perforation ratio A_h/A_T.

$$\alpha = \tanh[(k D_h)(A_h/A_T)] \tag{52}$$

This function is plotted in Figure 11. Table 2 gives the value of α for each perforated plate tested in this experiment. By the use of this α function in equation (51), it is found that the value of C in equation (49) can be correlated as a function of L^* ($= n\pi D_h[g(\rho_f - \rho_g)/\sigma]^{1/2}$) only. The plot of C for each plate against the Bond number L^*, as illustrated in Figure 12, shows that the relation between C and L^* can be represented by a simple linear function. By method of linear regression, this line is fitted as:

$$C = 1.07 + 4.33 \times 10^{-3} L^* \tag{53}$$

with coefficient of determination:

Table 2. The Values of α for Each Perforated Plate

Labels of Plates	D_h	$D_h k$	A_h/A_T	α
15 hole	10.5	3.2	.423	0.884
9 hole	10.5	3.2	.254	0.671
5 hole 5A hole	10.5	3.2	.141	0.422
3 hole 3A hole	10.5	3.2	.085	0.264
40 hole	4.8	1.5	.232	0.335
2 hole	28.6	9.0	.418	0.999

$$\alpha = \tanh[(D_h k)(A_h/A_T)]$$

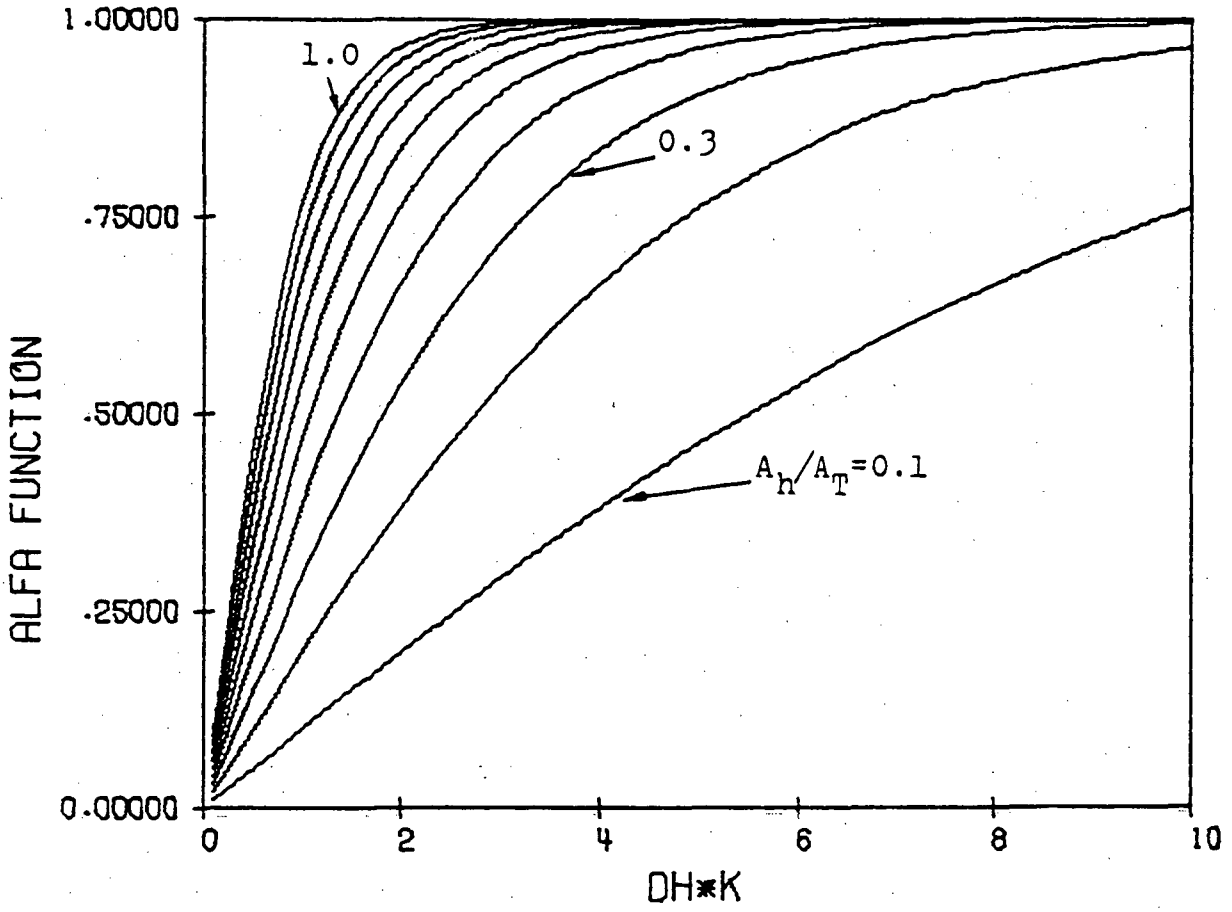

Figure 11. The α function given by equation (52).

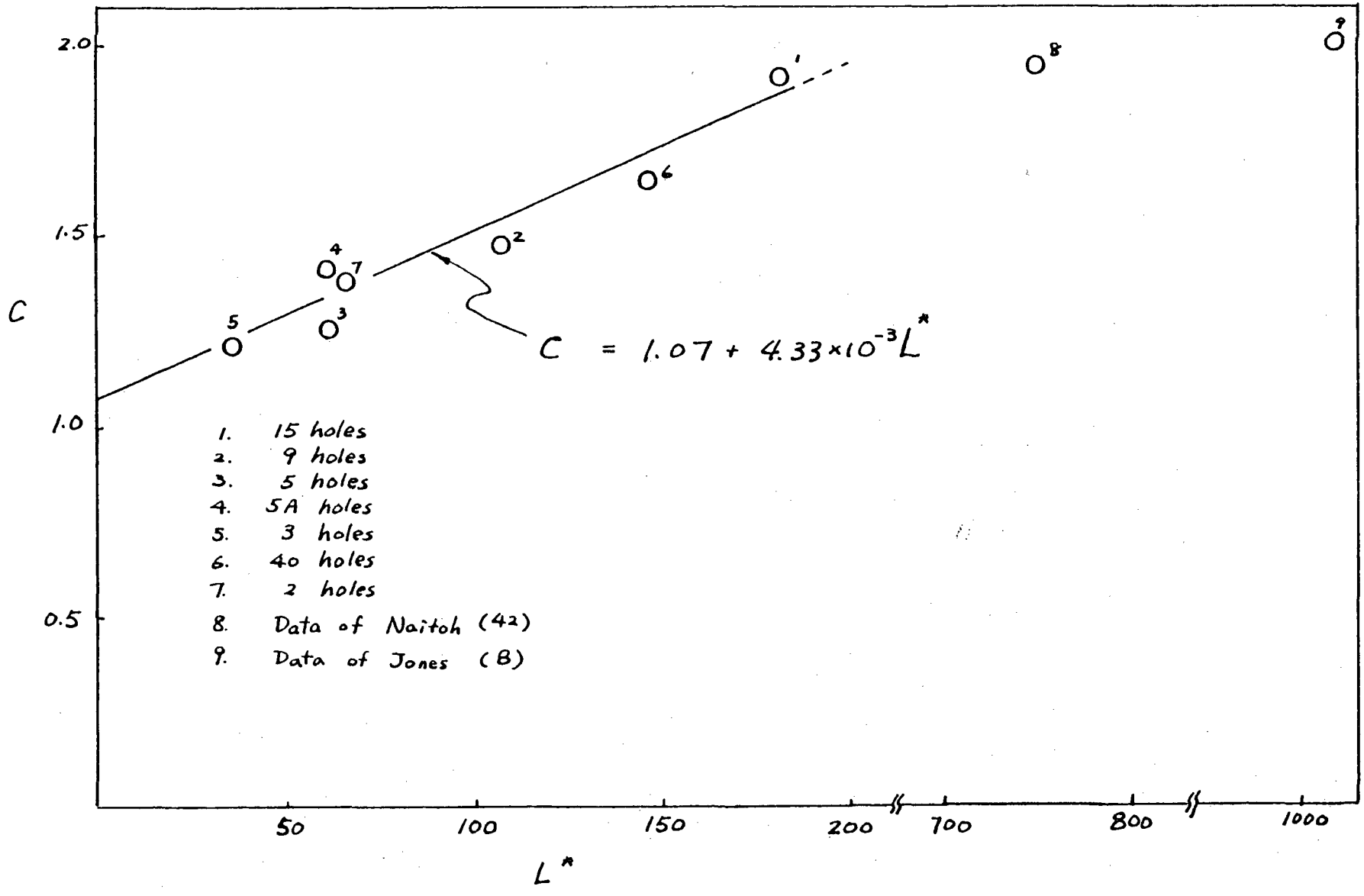

Figure 12. Coefficiency C in equation (55) as a function of L^*.

$$r^2 = 0.93 \qquad (54)$$

The applicable range of equation (49) is $30 < L^* < 200$. Data obtained in BWR upper tie plate geometries reveals that as L^* becomes large, the value of C approaches a upper limit of 2.0.

Therefore, a general equation for perforated plate weeping rate prediction is suggested as

$$H_g^{*1/2}/C + H_f^{*1/2}/C = 1 \qquad (55)$$

where $C = 1.07 + 4.33 \times 10^{-3} L^* < 2.0 \qquad (56)$

Figure 13 shows the data plotted with $H_g^{*1/2}/C$ vs. $H_f^{*1/2}/C$. Based on the data shown, it is reasonable to conclude that equation (55) are an adequate rate of weeping data correlation. This equation, along with equation (56) and (52) will then be used in the correlation of steam/cold water experimental data.

3.4 Effect of Liquid Inlet Rate

The dimensionless liquid inlet rate is plotted on the abscissa of Figure 13 as $H_f^{*1/2}/C$. The data for each perforated plate, though taken at several different liquid inlet rates, fit a single curve with a constant slope, which means the rate of weeping is independent of inlet liquid rate. This conclusion agrees with the results of other investigators(8, 42, 52).

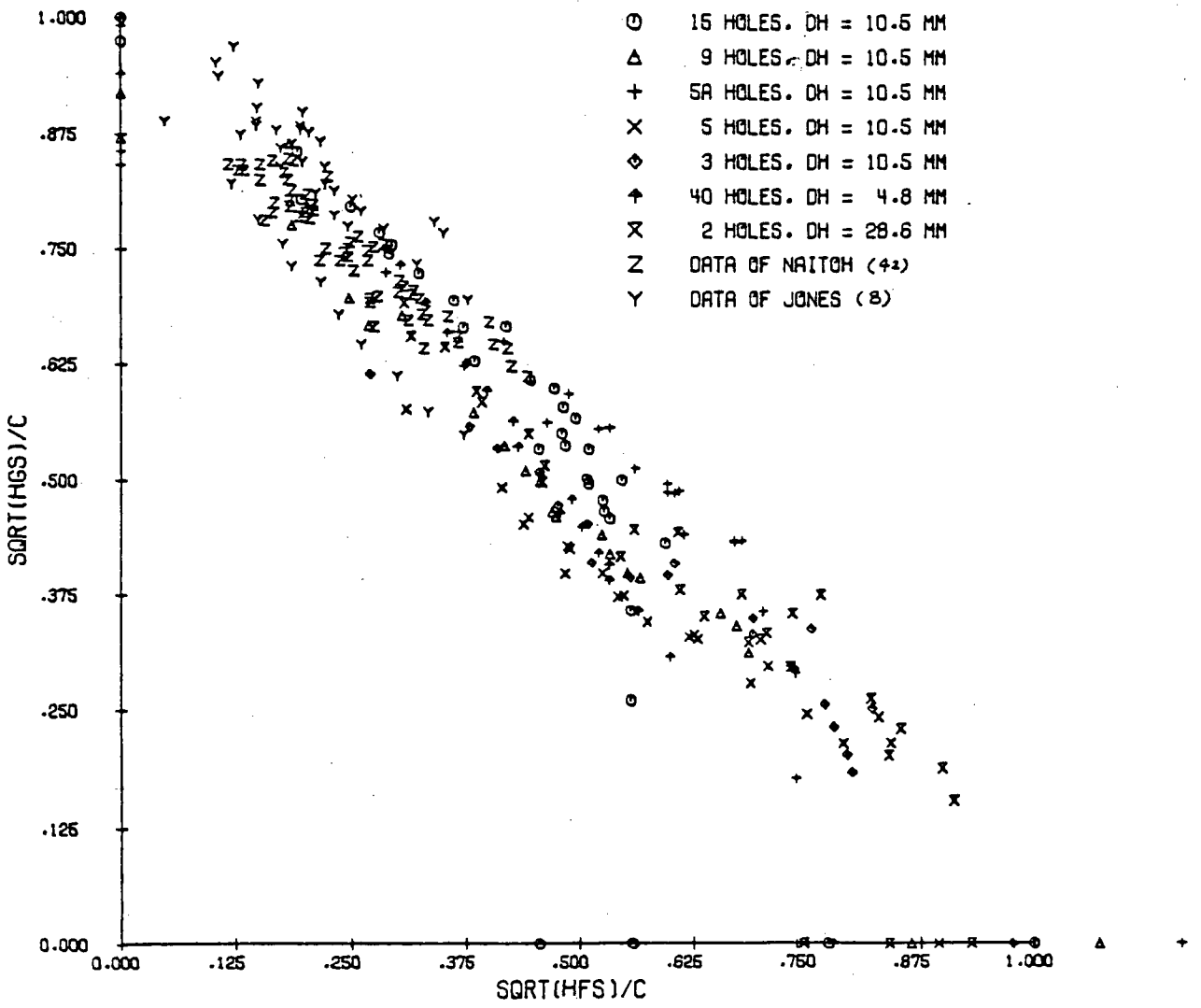

Figure 13. Data Correlation with Equation (55).

3.5 Effect of Head of Liquid Pool above the Plate

The liquid pool head(h_L0 has been varied between 1500 mm and 40 mm in Naitoh's BWR 8x8 upper tie plate weeping experiment (42). In this experiment h_L does not have observable effect on the rate of weeping. The effect of h_L on the rate of liquid delivery in annular geometry has also been investigated in Air/Water system at Dartmouth(37). As reported, the rate of liquid delivery is independent of liquid head as soon as the liquid head exceeds 50 mm. However, Mohr(43) proclaimed that increasing the liquid head h_L will cause a higher rate of liquid delivery.

Figure 14 shows the 15 hole test plate data obtained at two values of h_L. The rate of weeping is the same in both cases. Hence, we conclude that the rate of liquid downflow is independent of the liquid head h_L in the geometry studied.

3.6 Effect of Liquid Inlet Position and Soft Volume

The liquid inlet spray position has been varied between 5 mm and 600 mm. Since all the liquid streams are injected horizontally into the channel, the effect of liquid inlet momentum on the rate of weeping has been minimized. The position of liquid inlet spray, as expected, does not produce observable effect on the rate of weeping.

The soft volume range from 6.75×10^{-4} m^3 to 2.86×10^{-3} m^3 has been tested in a few runs on the 15 hole test plate. No effect of this factor on the rate of weeping has been observed.

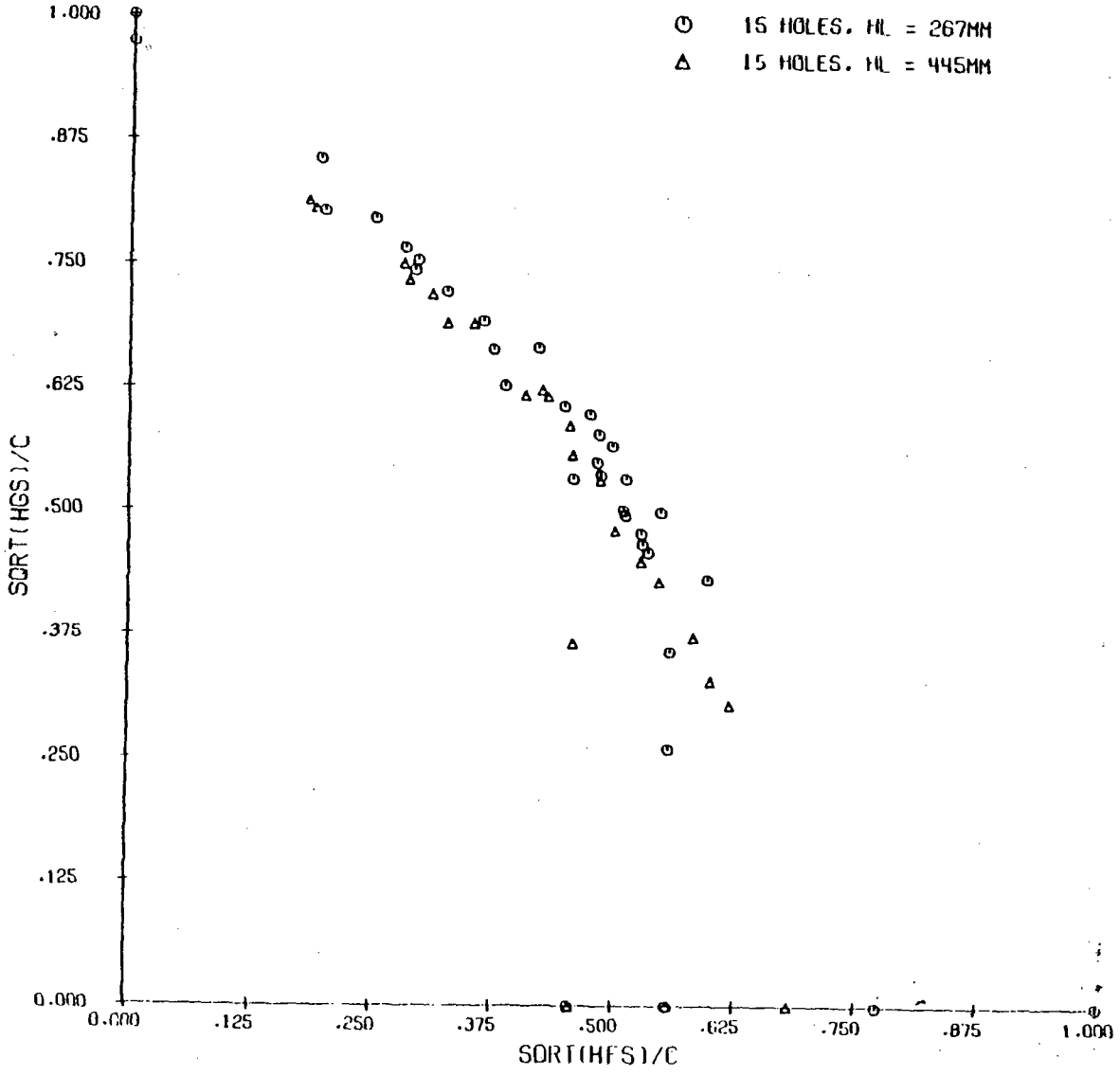

Figure 14. Effect of Head of Liquid Pool(h_L) on the Rate of Weeping

4. Steam/Cold Water Experiment

The objective of the steam/cold water experiment is to study the effect of subcooled water to the onset of weeping. At a fixed value of water flow rate and subcooling, the steam flow rate at which the water above the plate starts to leak through the perforations, along with all the thermocouples and pressure transducer readings at this point, is recorded. Water flow rates up to 0.7 kg/s, water temperature between 285 K and 359 K, and water inlet spray position between 5 mm and 710 mm have been tested. Depending on the combinations of these parameters, several types of weeping and dumping have been observed and studied.

4.1 Technical Background

Various aspects of condensation-driven fluid motions have been examined and discussed by Block(15). The thermodynamic ratio R_T($= C_f(T_{sat} - T_f)W_f/h_{fg}W_g$) is adopted as the main parameter in characterizing the performance of condensing two-phase flow systems. The line $R_T = 1$ separates the "universal flow regime map for direct contact condensation" into two major regions(Figure 15). The region $R_T > 1$, where complete condensation of the vapor is possible, is further divided into three sub-regions, but no detailed discussion was made for the performance characteristics of region $R_T < 1$.

The experiments held in annular or perforated plate geometries have revealed some new information to this flow regime map. In addition to the thermodynamic boundary $R_T = 1$, a hydrodynamic boundary is observed in the region $R_T < 1$. This hydrodynamic boundary can be expressed in the form of equation (12)

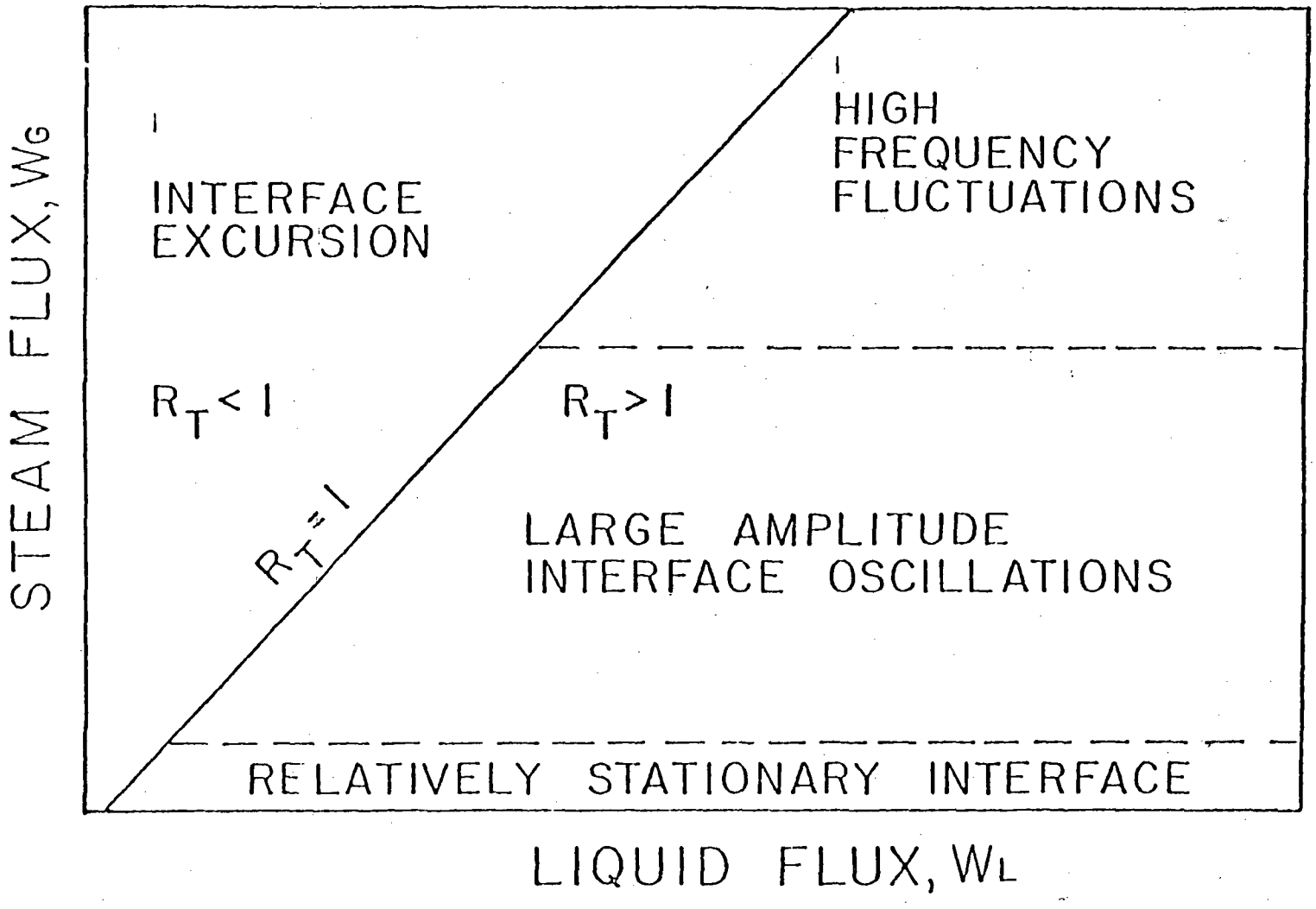

Figure 15. Block's "Universal Flow Regime Map for Direct Contact Condensation".

or equation (55).

Figure 16 is a typical flow regime map for PWR downcomer geometries. In the region (1), where the steam flow rate is so high that both the hydrodynamic and thermodynamic boundary are exceeded, the Emergency Core Coolant(ECC) can not flow down against the ascending steam, and it is called ECC bypass(6). The region (2) represents the operating condition where the end of ECC bypass may occur. The region (3) covers both sides of line $R_T = 1$. The flooding equation in this region can be expressed as(6, 35):

$$(J^*_{gc} - f[(T_{sat}-T_f)C_p/h_{fg}](\rho_f/\rho_g)^{1/2}J^*_{f,in})^{1/2} + m\, J^{*1/2}_{fd} = C \qquad (57)$$

where f, the condensation ratio, is correlated empirically as a function of operating pressure P and dimensionless liquid inlet flow rate $J^*_{f,in}$.

The boundary between the region (3) and the region (4) is given by

$$J^*_{gc} - f[(T_{sat}-T_f)C_p/h_{fg}](\rho_f/\rho_g)^{1/2}J^*_{f,in} = 0 \qquad (58)$$

All the steam will be condensed in the region (4), resulting a total delivery of the ECC water.

For perforated plate, both Jones(8) and Naitoh(42) indicated that once the temperature of downflowing liquid(T_f in equation (58)) is less than the saturated temperature(T_{sat}), some steam will be condensed before it can reach the plate. As a result, more water can flow down, and triggers the total dumping. In

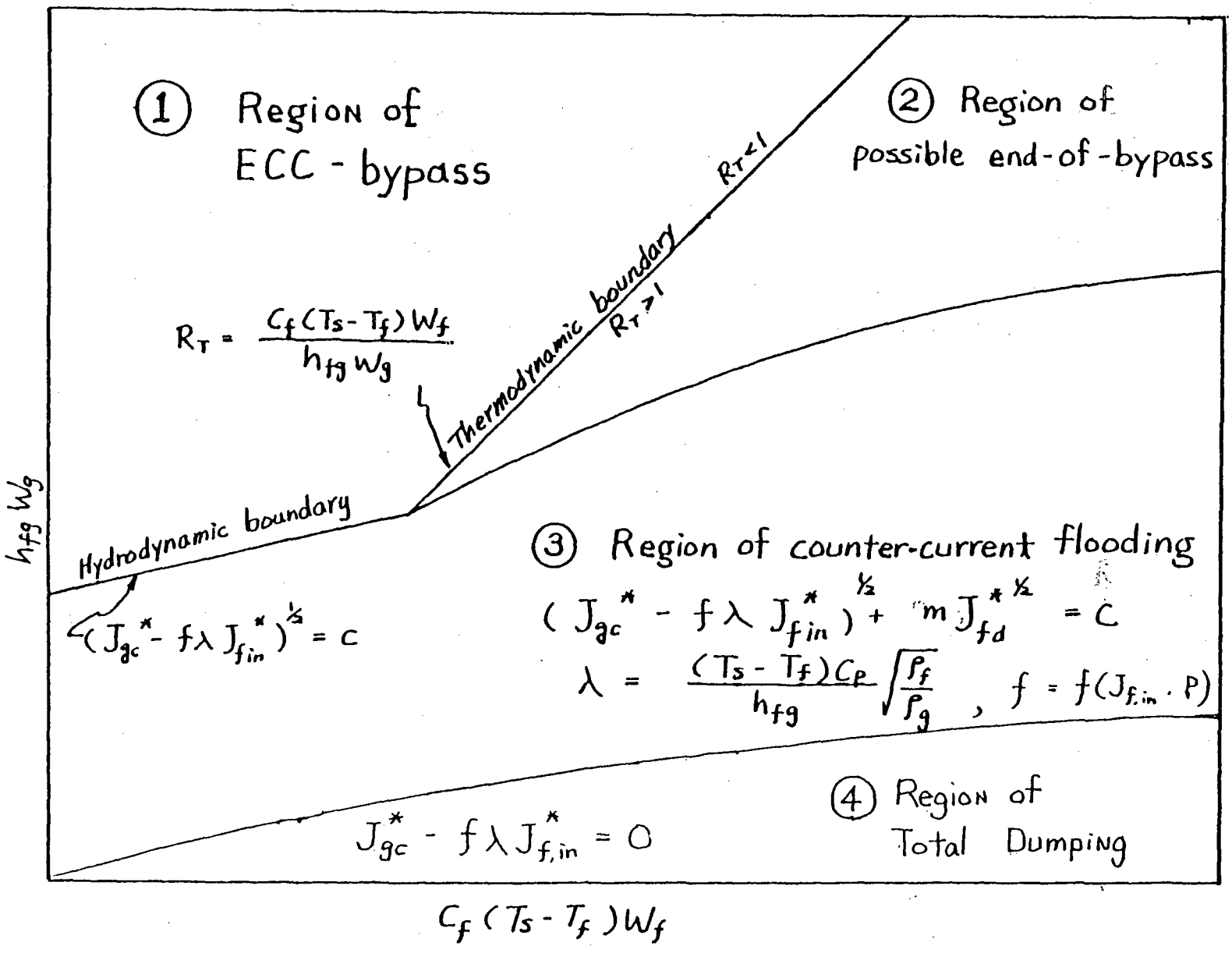

Figure 16. The Flow Regime Map of Direct Contact Condensation for the PWR Annular Downcomer Geometries.

other words, the condensation efficiency (f) is equal to one in this case. Setting f = 1 in equation (58), this equation will then reduced to R_T = 1. Hence, for perforated plate the boundary between the region (3) and (4) of Figure 16 will coincide with the thermodynamic boundary R_T = 1, resulting a flow regime map like Figure 17. Jones(8) and Naitoh(42) held their steam/water weeping experiments in region (2). Both of them indicated that in this region the rate of weeping is independent of the water subcooling. Operating in the region (3) and (4), Duffey(50) studied the time elapsed between injection of water and the transition to downflow. The present investigation in steam/cold water system is to locate the boundary between weeping and no weeping regions in this flow region map, and to study the mixing efficiency at this boundary.

4.2 Previous Works

The operating condition at the weep point has been studied by the investigators in Northwestern University(51) in the steam /water system. The test channel is made of a 2 inches I.D. pyrex glass tube. A 6.4 mm thick perforated plate with six holes of 6.4 mm diameter has been studied in this channel. Water is injected out horizontally through a tube which is attached to the center of the perforated plate. Holes in this tube, which admit the water into the channel, are 1 cated right above the plate.

In this experiment, water temperature is kept at building tap water temperature, which varied between 280 K and 288 K. The steam inlet temperatures have been varied between 373 K and 518 K to study the effect of steam superheat on the weep point.

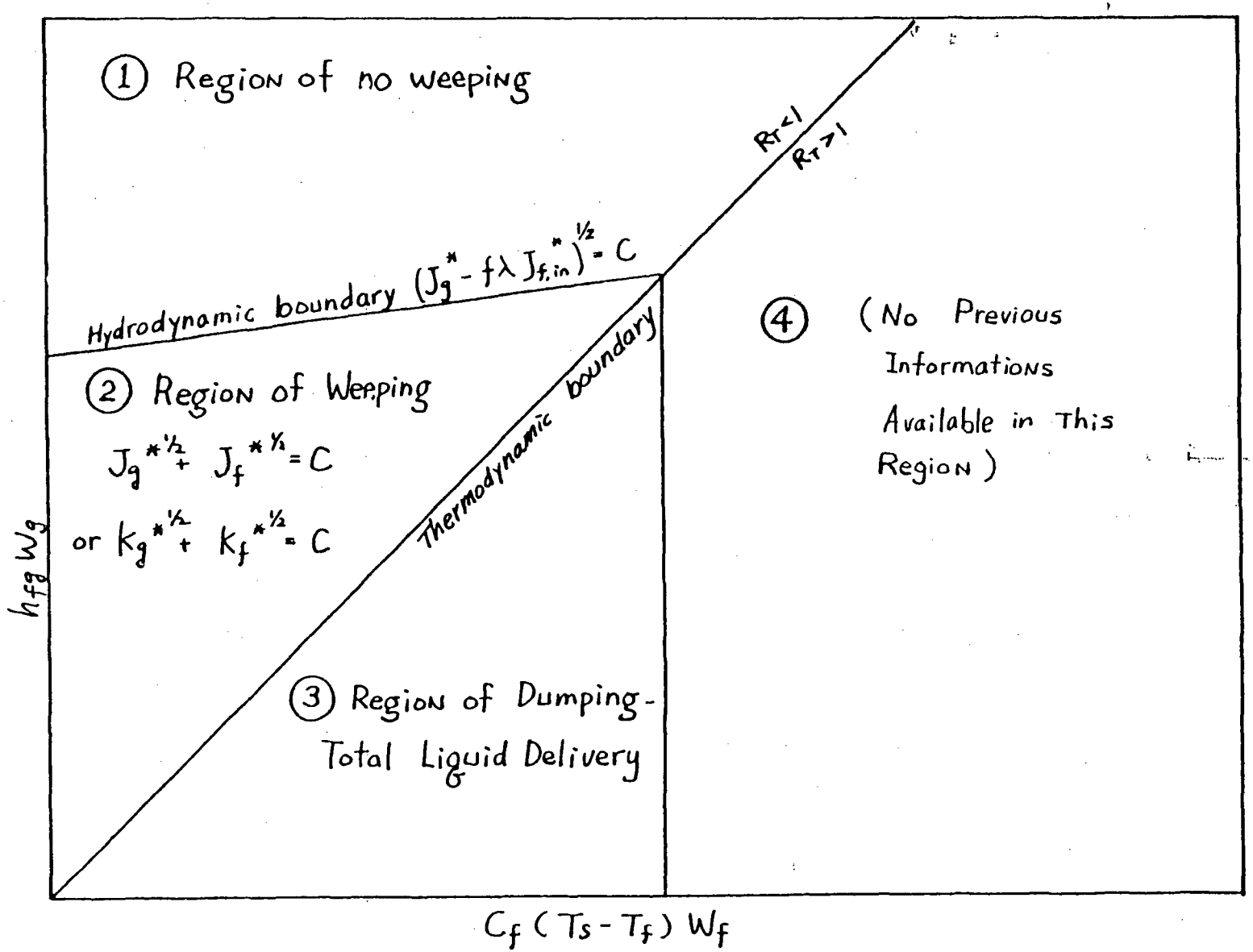

Figure 17. The Flow Regime Map of Direct Contact Condensation For Perforated Plate Plate Geometries.

Several important observations have been obtained in this experiment:

1. The head of liquid pool above the plate(h_L) between 50 mm and 350 mm did not have any discernible effect on the weep point.

2. At high water flow rate(0.151 kg/s) and large h_L(254 and 356 mm) two types of liquid delivery were observed--- "oscillatory weep" and "total dumping". The oscillatory weeping is characterized by its severe oscillation in the water pool above the plate. When the steam flow rate is reduced to a point where all the steam can be condensed right above the plate, the pressure fluctuation in the water pool is eliminated, and a stable no weeping condition is, therefore, maintained. Further decreasing the steam flow rate can trigger the total dumping.

3. The effect of steam superheat ranging between 0 K and 145 K can be correlated by taking into account the sensible heat of superheated steam in the thermal calculation and the change of steam density in the hydrodynamic calculation.

4.3 Experimental Apparatus

4.3.1 Test Channel

The same test facilities for the air/water experiment is used here for the steam/water experiment. The detailed descriptions of the apparatus and the channel are given in section 2.2. The perforated plates tested in this experiment include(Figure 1): 15 hole, 9 hole, 5 hole, 5A hole, 3 hole, and 3A hole.

4.3.2 Water Line

The water line used here is the same one used in air/water experiment. The water inlet temperature ranging between tap water temperature and 358 K can be adjusted by the control of steam purging rate to the water line. Two 3/8 inch steam purging lines are connected from 1 m upstream of the 1 inch steam venturi to 0.8 m upstream of the water rotameter. At any fixed water flow rate, the water temperature can be adjusted to within 0.2 K of the desired value by this device.

The water inlet temperature is measured by thermocouple T1 (Figure 6) located at 0.3 m upstream of the water rotameter. The temperature of the downflow water is measured by thermocouple T14, while the overflowing water is measured by thermocouple T15 located at the overflow port. A overflow weir of 25 mm height is installed in the port to guarantee the tip of T15 is immersed in the water. Detailed descriptions about the temperature measurement of the two phase mixture above the test perforated plate will be given in section 4.3.4.

Since the experiment is concentrated on a weep point study, no measurement on the rate of weeping has been made The rate of weeping at the weep point is equal to zero. It is, therefore, assumed that the rate of water overflow is equal to the sum of the water inlet rate and the rate of steam condensation. The rate of steam condensation is estimated by the water phase enthalpy balance.

4.3.3 Steam Line

Steam at 800 kPa is obtained from the building main steam line. Passing a water separator, the steam venturi system installed mainly for other experiments held in the same laboratory, and several valves, the dry steam is directed to the test channel via a 1 inch brass pipe. The degree of steam superheat can be controlled by a electrical heater. The steam flow rate is controlled by two 1 inch stainless steel globe valves installed before the 1 inch air and/or steam entrance nozzles of the test channel.

The soft volume upstream of the perforated plate can be adjusted by changing the liquid level in the lower chamber of the channel. Since the water temperature at the steam/water interface in this chamber can be saturated very soon, and the heat loss through the channel wall can be assumed negligible, the rate of steam condensation in this lower chamber is ignored.

After passing the two-phase mixture above the perforated plate, the steam left, if any, flows out of the test channel through a 3 inch hose. The pressure drop through this hose is small enough to keep the operating pressure of the channel

near atmospheric for the whole range of steam flow rate. The steam outlet temperature is measured by thermocouple T3 installed at the top plate of the test channel. A pressure relief valve is also installed on the side wall near the the top plate. Should the operating pressure in the channel exceed 200 kPa, this valve can relieve the pressure by venting the steam to the atmosphere.

4.3.4 Instrumentation

The detailed description of water rotameters is given in section 2.2.4.

The steam flow rate is usually measured by a BARCO 1/2"-402 venturi installed horizontally on the 1 inch steam line between the steam purge outlet nozzles and the electrical heater(Figure 6). Therefore, this venturi reading is independent of the steam purging rate. The standard piping arrangement for the steam venturi is given in Figure 18.Knowing the differential pressure reading of the venturi, along with the absolute pressure and temperature of the steam, the mass flow rate of the steam can be calculated with the aid of the calibration curve of the vanturi. For steam flow rate higher than the maximum measurement capacity of this venturi, a BARCO 3/4"-425 venturi, which belongs to the venturi system of the laboratory, is used.

Table 3 gives the locations and functions of all the thermocouples used in the experiment. All the thermocouples attached to the channel are fixed by Cajon Ultra-Torr Fittings installed on the side wall of the channel. These fittings can be made leak tight by finger-tightening, while traversing the thermocouples can easily be done by loosening the cap of the fitting. Among all the

Table 3. Function of Thermocouples

TI	Position	Phase
1	70 cm upstream of water rotameters	L
2	50 mm up stream of 1 inch steam venture	V
3	Top plate of the test channel	V
4	177 mm above the perforated plate	V-L
5	152 mm above the perforated plate	V-L
6	127 mm above the perforated plate	V-L
7	102 mm above the perforated plate	V-L
8	77 mm above the perforated plate	V-L
9	52 mm above the perforated plate	V-L
10	27 mm above the perforated plate	V-L
11	2 mm above the perforated plate	V-L
12	Steam inlet nozzle	V
13	Lower chamber of the channel	V
14	Lower chamber of the channel	L
15	Liquid overflow nozzle	L

Note: L : Liquid V : Vapor

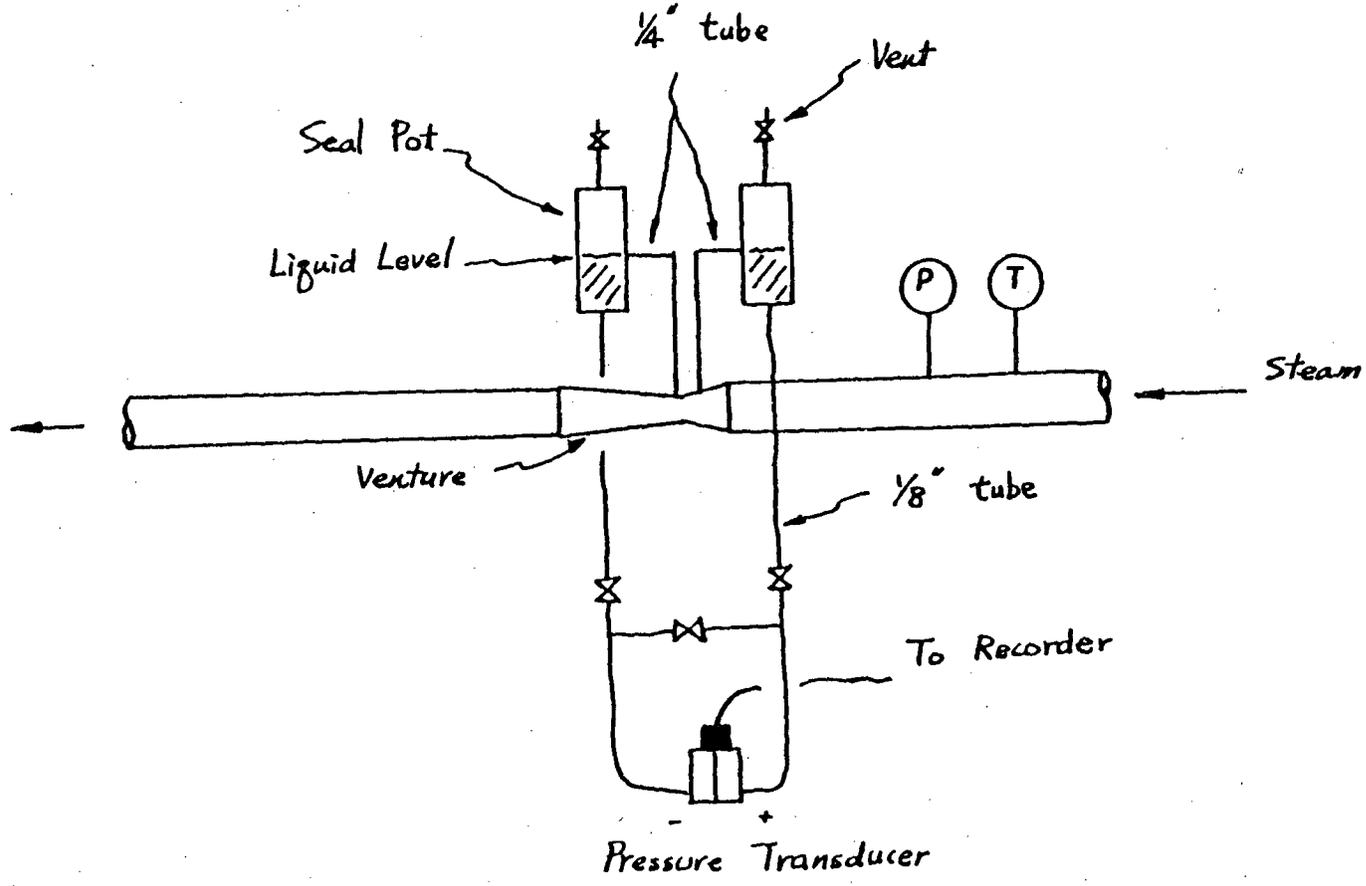

Figure 18. The Standard Piping Arrangement for Steam Venturi

thermocouples, more attention must be given to T12, which was installed to measure the dry steam temperature at the inlet nozzle. It tends to give a false reading of 373 K(sat ated steam temperature at 1 atmosphere) if the tip of the thermocouple is wetted by a water droplet.

The temperature of the vapor/liquid mixture above the perforated plate is measured by thermocouples T4 - T11. The tip of T11 is 2 mm above the perforated plate. By properly traversing this thermocouple, the temperature of two thirds of the cross-section area above the plate can be measured. Thermocouples T4 to T10, al igning on the centerline of the side wall of the channel with a equal spacing of 25 mm, can provide some picture about the temperature distribution above the plate.

Detailed description about the channel operating pressure measurement device is given in section 2.2.4 and Figure 8. Since the steam will tend to condense in the pipe line of the pressure transducer, a constant air purge is usually required to maintain a stable pressure reading.

4.3.5 Computer Program

A computer program written in FORTRAN IV language is used for the tasks of data reduction and plotting.

The steam flow rate through the 1/2"-402 venturi is calculated by equation (59):

$$W_s = 0.051\ (V/\rho_g) \qquad \text{lbs/sec.} \qquad (59)$$

where V is the voltage reading from the pressure transducer connected to the venturi. If the 3/4"-425 venturi is used, the steam mass flow rate is calculated by equation (60).

$$W_s = 0.35\ (V/\rho_g) \qquad \text{lbs/sec.} \qquad (60)$$

The physical properties of the steam(enthalpy, entropy and specific volume) can be calculated by the Subroutine PHIS2. The description and the calling sequence of this subroutine are given in Appendix II.

The liquid inlet flow rate is calculated by the following equations:

$$R = 0.4118 + 0.03611 \times W_1 + 0.001042 \times W_1^2 \qquad (61)$$

If $W_1 > 0.724$, set $W_1 = 0.724$

$$W_f = (W_1 \times R + W_2)/60 \qquad \text{lbs/sec.} \qquad (62)$$

where W_1 and W_2 are the readings of water rotameter A and B. These equations are obtained by rotameter flow rate calibration held in the laboratory.

In addition to these flow rates, several temperature readings are also sent into the program; the thermodynamic ratio and the enthalpy flux of the steam and the water can, therefore, be calculated.

The superficial steam and water velocity through the holes and the dimensionless flow rate H_g^* and H_f^*, are also calculated in this program. Finally, the reduced data is plotted by plotter 565 of Northwestern University Computer Center via CalComp Basic

Plotting Package.

A list of this program is given in Appendix II.

4.4 Experimental Procedure

Since visual observation is the only method used in weep point determination, the repeatability of the experiment must be constantly verified. A standard experimental procedure designed for this purpose is listed as follow:

1. Select a test perforated plate. Fix it into the channel.

2. Fix the height of the water inlet spray. Four different water inlet spray positions have been tested: 5 mm, 102 mm, 305 mm, and 710 mm.

3. Open all the valves from the main steam supply pipe to the steam flow rate control valves at the channel steam inlet nozzles. Run the steam for 3 - 5 minutes to clear the steam line from the condensed water and possibly the accumulated air.

4. Zero the voltage readings of pressure transducer of the steam venturi and DP103 differential pressure transducers of the channel pressure measurement.

5. Check the function of all the thermocouples.

6. Turn off the steam.

7. Open the water. Usually, the water flow rate starts at 0.023 kg/s. Gradually increase the steam flow rate to the weep point, which is defined as the point where the water downflow ceases. Record the steam flow rate and pressure, water flow rate and all the relative thermocouples readings. The operating pressure in the channel can also be measured at this point.

8. Further increase the steam flow rate. Then approach the weep point from a high steam flow rate. Record the same informations mentioned in step 7 at this point.

9. Increase the water flow rate, 0.03 kg/s each time. Repeat step 7 to step 8. A complete set of test runs is finished at the maximum water flow rate of 0.65 kg/s.

10. Repeat step 7 to step 9. This time the water flow rate is changed randomly in the range between 0.03 kg/s and 0.65 kg/s. A comparison between the data obtained in step 9 and in step 10 can serve as an indication of the repeatability of the visual weep point determination.

11. Repeat step 2 to 10 at different water inlet height.

12. Repeat step 1 to 11 for different perforated plates.

For the 15 hole perforated plate, steps 2 to 10 have been repeated at 6 different water inlet temperature between 285 K to 359 K in an attempt to study the effect of water subcooling.

5. Results and Discussion for Steam/Water Experiments

The flooding phenomena above a perforated plate are quite different in the steam/cold water system from those in the air/water system. Since the ascending steam contacts the cold water directly above the perforated plate, condensation-driven fluid motions can play a significant role in triggering water breakthrough. This thermal effect may be governed by several factors including : water subcooling, steam superheat, and above all, the position of the water inlet spray nozzle, which determines the mixing efficiency.

In the current steam/water test matrix, steam temperatures ranged from 373 K to 421 K, and water temperatures varied between 285 K and 359 K; the number of holes in the support plate ranged from 3 to 15; and the water inlet position was varied from 5 to 710 mm above the plate. Because of the strong effect of the water inlet position, the data for high and low position are discussed separately below.

5.1 Water Inlet Spray Above The Pool

During those experiments, the distance between the centerline of the water overflow port and the top of the perforated plate(and hence the height of the liquid pool above the plate, h_L) was fixed at 267 mm. A liquid inlet height of 305 or 710 mm, therefore, means the liquid inlet spray was above the pool surface.

Water spraying out from the inlet nozzle fell gravitationally after hitting the side wall of the test channel. Only a portion of this water contacted with the steam, with the remainder bypassing through the overflow port.

5.1.1. 15 Hole Data

Figure 19 shows the 15 hole weep point data obtained at five different temperatures. The effect of water subcooling, as shown, can be correlated in this total enthalpy flux plot. The steam enthalpy flux required to stop the weeping, starting at a value of 40 KW, gradually approaches a maximum limit of 71 KW as the water enthalpy is increased. No relation can be found between this line of weep point and the line of thermodynamic ratio $R_T = 1$.

Two types of weeping were observed during the experiment. Continuous weeping(Figure 20) happened when the liquid enthalpy flux is very low($W_f C_p (T_{sat} - T_f) < 15$ KW). All the inlet water was well saturated at this condition, and the steam can flow through the two-phase mixture above the plate without much being condensed. The pressure transducer readings showed that except for high frequency noise, operating pressures both upstream and downstream of the perforated plate were fairly constant. If the steam velocity through the holes is lower than a certain value, its frictional drag can no longer hold all the liquid above the plate, resulting in continuous weeping.

When the liquid enthalpy flux was increased, more steam was required to keep the plate from weeping. The amount of this extra steam is determined by the condensation effect in a two-phase mixture layer close to the plate. This condensation effect is proportional to the total liquid enthalpy flux with a proportional constant f of 0.24 for 15 hole data(Figure 19). The proportional constant is named the mixing efficiency, because it represents the degree of mixing between the water inlet and the plate. As shown in Figure 20, the ascending two-phase mixture

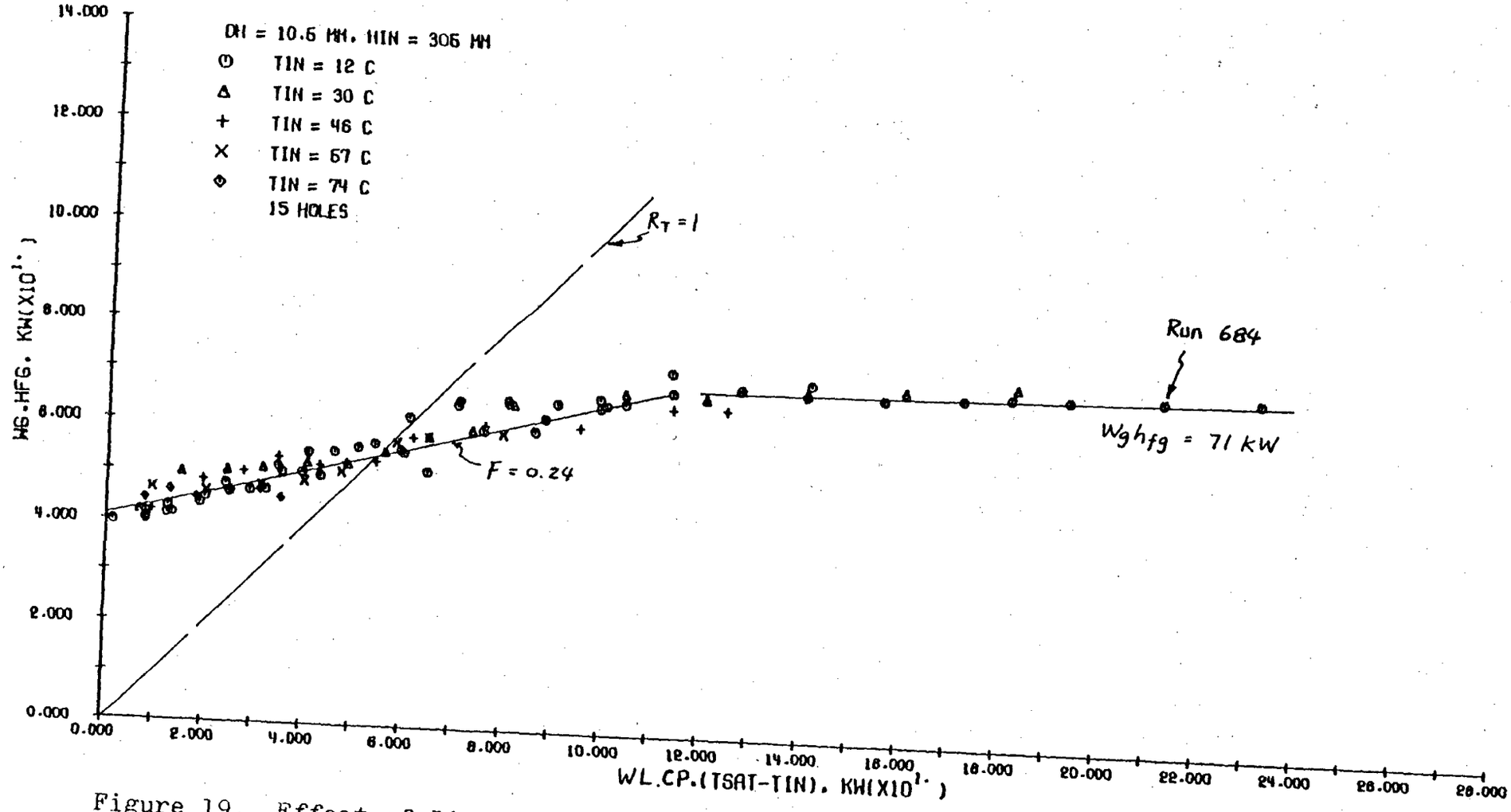

Figure 19. Effect of Liquid Subcooling to the Weep Point, h_{in} = 305 mm, 15 Hole Data

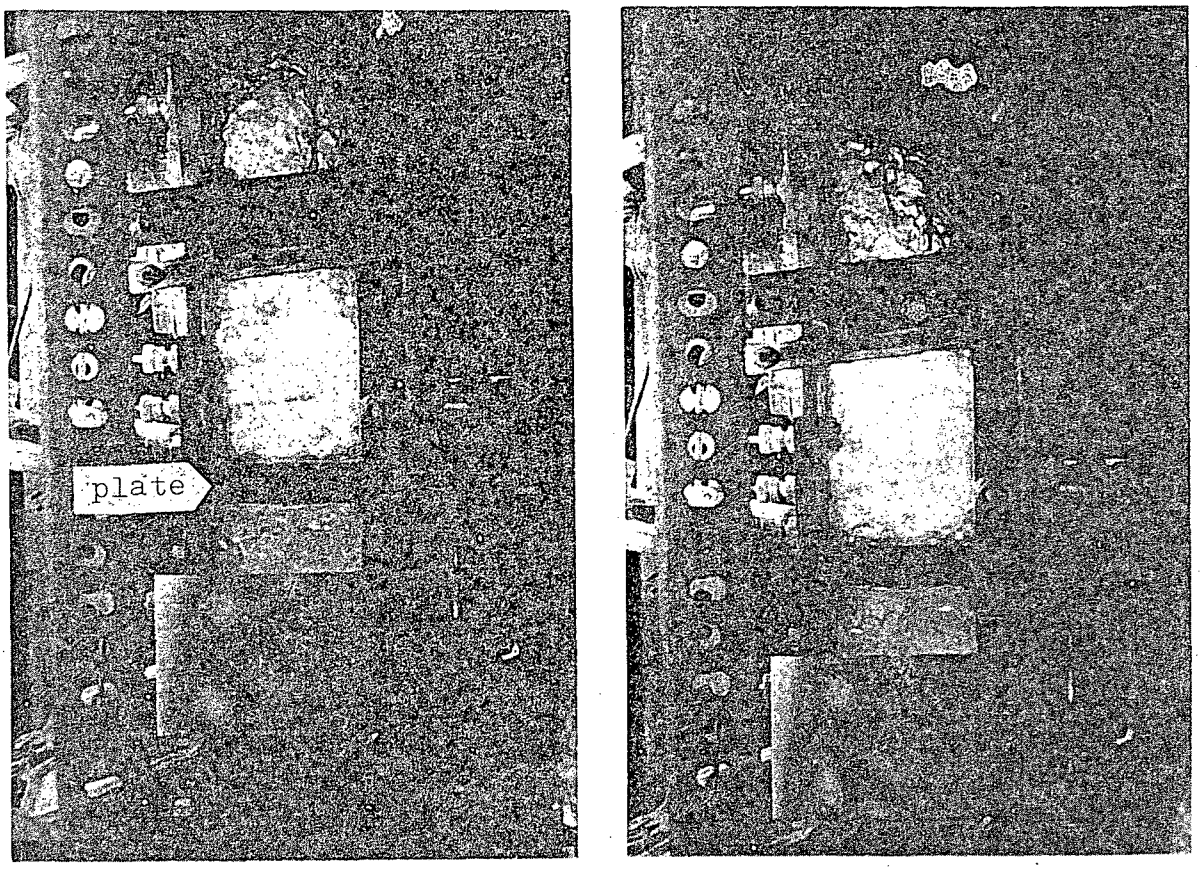

W_f = 0.076 kg/s T_f = 285 K

W_g = 0.018 kg/s T_g = 413 K

Figure 20. Some Pictures of Continuous Weeping, h_{in} = 305 mm

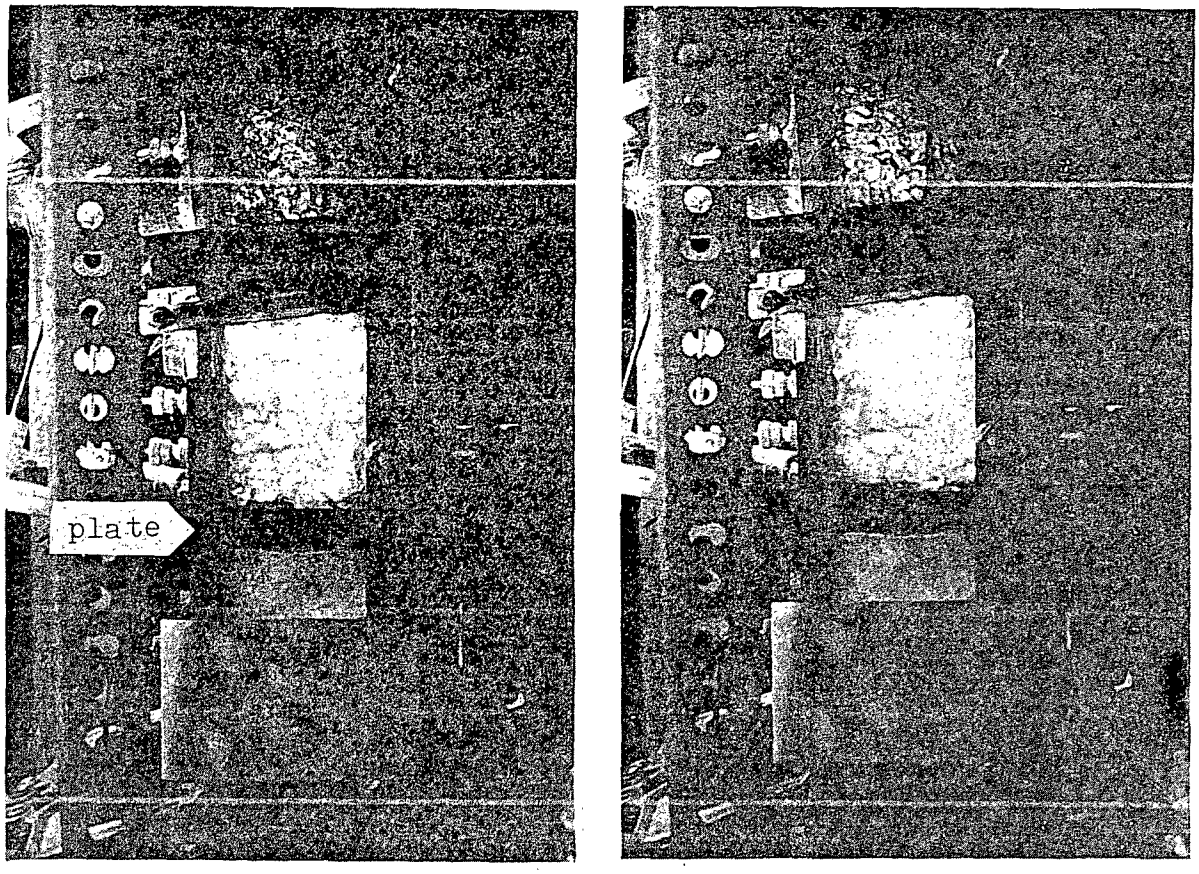

Figure 20. (Continued)

essentially covered the whole cross-section of the channel, water from above had no means of bypassing down to the plate, resulting in a poor mixing efficiency(0.24) in this case.

Once the liquid enthalpy flux exceeded 50 KW, the steam could all be condensed before it reached the top of the pool. A layer of water was then formed above the two-phase mixture above the plate. Along with the increasing of liquid enthalpy flux, this water layer become thicker, and its buffer effect become larger. Eventually, the degree of mixing reaches a maximum. Further increasing the water enthalpy flux can only resulting in a larger portion of cold water overflow without much influence on the two-phase mixture above the plate. This phenomenon can clearly be identified in Figure 19 when the liquid enthalpy flux is greater than 120 KW.

When liquid enthalpy flux was increased, the type of weeping at the weep point also changed from continuous to oscillatory(Figure 21). Oscillatory weeping is characterized by the intermittent downflow of cold water along with the fluctuation of the operating pressure. Figure 22 shows a typical thermocouple reading obtained at Run 684 operating in high liquid enthalpy flux region. As shown by the reading of this thermocouple, which is located 2 mm above the plate, cold water penetrated all the way down to the plate, and then passed through the holes of the plate. The oscillatory weeping of this run has a frequency around 1 cps.

5.1.2 Comparison between 15 Hole and 9 Hole Data

Figure 23 shows both the data of 15 hole and 9 hole experi-

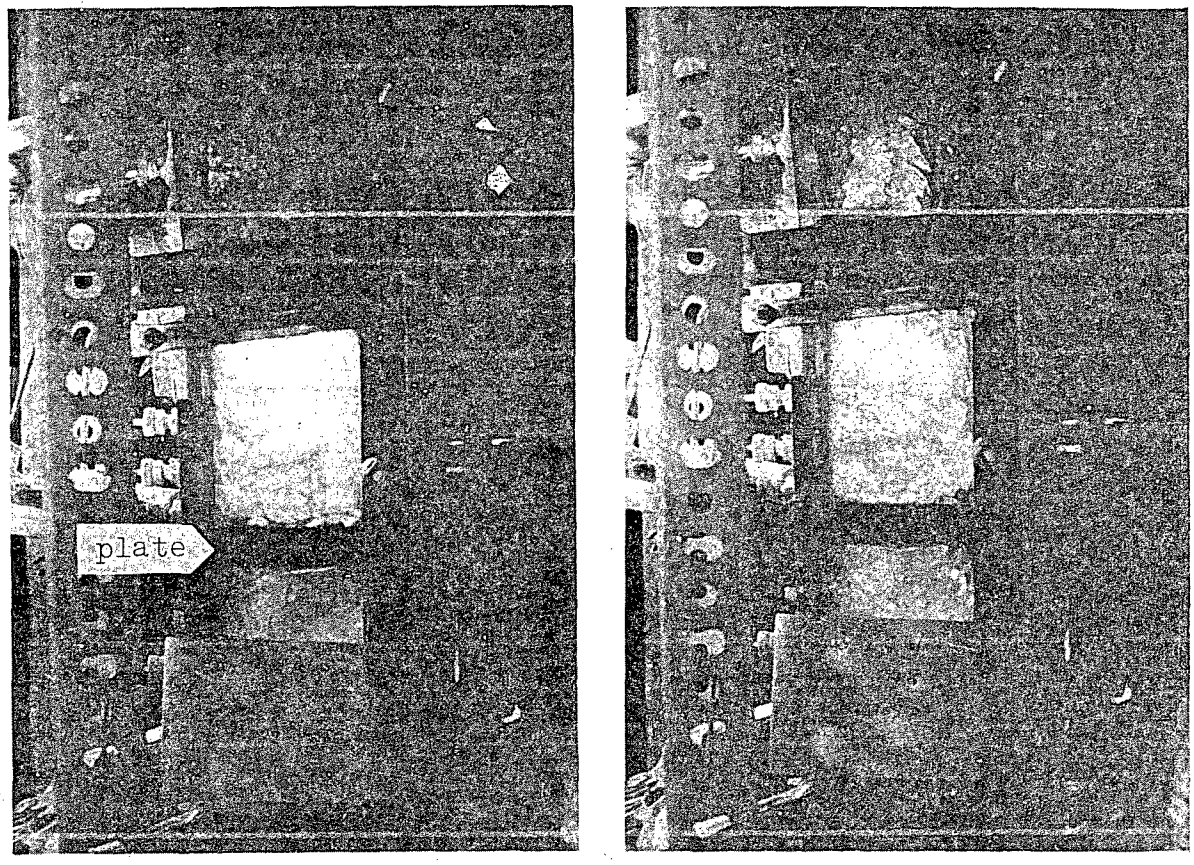

W_f = 0.68 kg/s T_f = 285 K

Wg = 0.056 kg/s T_g = 413 K

Figure 21. Some Pictures of Oscillatory Weeping, h_{in} = 305 mm.

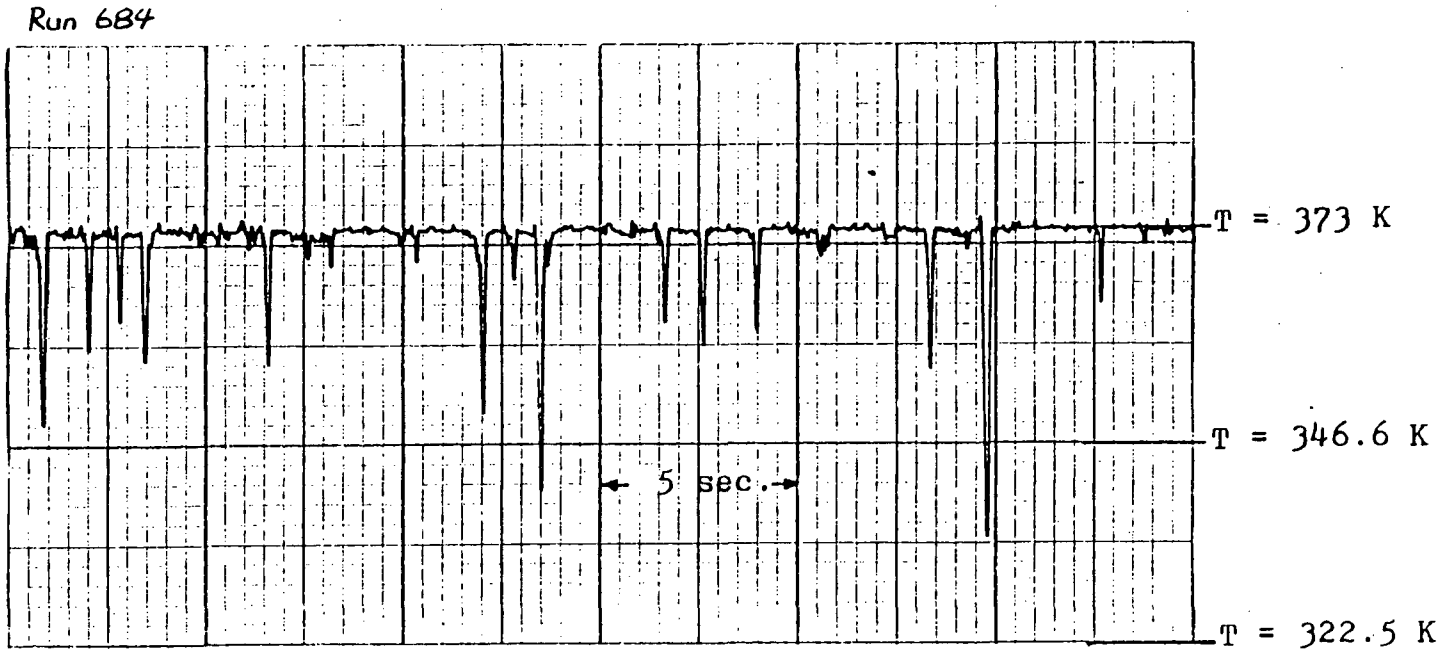

Figure 22. Thermocouple T11 Readings at Weep Point.

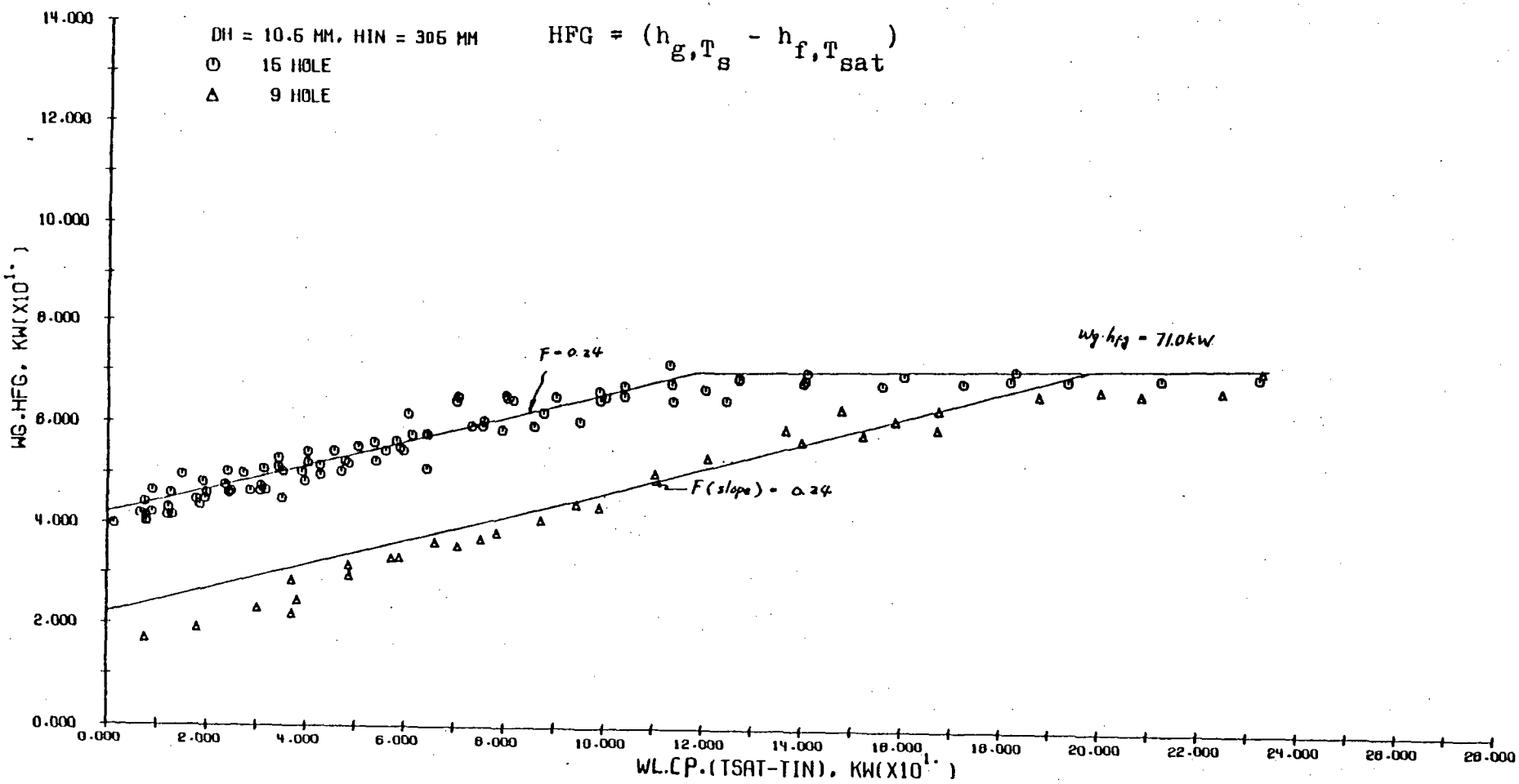

Figure 23. Total Enthalpy Flux at Weep Point, 15 Holes and 9 Holes Data, h_{in} = 305 mm.

ment. Two common features can be discerned easily from this Figure:

1. The mixing efficiency of both experiments are equal to 0.24.

2. Both experiments show the same maximum required total steam enthalpy flux at 71 KW.

Visual observation confirmed that the two-phase mixture zone above the plate in 9 hole experiment still covered the whole cross-section area of the channel ; therefore, cold water can not find any bypass to reach the vicinity of the plate. As a result, the 9 hole experiment shows a mixing efficiency of 0.24, the same as 15 hole data.

A same maximum steam enthalpy flux for both 15 hole and 9 hole data suggested that these two plates not only have the same mixing efficiency, but also have the same upper limit of the degree of mixing, which can not be exceeded by further increasing the water enthalpy flux. Since Figure 23 is a total enthalpy plot, the same maximum total steam enthalpy flux means that the weep point at this high enthalpy flux condition depends on the mixing condition of the channel as a whole, and not on the flow condition at each hole.

Figure 24 is the same data plotted with the superficial steam velocity through the holes vs. the total water enthalpy flux. A comparison between this Figure and Figure 23 shows that:

1. At low water enthalpy flux, though the total amount of steam enthalpy required to stop the weeping is different, the steam velocity through the holes is the same, which means the hydrodynamic effect is the dominant factor of the onset of weep-

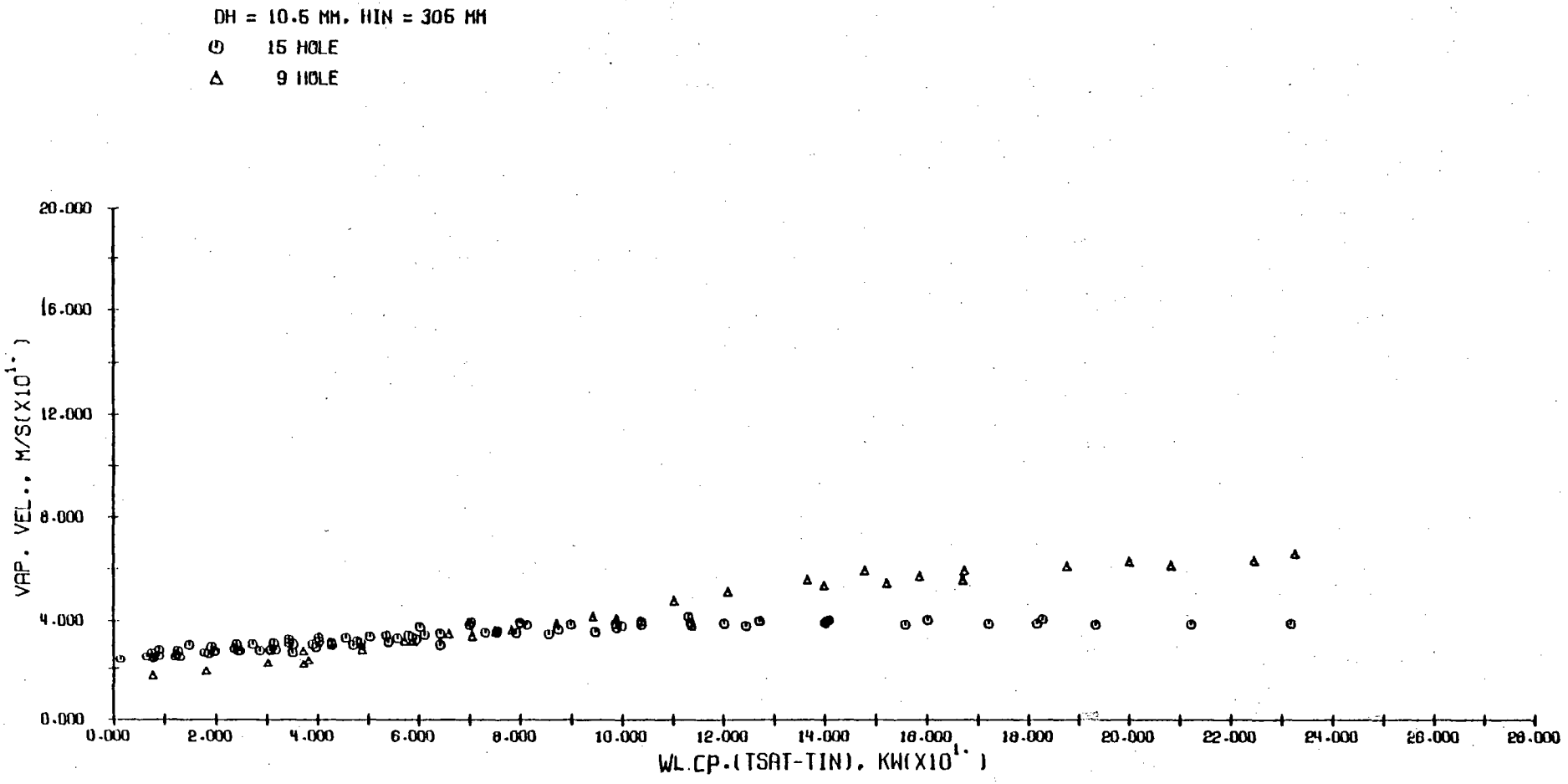

Figure 24. Superficial Steam Velocity through the Holes, 15 Holes and 9 Holes Data, h_{in} = 305 mm.

ing.

2. At high water enthalpy flux, the total steam enthalpy flux is the same, but the superficial steam velocity through the holes of 9 hole experiment is 1.7 times larger than that of 15 hole data. It is suggested that at high water enthalpy flux the condensation effect governed by the degree of mixing of the channel as a whole is the controlling factor of the onset of weeping.

In order to combine these two effects into one equation, the ideal of the effective steam flow rate(5, 6, 33) is considered. for the data correlation.

5.1.3 Data Correlation

The dimensionless effective steam flow rate in the form of H^* scaling is defined as

$$H^*_{g,e} = H^*_g - f[C_p(T_{sat}-T_f)/h_{fg}](\rho_f/\rho_g)^{1/2}H^*_{f,in} \quad (63)$$

where H^* scaling is suggested from the air/water data correlation, and f is the mixing efficiency obtained from Figure 23.

By the use of this effective steam flow rate, the flooding equation obtained in air/water experiment, i.e., equation (55), becomes:

$$H^{*1/2}_{g,e}/C + H^{*1/2}_f/C = 1 \quad (64)$$

At the weep point no water will fall through the holes;

hence, H_f^* is equal to zero, and equation (64) is reduced to

$$H_{g,e}^{*1/2}/C = 1 \qquad (65)$$

where the coefficient C is given in equation (56).

Equation (65) is then used to correlate the 15 hole and 9 hloe steam/cold water weep point data by setting f = 0.24 with an upper limit of steam enthalpy flux of 71 KW.

Figure 25 is the dimensionless steam and water inlet flow rate plotted in the form of $H^{*1/2}/C$. It shows the value of $H_g^{*1/2}/C$ is very close to one at low water inlet flow rate. This means that the steam/water data agree fairly well with the air/water data when the condensation effect is insignificant.

Once the liquid enthalpy flux, and hence the condensation effect is increased, the dimensionless steam inlet flow rate is replaced by the effective steam flow rate. Figure 26 is the same data plotted with the left hand side of equation (65) against the dimensionless liquid inlet flow rate. It shows the concept of effective steam flow rate has successfully related the steam /cold water data obtained at high water inlet position to the air/water correlation.

5.1.4 5(5A) Hole and 3(3A) Hole Data

Figure 27 shows the results of 5, 5A, 3, and 3A hole experiments. Comparing with the data shown in Figure 23, one can find that:

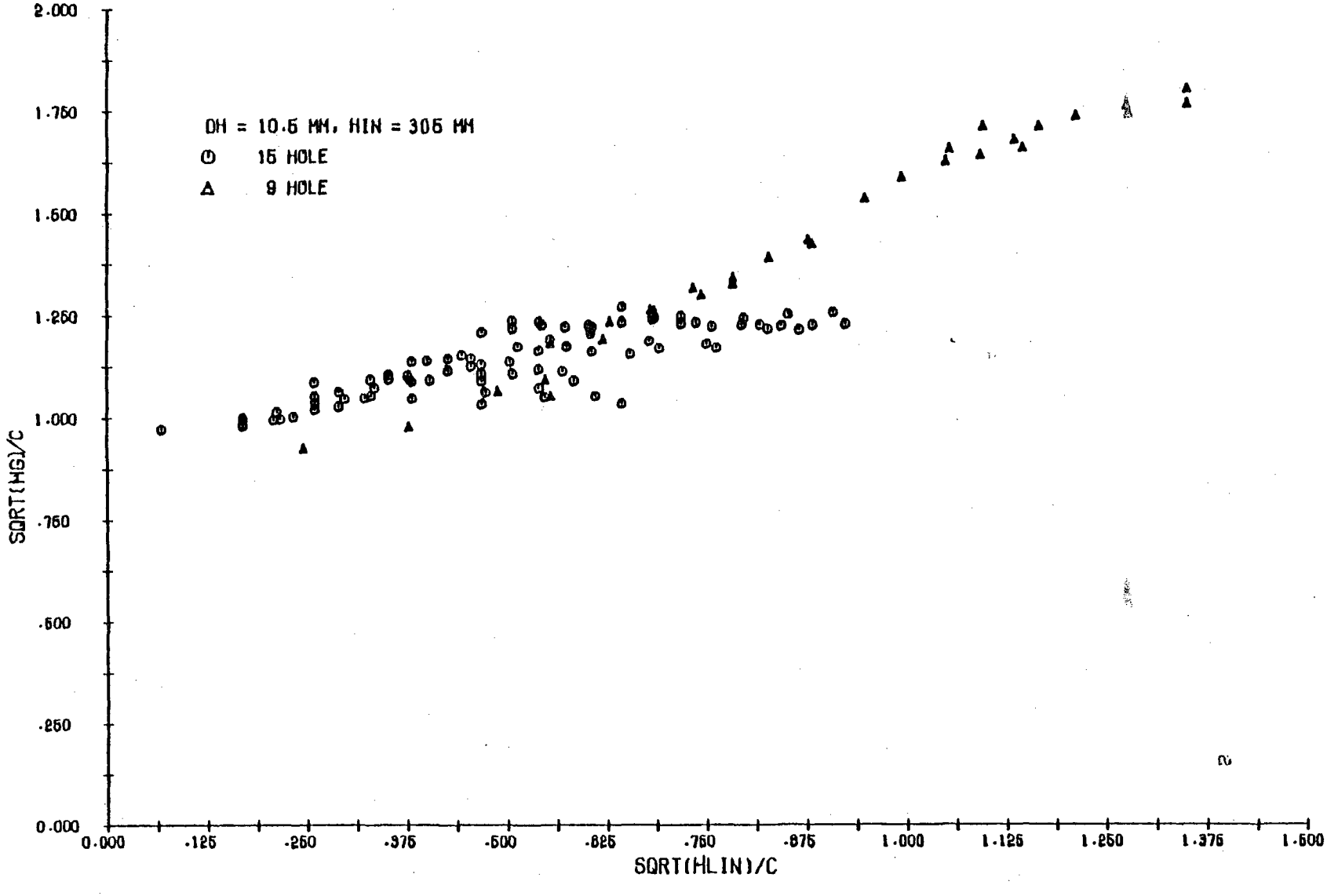

Figure 25. Dimensionless Steam and Water Inlet Flow Rate at Weep Point, 15 Holes and 9 Holes Data, h_{in} = 305 mm.

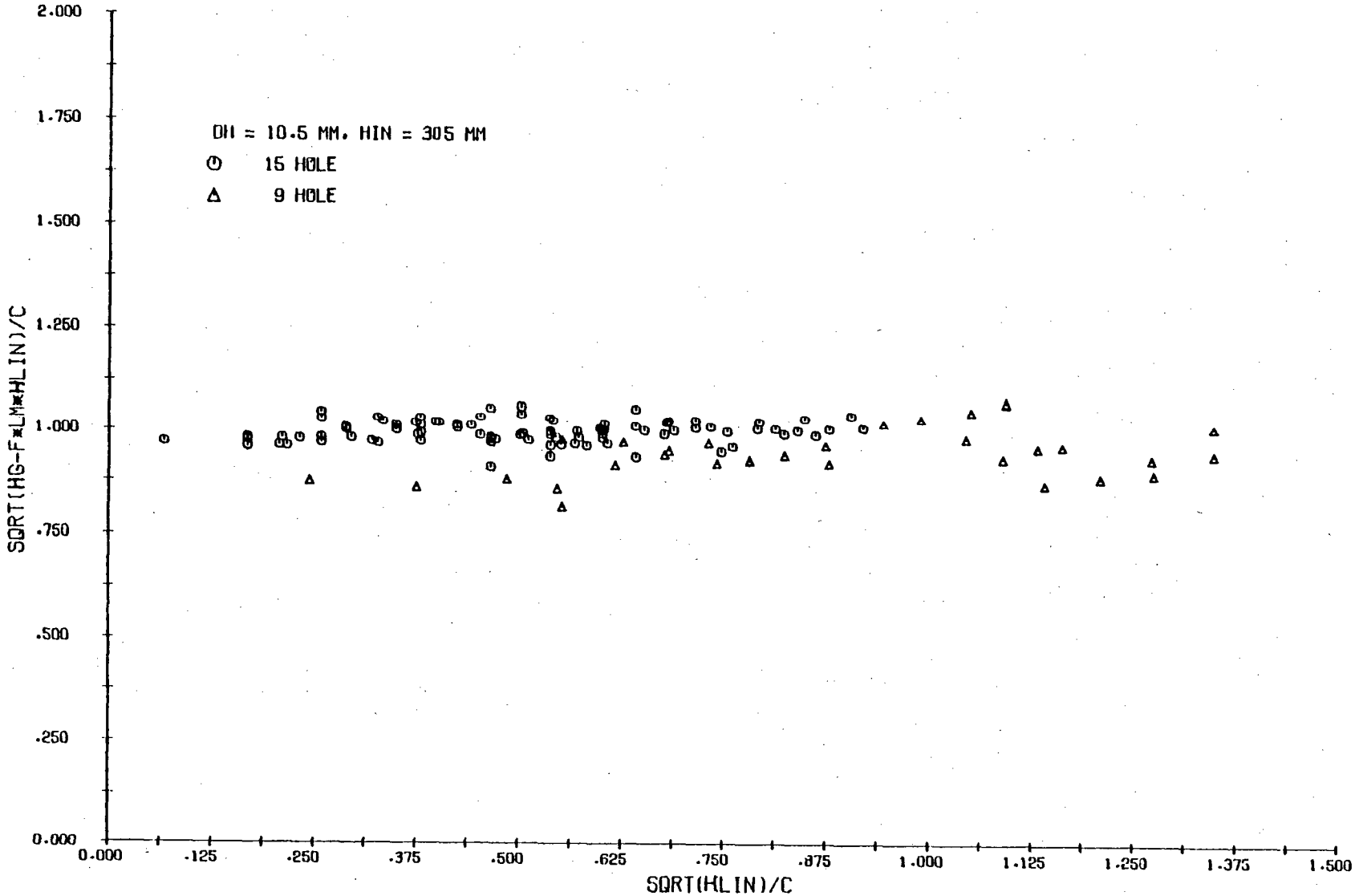

Figure 26. Condensation Effect on Weep Point Correlation, 15 Holes and 9 Holes Data, h_{in} = 305 mm.

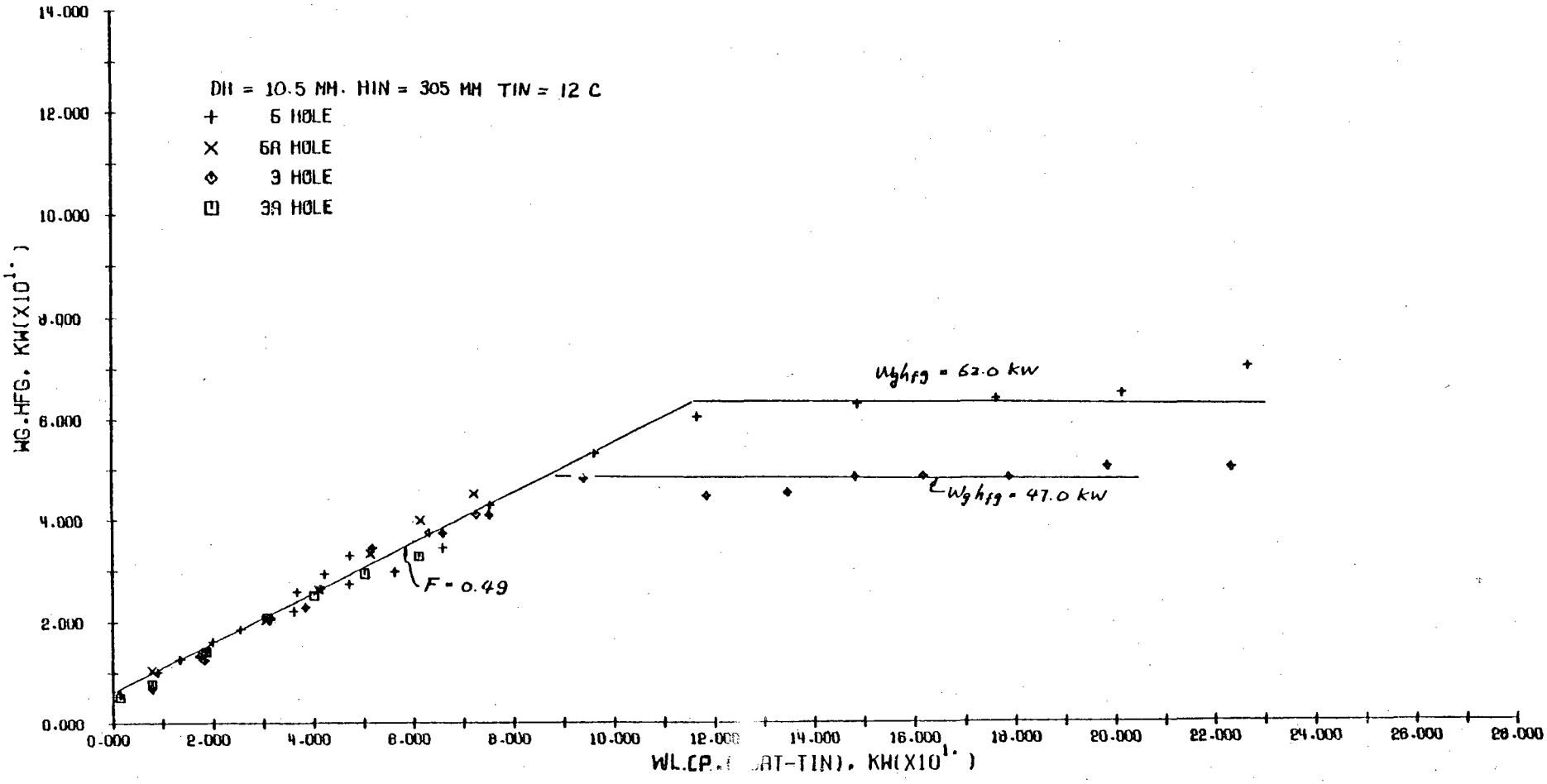

Figure 27. Comparison of the Weep Point Data of 5 Holes, 5A Holes, 3 Holes, and 3A Holes Experiment Result.

1. The mixing efficiency here(f = 0.49) is almost two times larger than that of 15 hole and 9 hole experiment.

2. The maximum steam enthalpy flux required to stop the weeping is lower than that of 15 hole and 9 hole experiment.

With the number of holes equals to or less than 5, the total hole area is less than 15% of the whole cross-section area of the channel. It can be observed that the two-phase mixture will now cover only the middle portion of the channel cross-section area, leaving the rest of the area filling by water. Water can easily reach the vicinity of the perforated plate, resulting a higher mixing efficiency of 0.49.

Since more steam will be condensed in the vicinity of the plate, the height of the two-phase mixture zone will then be decreased. This means a thicker water layer with a higher buffer effect will be builtup between the top of this zone and the overflow port. As a result, the upper limit of the degree of mixing, and hence the maximum steam enthalpy flux required to stop the weeping will be decreased. Figure 27 shows that this maximum steam enthalpy flux has a value of 62 KW for the 5 hole experiment data and a value of 47 KW for the 3 hole experiment data.

Figure 28 is the superficial steam velocity through the holes for these runs. At low water enthalpy fluxes, where the condensation effect is not dominant, the velocity through the holes is almost the same for all these plates. Once the condensation effect starts playing a role in triggering the weeping, the steam velocity of the 3 hole experiment is higher than that of the 5 hole experiment in order to maintain the same amount of total steam enthalpy flux.

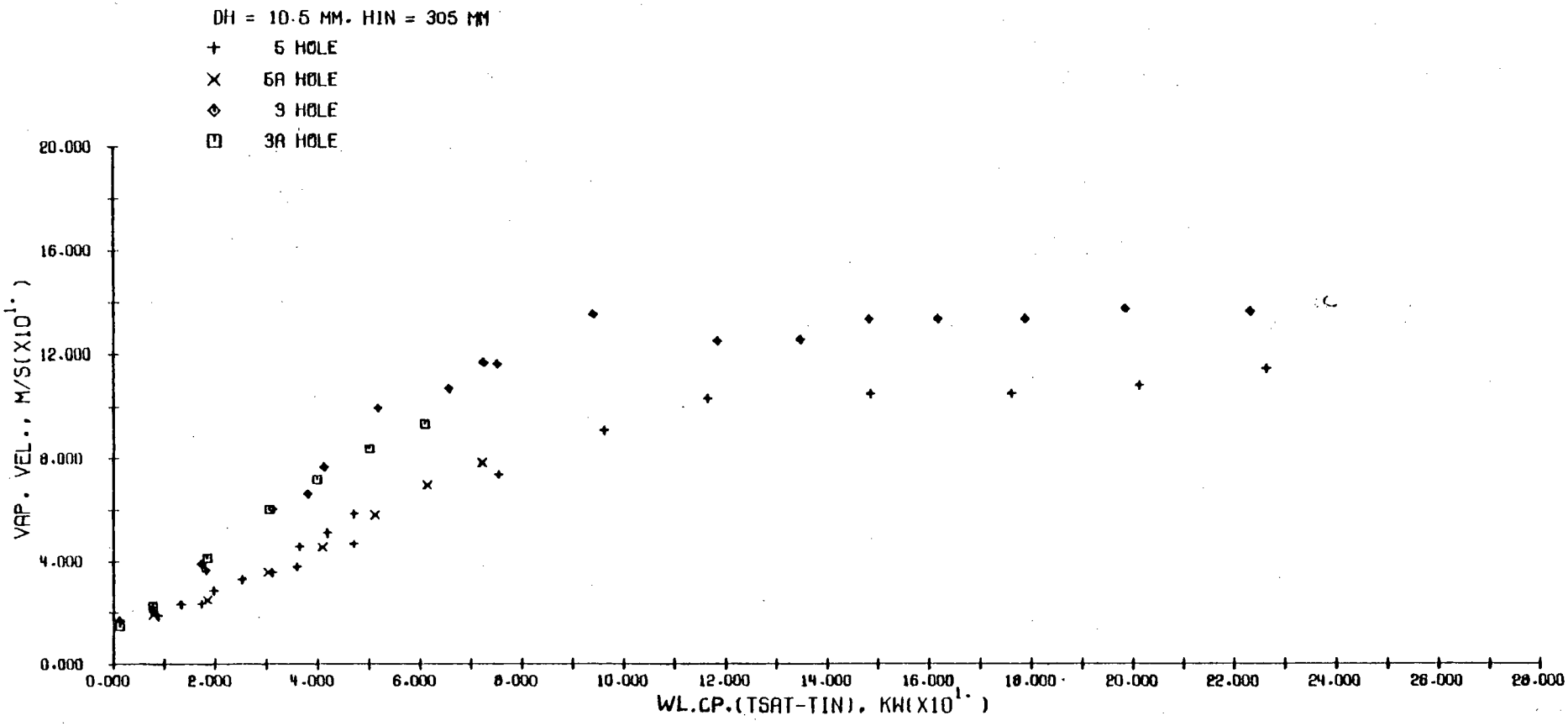

Figure 28. Comparison of Superficial Steam Velocity through Holes for 5 Holes, 5A Holes, 3 Holes, and 3A Holes Data.

Figure 29 is the same data plotted as $H_g^{*1/2}$ vs. $H_f^{*1/2}$. Again, it shows at low water flow rate the data agrees with the air/water correlation very well($H_g^{*1/2}/C = 1$).

Figure 30 then replaced the steam flow rate with the effective steam flow rate defined in equation (63). It shows that the data are still in close agreement with the air/water correlation. Therefore, one can conclude that so long as the mixing efficiency f can be determined for the particular geometry of the channel and plate, equation (55) and (56) are suitable for both steam/water and air/water weeping data correlation.

5.2 Water Inlet Spray at the Plate

As the water inlet spray been positioned right above the plate, essentially all the inlet water will have the chance to contact with the steam before leaving the channel, and huge condensation rate will occur in the vicinity of the plate. As a result, the weeping phenomenon at this operating condition can be significantly different from that of a high liquid inlet position experiment.

With the water inlet spray height kept at 5 mm, Figure 31 shows the 15 hole weep point data obtained at six different water inlet temperatures. Comparing with the data obtained at high water spray experiment, two distinct phenomena are shown by the data point of 12 ^{o}C(285 K) experiment:

1. In the region $R_T > 1$, the oscillatory weep point boundary is close to the thermodynamic boundary $R_T = 1$.

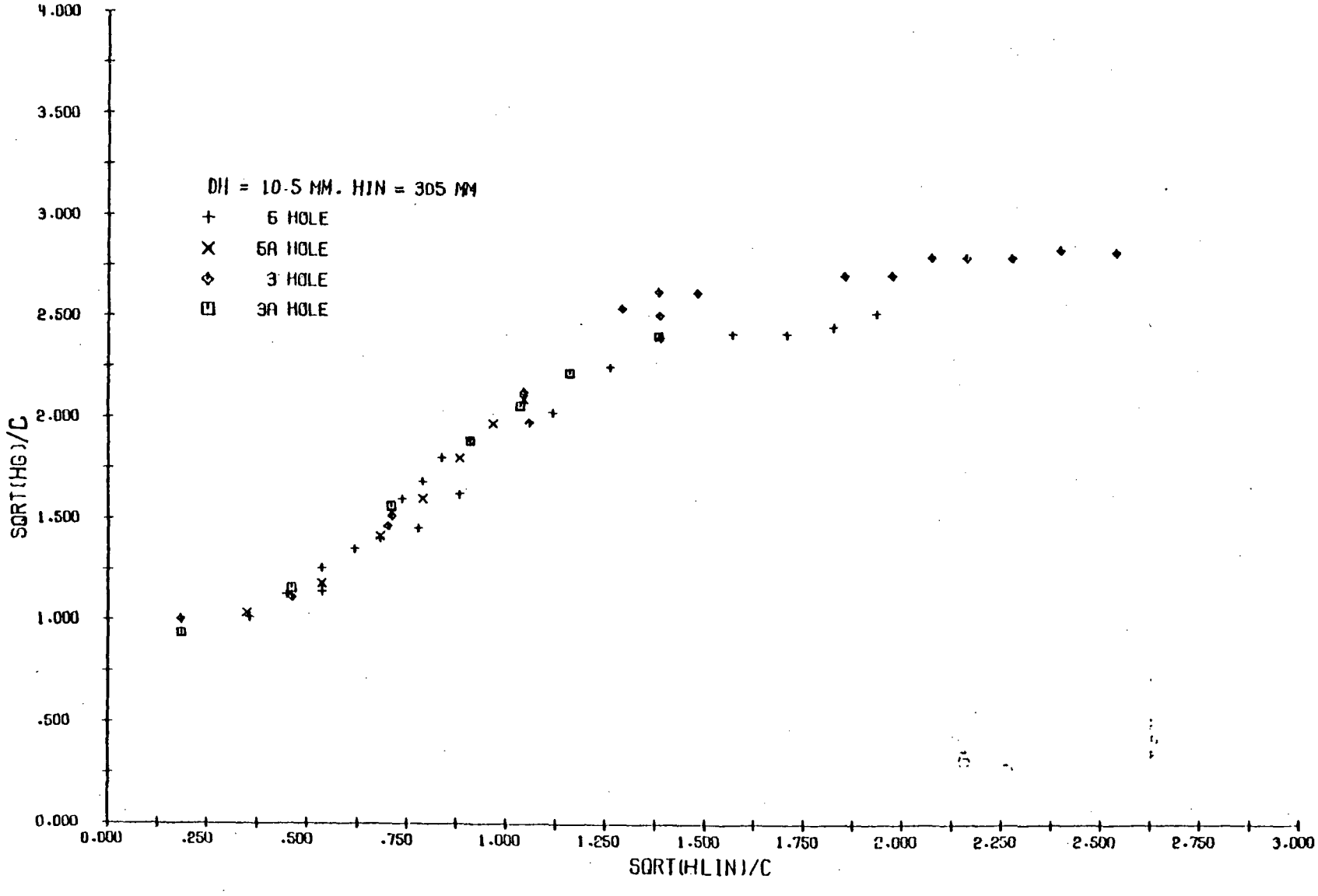

Figure 29. Dimensionless Steam and Water Inlet Flow Rate at Weep Point, 5 Holes, 5A Holes, 3 Holes, and 3A Holes Data, h_{in} = 305 mm.

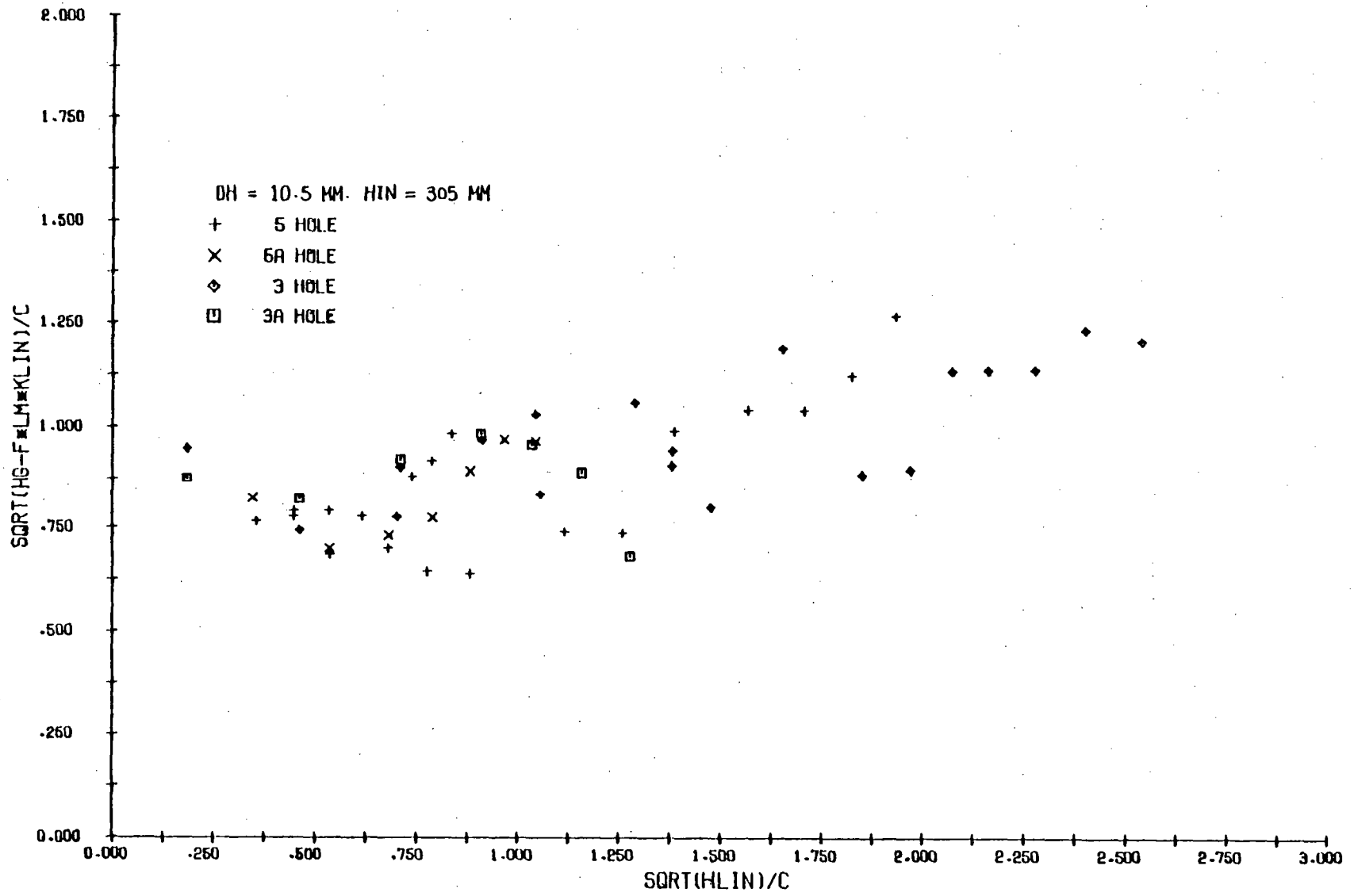

Figure 30. Condensation Effect on Weep Point Correlation, 5 Holes, 5A Holes, 3 Holes, and 3A Holes Data, h_{in} = 305 mm.

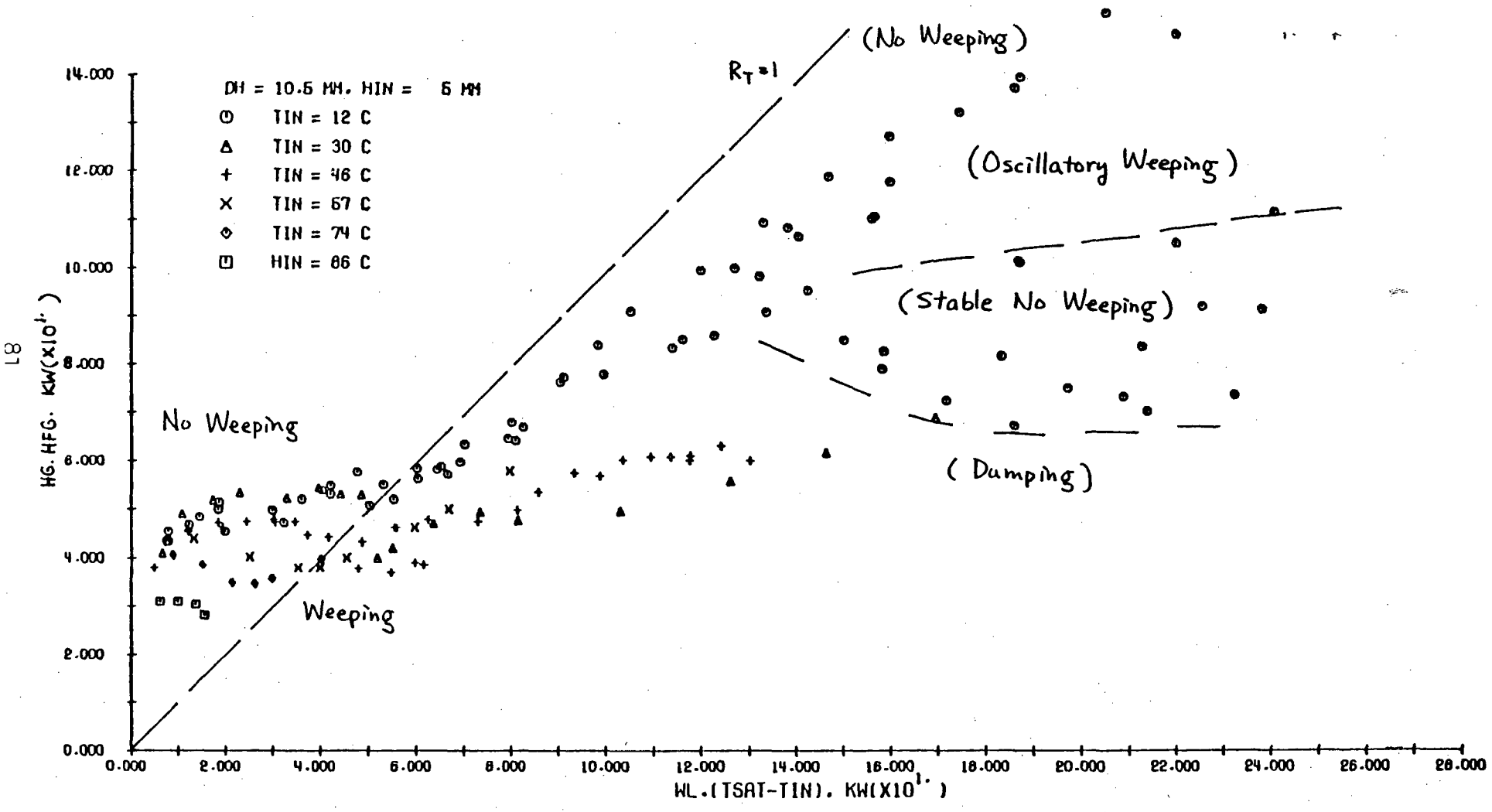

Figure 31. 15 Hole Weep Point Data Obtained at Low Water Inlet Position

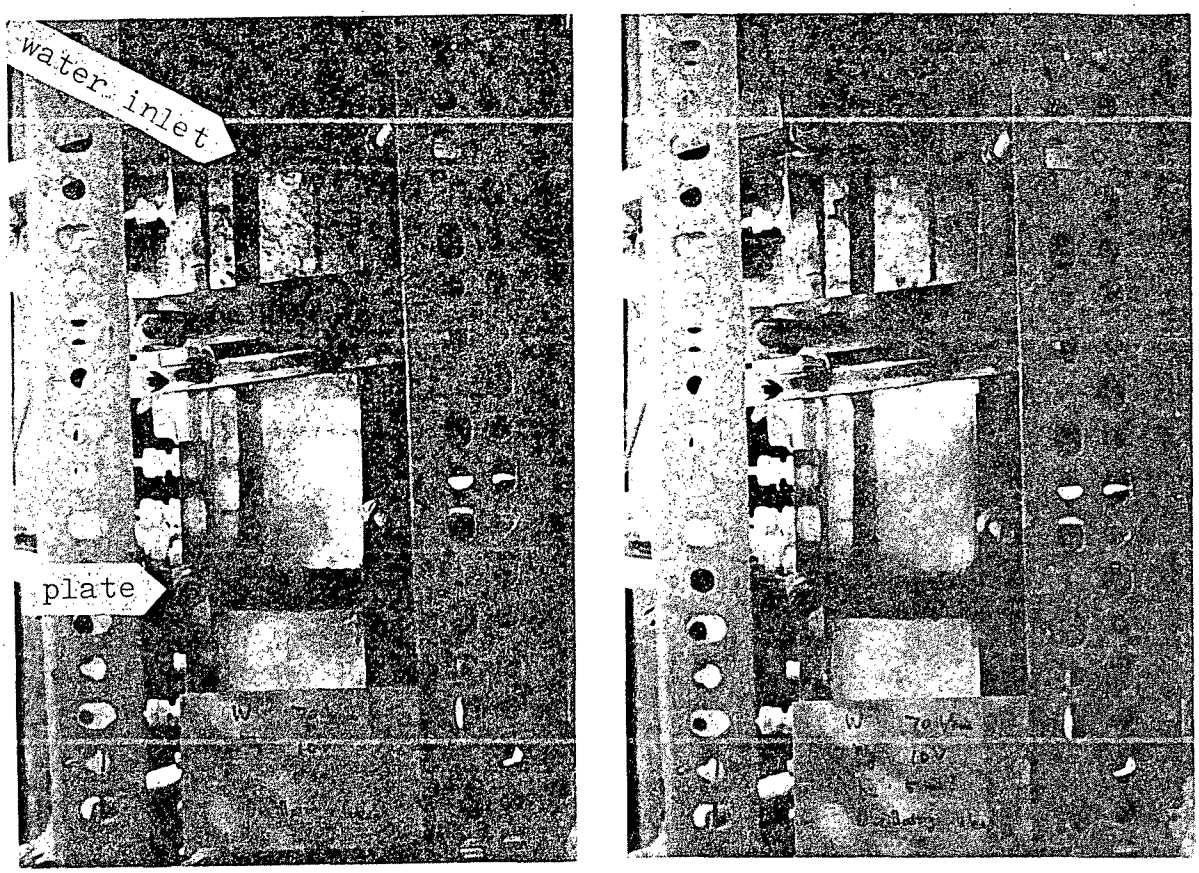

W_f = 0.53 kg/s T_f = 285 K

W_g = 0.12 kg/s T_f = 413 K

Figure 32. Some Pictures of Oscillatory Weeping.

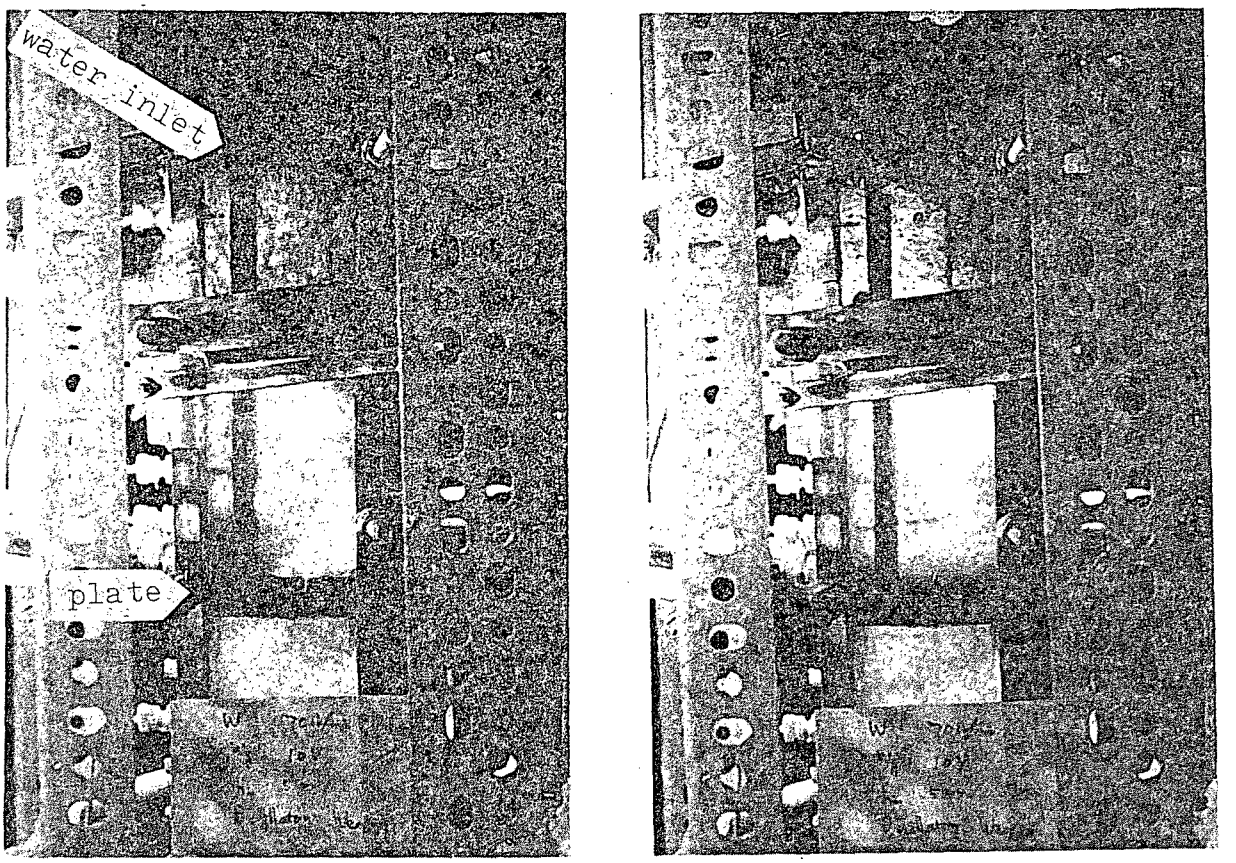

Figure 32. (Continued)

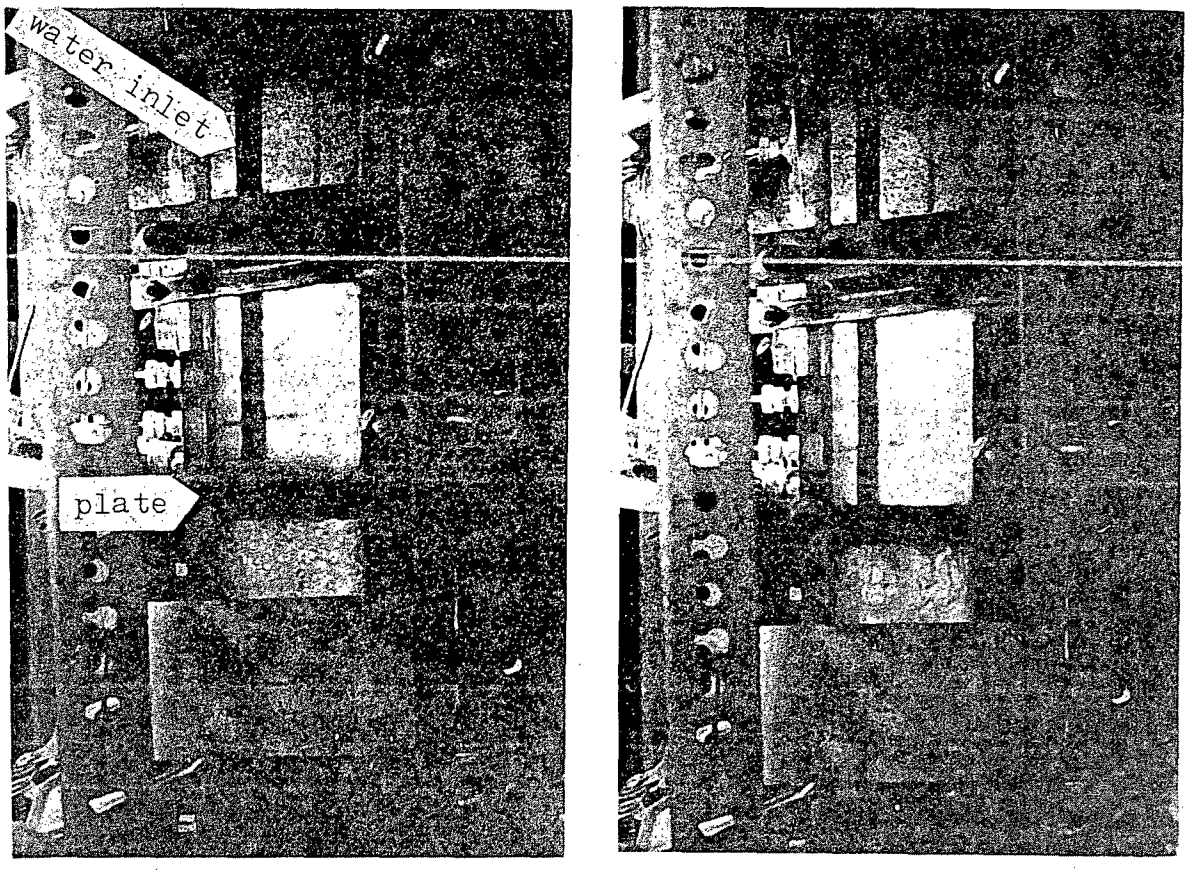

W_f = 0.53 kg/s. T_f = 285 K

W_g = 0.072 kg/s T_g = 413 K

Figure 33. Some Pictures of Stable No Weeping.

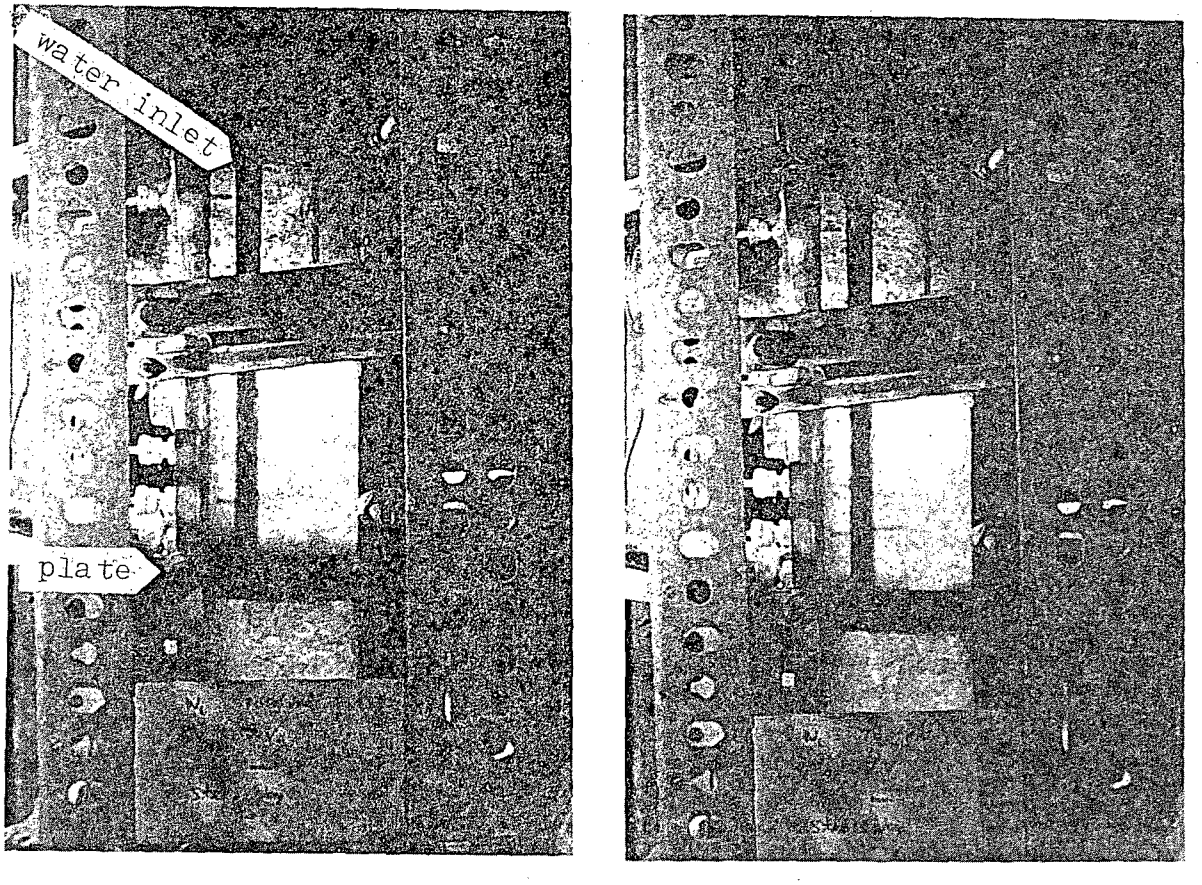

Figure 33. (continued)

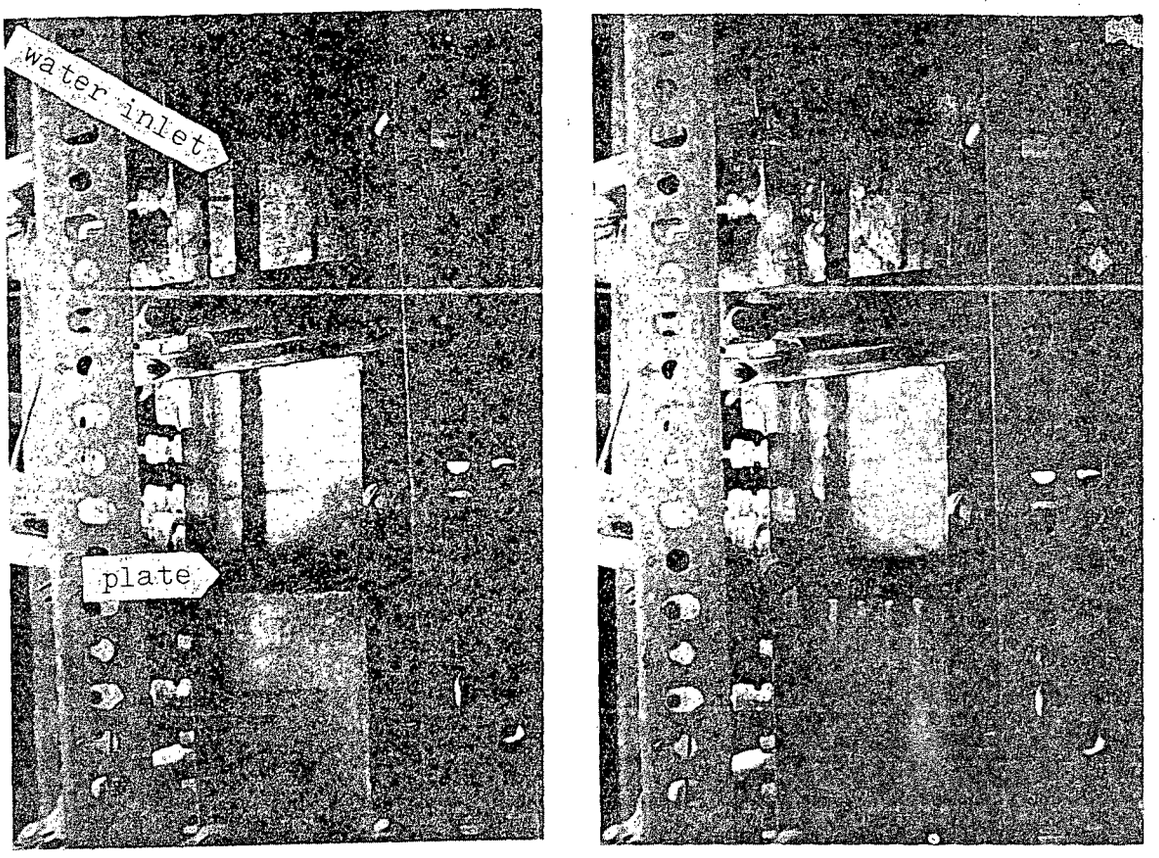

before the Dumping

at the Dumping

Figure 34. Some pictures of Total Dumping

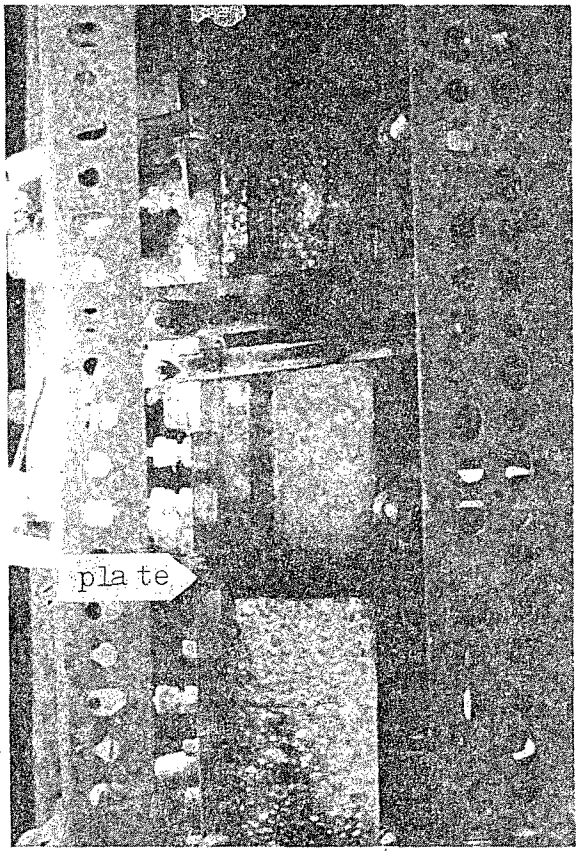

Figure 35. A Picture after the Total Dumping

2. A stable no weeping region is observed when the steam enthalpy flux is decreased from the oscillatory weeping. Further decreaseing the steam flow rate from the stable no weeping region will cause total water dumping.

Figure 32 shows some pictures taken at the oscillatory weeping condition. Severe pressure fluctuation is observed. As shown in these pictures, the steam/water interface is quite unstable, and the weeping is accompanied with the collapse of the steam region above the plate.

Figure 33 shows some pictures taken at the stable no weeping condition. All the steam is condensed at the vicinitiy of the plate, leaving a clear layer of liquid between the plate and the overflow port. Except for high frequency noise, no pressure fluctuation was observed in this region.

Further decreaseing the steam flow rate will cause total dumping, which is shown by some pictures taken before, at, and after the dumping. The clear water pool accumulated in the stable no weeping condition now all dumped through the plate(Figure 34,35).

The other data in Figure 31 are obtained at some higher temperatures. The whole phenomenon discussed above disappeared, and the hydrodynamic effect seems to be the dominant factor in this operating condition. Presently, no correlation has been obtained for the subcooling effect in this case.

Figure 36 shows the weep point data collected for different plates with the water inlet temperature at 12 ^{o}C and water inlet height of 5 mm. Two common features are observed among these data:

1. Starting from the $R_T < 1$ region(the hydrodynamic control

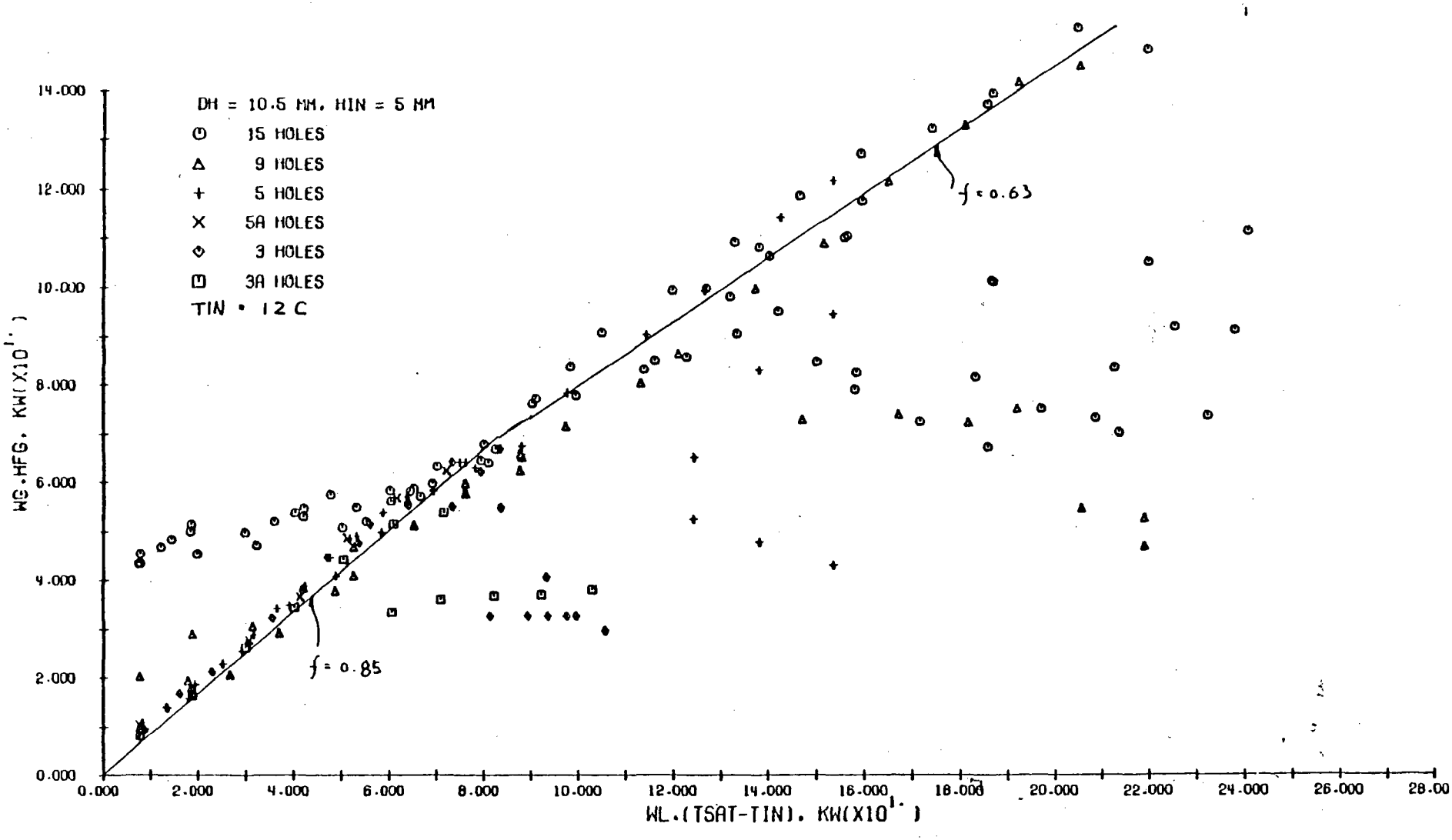

Figure 36. Weep Point Data Taken at T_{in} = 12 ^{o}C and h_{in} = 5 mm.

region) where the weeping is continuous, the oscillatory weeping will occur once the thermodynamic boundary is reached. After passing the $R_T = 1$ line, the oscillatory weep point boundary is close to the thermodynamic boundary $R_T = 1$. The mixing efficiency(f) for 3 hole and 5 hole data is 0.85, the mixing efficiency(f) for 9 hole and 15 hole data is 0.63.

2. A stable no weeping have been observed for all the experiments with different plates.

By assuming the steam is condensed in a hemispherical steam jet with its diameter equal to the diameter of the hole, the condensation heat transfer coefficients in this stable no weeping condition can be estimated with the aid of the thermocouples reading at the vicinity of the plate:

Therefore, for 15 hole data, the steam enthalpy flux at the begining of the stable no weeping condition is around 9.6 KW, the temperature at the vicinity of the plate is 340 K, and the heat transfer area per hole is

$$A_b = 0.5 \quad D_h^2 = 1.73 \times 10^{-4} \ m^2 \tag{66}$$

$$h' = Q/A_b \Delta T = 96000/(15 \times 1.73 \times 10^{-4})(373-340)$$
$$= 1.12 \times 10^6 W/m^2 \ K \tag{67}$$

For 9 hole,

$$h' = 74000/(9 \times 1.73 \times 10^{-4})(373-337) = 1.32 \times 10^6 W/m^2 \ K \tag{68}$$

For 5 hole,

$$h' = 52000\ W/(5x1.73x10^{-4}\ m^2)(373-339) = 1.76x10^6\ W/m^2K \quad (69)$$

and for 3 hole

$$h' = 33000\ W/(3x1.73x10^{-4}\ m^2)(373-333)$$
$$= 1.58 \times 10^6\ W/m^2\ K \quad (70)$$

All these condensation heat transfer coefficients are of the same order of magnitude. As a result of this high rate of condensation right above the plate, the possibility of the collapse of steam in the liquid pool and the oscillatory weeping along with this collapse are totaly eliminated.

Decreasing the steam enthalpy flux below the stable no weeping region will allow some cold water to penetrate through the holes of the plate. This cold water will condense some steam before it can reach the plate; as a result, more cold water will be drawn down through the plate, triggering total dumping.

5.3 Effect of Liquid Inlet Spray Position

Figure 37 and 38 are the 15 hole and 9 hole data taken at different water inlet spray position. It shows that the weep point data obtained at h_{in} = 305 and 710 mm(water spray above the pool) are the same. The data taken at h_{in} = 102 mm lie between the data of h_{in} = 5 mm and h_{in} = 305 mm.

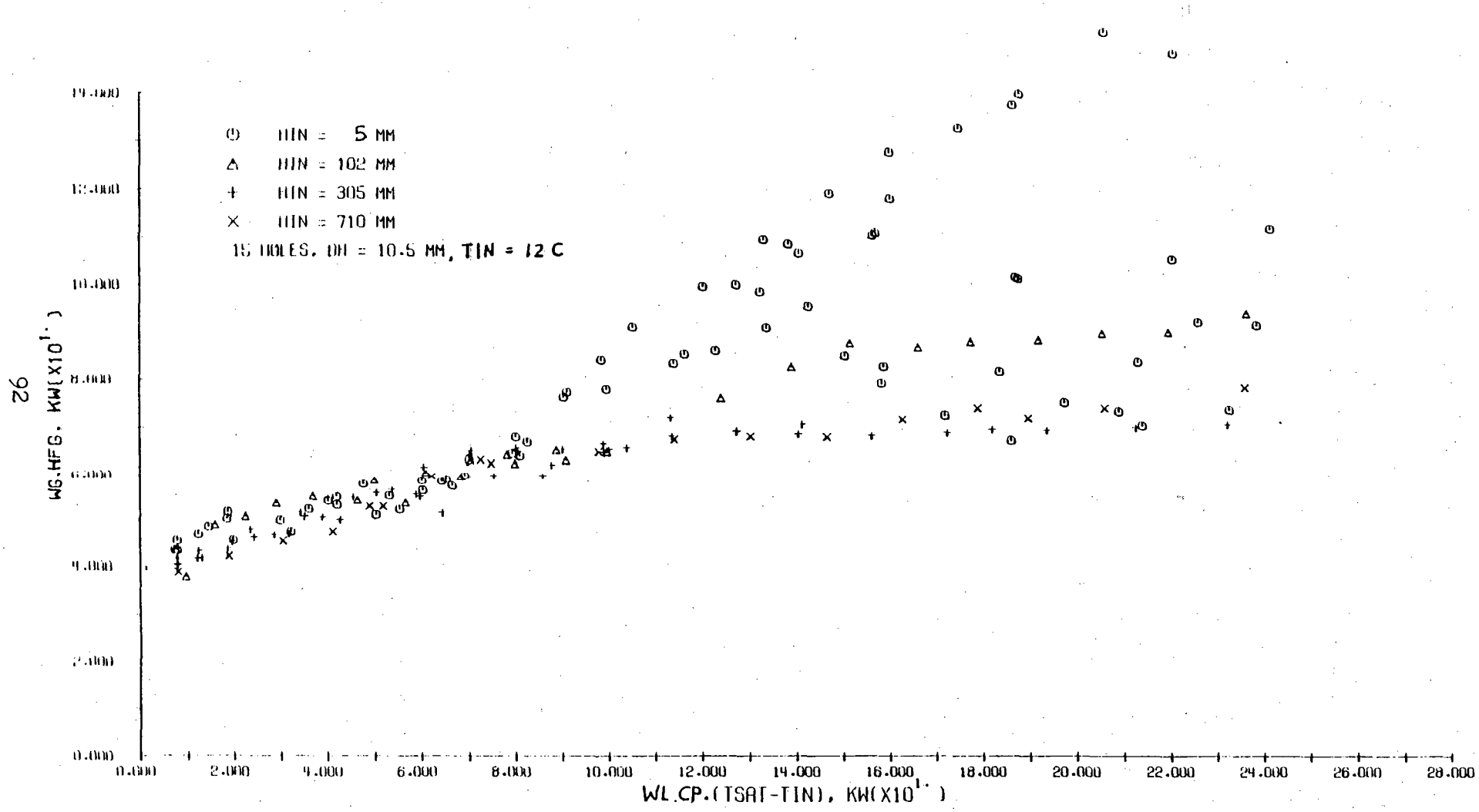

Figure 37. Effect of Liquid Inlet Spray Nozzle Position on Weep Point, 15 Holes Data.

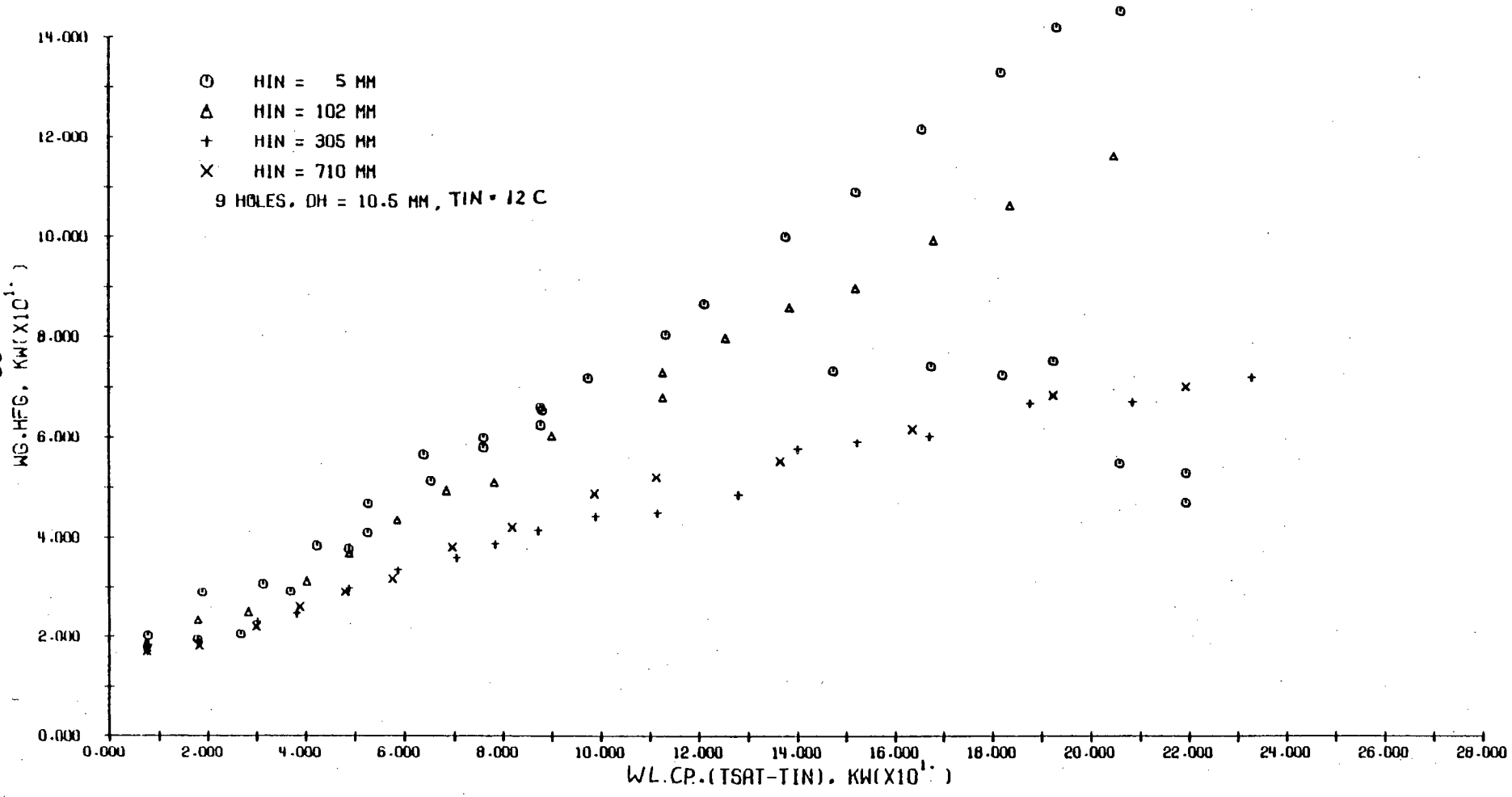

Figure 38. Effect of Liquid Inlet Spray Nozzle Position on Weep Point, 9 Holes Data.

6. Conclusions and Suggestions

Based on the information collected in the present study, the following conclusions can be made:

a. By introducing the new dimensionless flow rate scaling H^*, which represents a smooth transition between J^* and K^* scaling, the air/water data obtained at 7 perforated plates with different numbers and diameters of holes can be correlated by a conventional flooding equation in the form of

$$H_g^{*1/2} + H_f^{*1/2} = C \qquad (55)$$

where $H^*_{f,g} = [\rho_{f,g}/gw(\rho_f - \rho_g)]^{1/2} j_{f,g}$ (50)

and w is given in equation (51) and (52), the coefficient C is given in equation (56).

b. The liquid spray position, liquid inlet flow rate, soft volume and the head of liquid pool above the plate do not have any discernible effect on the rate of weeping in the present air/water experiment.

c. The steam/cold water weep point data which were obtained at high liquid inlet spray position can be related to equation (55) by introducing an effective steam flow rate, which is defined by equation (63).

d. Two types of weeping were observed when the the channel was running in high liquid spray experiment: For low water flow rate and subcooling the weeping at the weep point is smooth and continuous; As the water flow rate or subcooling becomes high, oscillatory or intermittent weeping was observed.

e. For water inlet near the plate, a stable no weeping region was observed at high water flow and subcooling. In this region, all the steam was condensed right above the plate, leaving a clear layer of liquid above a bubbly region. Increasing the steam flow rate causes oscillatory weeping, while decreasing the steam flow below this region will result in total dumping.

Several suggestions are made for further investigations:

a. The validity of H^* scaling, which is highly dependent on the construction of the α function, should be checked over a larger parameter range, and larger scale.

b. The void fraction of the two-phase mixture above the plate should be checked by pressure measurenent.

c. The mixing efficiency, which could be a function of liquid spray position, method of liquid injection, perforation ratio of the plate, and channel geometry, should be further studied.

7. Reference:

(1). Sherwood, T. K., et al., Ind. Eng. Chem. 30, pp765 (1938).

(2). Lobo, W. E., et al., Trans. ALCHE, 41, pp693 (1945).

(3). Bulletin HY-30, Hy-Park Packings, Norton Co., (1977).

(4). Sherwood, T. K., et al, "Mass Transfer", pp599-603 McGraw-Hill, Inc., New York (1975).

(5). Tien, C. L. and C. P. Liu, "Survey on Vertical Two-Phase Countercurrent Flooding" NP-984 (1979).

(6). Wallis, G. B., et al., "Analysis of ECC Delivery", CREARE TN-231 (1976).

(7). Ueda, T. and S. Suzuki, "Behaviour of Liquid Films and Flooding in Counter-Current Two-Phase Flow. Part 2. Flow in Annuli and Rod Bundles", Int. J. Multiphase Flow, 4, pp157-170 (1978).

(8). Jones, D. D., "Subcooled Counter-Current Flow Limiting Characteristics of the Upper Region of a BWR Fuel Bundle", General Electric Company, Nuclear Systems Products Division, BD/ECC Program, NEDG-NUREG-23549 (1977).

(9). Mayfield, F. D., et al., "Perforated-Plate Distillation Columns", Ind. Eng. Chem., 44 9, pp2238-49, Sept. (1952).

(10). Arnold, D. S., et al., "Performance of Perforated-Plate Distillation Columns", Chem. Eng. Prog., 48 12, pp633-42, (1952).

(11). Zenz, F. A., "How to Calculate Capacities of Perforated-Plates", Petroleum Refiner, 33 2, pp99-102, Feb. (1954).

(12). Hunt, C. D., et al., "Capacity Factors in the Performance of Perforated-Plate Columns", AICHE J., 1 4, pp441-51, (1955).

(13). Jones, P. D., and Ma~~thew~~ Van Winkle, "Variables in Perforated-Plate Column Efficiency and Pressure Drop", Inc. Eng. Chem., 49 2, pp232-38, (1957).

(14). Leibson I., et al., "Design of Perforated Plate Fractionating Towers", Chem. Eng. Prog., 53 3, pp127-33, (1957).

(15). Block, J. A., "Condensation-Driven Fluid Motion", EPRI Workshop on Basic Two-Phase Flow Modeling, Tampa, Florida, March 1, (1979).

(16). Biddulph, M. W., and D. J. Stephens, "Oscillating Behavior on Distillation Trays", AICHE J., 20 1, pp60-66 (1974).

(17). Hughmark, G. A., et al., "How to Design Perforated Trays", petroleum Refiner, 37 2, pp127-33,(1957).

(18). Huang, C. J., et al., "Design of Perforated Plate Fractionating Towers", Chem. Eng. Prog., 53 3, pp127m-132m, (1957).

(19). Eduljee, H. E., "Design of Sieve-Type Distillation Plates", British Chem. Engineering, pp320-26, June (1959).

(20). Davies, J. A., "What to Consider in Your Fractionator Tray Design, Part 2 Perforated Trays", Petro/Chem. Engineer, pp250-3, Nov. (1961).

(21). Smith, B. D., W. L. Bolles and J. R. Fair, "Design of Equilibrium Stage Process", pp548, McGraw-Hill Book Company, New York (1963).

(22). Perry, R. H. and C. H. Chilton, "Chemical Engineers' Hand book", 5th edition, pp18-7, McGraw-Hill Book Company, New York (1973).

(23). McCann, D. J. and R. G. H. Prince, "Bubble Formation and

Weeping At a Submerged Orifice", Chem. Eng. Science, 24, pp801-814 (1969).

(24). Showkry E. and V. Kolar, "On the Hydrodynamcis of Sieve Plates Without Downcomers", The Chem. Eng. J., 8, pp41-51 (1974).

(25). Wallis, G. B., "One-Dimensional Two-Phase Flow", pp343-344, McGraw-Hill, Inc., New York (1969).

(26). Pushkina, O. L. and Y. L. Sorokin, "Breakdown of Liquid Film Motion in Vertical Tubes", Heat Transfer-Soviet Research, 1 5, pp56 (1969).

(27). Sun, K. H. and R. T. Fernandez, "Counter-Current Flow Limitation Correlation for BWR Bundles During LOCA", ANS Transaction, 27, pp605 (1977).

(28). Sun, K. H., "Flooding Correlations for BWR Bundle Upper Tieplates and Bottom Side-Entry Orifices", Second Multi-Phase Flow and Heat Transfer Symposium-Workshop, Miami Beach, Florida, April (1979).

(29). Bharathan, D., "Air-Water Countercurrent Annular Flow in Vertical Tubes", EPRI Report NP-786 (1978).

(30). Shires, G. L. and A. R. Pickering, "The Flooding Phenomena in Countercurrent Two-Phase Flow", Symposium on Two Phase Flow, ppB501-B538, Exeter, (1965).

(31). Block, J. A. and Crowley, C. J., "Effects of Steam Up-Flow and Superheated Walls on ECC Delivery in a Simulated Multiloop PWR Geometry", Creare Technical Note TN-210, May (1975).

(32). Block, J. A. and Crowley, C. J., "Effects of Cold Leg Steam and Flow Baffles on ECC Delivery in a Simulated Multiloop PWR Geometry with Steam Upflow", Creare Tech-Nical Note TN-214, July (1975).

(33). Crowley, C. J. and Block, J. A., "ECC Delivery Study-Experimental Results and Discussion", Creare Technical Note TN-217, October (1975).

(34). Cudnik, R. A., et al., "Steam-Water Mixing and System Hydrodynamics Program, Task 4", NUREG/CR-0147, BMI-2003, Battelle Columbus Laboratories (1978).*

(35). Block, J. A. and H. Rothe, "Progress on ECC By Pass Scaling", Creare TN-272, NUREG/CR-0048, R-2 (1977).*

(36). Garbiener, W. A., et al., "Steam-Water Mixing and System Hydrodynamics Program, Task 4", NUREG/CR-0034, BMI-1993, Battelle Columbus Laboratories (1977).*

(37). Richter, H. J. and S. L. Murphy, "Effect of Scale on Two-Phase Countercurrent Flow Flooding in Annuli, Final Report", Thayer School of Engineering, Dartmouth College, Hanover, N. H., NUREG/CR-0822 (1979).**

(38). Wallis, G. B., "One-Dimensional Two-Phase Flow", pp288, McGraw-Hill, Inc., New York (1969).

(39). Wallis, G. B. and S. Makkenchery, "The Hanging Film Phenomena in Vertical Annular Two-Phase Flow", ASME Journal of Fluids Engineering, pp297-298, Sept. (1974).

(40). Collier, R. P., et al., "Steam-Water Mixing and System Hydrodynamics Program, Quarterly Progress Reprot, Jan.-Mar. 1979", NUREG/ CR-0897, BMI-2029, Battelle Columbus Laboratories (1979).**

(41). Tobin, R., "CCFL Test Results, Phasel-TLTA 7x7 Bundle", General Electric Company, Nuclear System Products Divison, BD/ECC Program, GEAP-21304-5 (1977).

(42). Naitoh, M., K. Chino and R. Kawabe, "Restrictive Effect of Ascending Steam on Falling Water During Top Spray Emergency Core Cooling", J. of Nuclear Science and Technology, 15 11, pp806 (1978).

(43). Jacoby J. K., et. al., "Final Report on 3-D Experiment Project Air/Water Upper Plenum Experiments", USNRC, 3DP-TR-001, Nov. (1978).

(44). Jones, D. D., "Test Report TLTA Components CCFL Tests", General Electric Company, NEDG-NUREG-23732 (1977).

(45). Graham, G., "Summary of Recent Thayer School Annulus Penetration Results; Memorandum", Thayer School of Engineering, Dartmouth College, May 20 (1975).

(46). Cudnik, R. A. and R. O. Wooton, "Penetration of Injected ECC Water through the Downcomer Annulus in the Presence of Reverse Core Steam Flow", Battelle Columbus Laboratories Report, November (1974).

(47) Wallis, G. B., J. T. Kuo, "The Behavior of Gas-Liquid Interface in Vertical Tubes", Int. J. of Multiphase Flow, 2 521 (1976).

(48) Cudnik, R. A. et. al., "Flooding of Counter-Current Steam-

Water Flow in An Annulus", Topics in Two-Phase Heat Transfer and Flow, pp107-113, ASME(1978).

(49). Block, J. A., "Condensation-Driven Fluid Motions", Creare Incorporated, Paper submitted to the International Journal of Multiphase Flow(1979).

(50). Duffey, R. B., et. al., "The Condensation Induced Transition from Bubbling to Liquid Downflow in a Turbulent Two -Phase Pool", Paper submitted to the 18th National Heat Transfer Conference, SanDiego, (1979).

(51). Bankoff, S. G., et. al., "Condensation Rates in Steam-Water Mixing", Annual Progress Report, Northwestern University, Evanston, Ill., Feb., (1979).

(52). Jacoby, J. K., et. al., "Quick Look Report on KUU Support Column Air-Water Experiment", EG&G Report, RDW-23-78 (1978).

*Available for purchase from the National Technical Information Service, Springfield, VA 22161.
**Available for purchase from the NRC/GPO Sales Program, U.S. Nuclear Regulatory Commission, Washington, DC 20555, and the National Technical Information Service, Springfield, VA 22161.

Appendix I. Computer Program List and the Air/Water Reduced Data.

The input of this program includes: IP,WF,WG, and PG. where

IP = 1, 15 hole data
2, 9 hole data
3, 5(5A) hole data
4, 3(3A) hole data
5, 40 hole data
6, 2 hole data

WF : liquid mass flow rate, lbs/sec.
WG : air rotameter reading, SCFM.
PG : air rotameter pressure gauge reading, psig.

Depending the selection of DH(characteristic length), the program can calculate the dimensionless velocity in the form of J^*, K^*, or H^*.

The output of the program includes:

JG, JF : superficial gas and liquid velocity through holes, (m/s).
JGS, JFS : dimensionless velocity, either J^*, K^*, or H^*. the data shown are in H^*.
JGS5, JFS5 : square root of the dimensionless velocity.
C : coefficient C in the flooding equation.

The data will also be plotted as JGS5 vs. JFS5.

```
      PROGRAM JFGS(INPUT,OUTPUT,TAPE 99)
      REAL JG,JF,JGS,JFS,JGSA,JFSA
      DIMENSION A(6),AS(6),AC(6),AL(6)
      DIMENSION E(65),B(65),C(50),D(50),ALS(8)
      REAL JGS1(50),JFS1(50),JGS11(50),JFS11(50),JGS2(50),JFS2(50),JGS22
     A(50),JFS22(50),JGS3(50),JFS3(50),JGS33(50),JFS33(50),JGS4(50),JFS4
     B(50),JGS44(50),JFS44(50)
      REAL JGS5(50),JFS5(50),JGS55(50),JFS55(50),JGS6(50),JFS6(50),
     CJGS66(50),JFS66(50),JGS7(50),JFS7(50),JGS77(50),JFS77(50)
      DATA GC,CG,DL,DH/32.2,.0744,62.4,.00894/
      DATA (A(I),I=1,6)/.0133807,.0083884,.0046602,.0027361,.0076699,
     A.0138058/
      DATA (AL(I),I=1,6)/181.50,108.7,60.32,36.13,146.42,65.88/
      DATA(AS(I),I=1,6)/.413,.413,.413,.413,.1875,1.125/
      DATA (ALS(I),I=1,6)/181.6,108.7,60.3,36.1,146.4,65.9/
      IR=0
    1 I=0
      PRINT 19
      IP=IR+1
      READ*,IP
    2 READ*,WF,WG,PG
      IF(WF.LE.-2.) GO TO 300
      IF(WF.LE.-.5) GO TO 5
      I=I+1
      PLG=ALOG(PG)
      FG=-0.0508859721+.02841336269*PLG-0.05218174597*PLG*PLG
      FG=EXP(FG)
      JG=(WG/FG)/60./A(IP)
   12 JGS=(DG/(GC*DH*(DL-DG)))**.5*JG
      JF=WF/DL/A(IP)
      JFS=(DL/(GC*DH*(DL-DG)))**.5*JF
       W1=AS(IP)/.787*6.2832*A(IP)/.03302
      ALF=TANH(W1)
      CK=(AS(IP)/12./DH)**((1.-ALF)/4.)
      CS=CK*(1.07+4.33E-3*ALS(IP))
      JFSA=SQRT(JFS)/CS
      JGSA=SQRT(JGS)/CS
      IF(IR.EQ.1) GO TO 101
      IF(IR.EQ.2) GO TO 111
      IF(IR.EQ.3) GO TO 121
      IF(IR.EQ.4) GO TO 131
      IF(IR.EQ.5) GO TO 141
      IF(IR.EQ.6) GO TO 151
      IF(IP.EQ.7) GO TO 161
  141 JGS5(I)=JGS
      JFS5(I)=JFS
      JGS55(I)=JGSA
      JFS55(I)=JFSA
      GO TO 200
  151 JGS6(I)=JGS
      JFS6(I)=JFS
      JGS66(I)=JGSA
      JFS66(I)=JFSA
      GO TO 200
  161 JGS7(I)=JGS
      JFS7(I)=JFS
      JGS77(I)=JGSA
      JFS77(I)=JFSA
      GO TO 200
  131 JGS4(I)=JGS
      JFS4(I)=JFS
      JGS44(I)=JGSA
      JFS44(I)=JFSA
      GO TO 200
  101 JGS1(I)=JGS
      JFS1(I)=JFS
      JGS11(I)=JGSA
      JFS11(I)=JFSA
      GO TO 200
  111 JGS2(I)=JGS
      JFS2(I)=JFS
      JGS22(I)=JGSA
      JFS22(I)=JFSA
      GO TO 200
  121 JGS3(I)=JGS
      JFS3(I)=JFS
      JGS33(I)=JGSA
      JFS33(I)=JFSA
  200 JG=JG/3.28
```

```
      JF=JF/3.28
      Z=JGSA+JFSA
      PRINT 20,JG,JGS,JGSA,JF,JFS,JFSA,Z
   20 FORMAT(18X,7F12.3,/)
   19 FORMAT(22X,'JG,M/S          JGS            JGS5           JF,M/S        JFS
     C           JFS5              C                 ',//)
      GO TO 2
    5 IF(IR.EQ.1) GO TO 71
      IF(IR.EQ.2) GO TO 72
      IF(IR.EQ.3) GO TO 73
      IF(IR.EQ.4) GO TO 74
      IF(IR.EQ.5) GO TO 75
      IF(IR.EQ.6) GO TO 76
      IF(IR.EQ.7) GO TO 77
   71 I1=I+1
      IA=I
      I2=I+2
      JFS11(I1)=0.
      JGS11(I1)=0.
      JFS11(I2)=.125
      JGS11(I2)=.125
      GO TO 1
   72 I1=I+1
      IB=I
      I2=I+2
      JGS22(I1)=0.
      JFS22(I1)=0.
      JGS22(I2)=.125
      JFS22(I2)=.125
      GO TO 1
   73 I1=I+1
      IC=I
      I2=I+2
      JGS33(I1)=0.
      JFS33(I1)=0.
      JFS33(I2)=.125
      JGS33(I2)=.125
      GO TO 1
   74 I1=I+1
      ID=I
      I2=I+2
      JGS44(I1)=0.
      JFS44(I1)=0.
      JGS44(I2)=.125
      JFS44(I2)=.125
      GO TO 1
   75 I1=I+1
      IE=I
      I2=I+2
      JGS55(I1)=0.
      JFS55(I1)=0.
      JGS55(I2)=.125
      JFS55(I2)=.125
      GO TO 1
   76 I1=I+1
      IF=I
      I2=I+2
      JGS66(I1)=0.
      JFS66(I1)=0.
      JFS66(I2)=.125
      JGS66(I2)=.125
      GO TO 1
   77 I1=I+1
      IG=I
      I2=I+2
      JGS77(I1)=0.
      JFS77(I1)=0.
      JGS77(I2)=.125
      JFS77(I2)=.125
      GO TO 1
  300 DO 305 K=1,61
      READ*,AI,BI
      E(K)=AI/.2233/2.06
  305 B(K)=BI/.2233/2.06
      DO 310 M=1,43
      READ*,CZ,DZ
      C(M)=CZ/2.06
  310 D(M)=DZ/2.06
      E(62)=0.
```

```
                      B(62)=0.
                      B(53)=.125
                      B(63)=.125
                      C(44)=0.
                      C(45)=.125
                      D(44)=0.
      163             D(45)=.125
                      CALL NAMPLT
                      CALL PLOT(0.,1.,-3)
                      CALL AXIS(0.,0.,12HSORT(KGS)/C ,12,8.,90.,0.,.125,10.)
                      CALL AXIS(0.,0.,12HSORT(KFS)/C ,-12,8.,0.,0.,.125,10.)
      170             CALL LINE(JFS11,JGS11,IA,1,-1,1)
                      CALL LINE(JFS22,JGS22,ID,1,-1,2)
                      CALL LINE(JFS33,JGS33,IC,1,-1,3)
                      CALL LINE(JFS44,JGS44,ID,1,-1,4)
                      CALL LINE(JFS55,JGS55,IE,1,-1,5)
      175             CALL LINE(JFS66,JGS66,IF,1,-1,6)
                      CALL LINE(JFS77,JGS77,IG,1,-1,7)
                      CALL LINE(3,6.61,1,-1,8)
                      CALL LINE(3,6.43,1,-1,9)
                      CALL PLOT(2.5,2.0,-3)
      180             CALL SYMBOL(2.,5.96,.12,1,0.,-1)
                      CALL SYMBOL(2.5,5.9,.12,22H15 HOLES, CH = 10.5 MM,0.,22)
                      CALL SYMBOL(2.,5.66,.12,2,0.,-1)
                      CALL SYMBOL(2.5,5.6,.12,22H 9 HOLES, CH = 10.5 MM,0.,22)
                      CALL SYMBOL(2.,5.36,.12,3,0.,-1)
      185             CALL SYMBOL(2.5,5.3,.12,22H54 HOLES, CH = 10.5 MM,0.,22)
                      CALL SYMBOL(2.,5.06,.12,4,0.,-1)
                      CALL SYMBOL(2.5,5.0,.12,22H 5 HOLES, CH = 10.5 MM,0.,22)
                      CALL SYMBOL(2.,4.76,.12,5,0.,-1)
                      CALL SYMBOL(2.5,4.7,.12,22H 3 HOLES, CH = 10.5 MM,0.,22)
      190             CALL SYMBOL(2.,4.46,.12,6,0.,-1)
                      CALL SYMBOL(2.5,4.4,.12,22H40 HOLES, CH =  4.8 MM,0.,22)
                      CALL SYMBOL(2.,4.16,.12,7,0.,-1)
                      CALL SYMBOL(2.5,4.1,.12,22H 2 HOLES, CH = 28.6 MM,0.,22)
                      CALL SYMBOL(2.0,3.86,.12,8,0.,-1)
      195             CALL SYMBOL(2.5,3.8,.12,14HDATA OF NAITOH,0.,14)
                      CALL SYMBOL(2.0,3.56,.12,9,0.,-1)
                      CALL SYMBOL(2.5,3.5,.12,13HDATA OF JONES,0.,13)
                      CALL ENDPLT
                      STOP
      200             END
```

SYMBOLIC REFERENCE MAP (R=1)

ENTRY POINTS
6211 JFGS

VARIABLES

7502	A	REAL	ARRAY	7516	AC	REAL	*UNDEF
7475	AI	REAL		7524	AL	REAL	ARRAY
7457	ALF	REAL		10100	ALS	REAL	ARRAY
7510	AS	REAL	ARRAY	7633	B	REAL	ARRAY
7476	BI	REAL		7734	C	REAL	ARRAY
7460	CK	REAL		7461	CS	REAL	
7500	CZ	REAL		10015	D	REAL	ARRAY
7254	DG	REAL		7256	DH	REAL	
7255	DL	REAL		7501	DZ	REAL	
7532	E	REAL	ARRAY	7455	EG	REAL	
7253	GC	REAL		7467	I	INTEGER	
7464	IA	INTEGER		7466	ID	INTEGER	
7467	IC	INTEGER		7470	IO	INTEGER	
7471	IE	INTEGER		7472	IF	INTEGER	
7473	IG	INTEGER		7450	IP	INTEGER	
7446	IR	INTEGER		7463	I1	INTEGER	
7455	I2	INTEGER		7441	JF	REAL	
7443	JFS	REAL		7445	JFSA	REAL	
10172	JFS1	REAL	ARRAY	10336	JFS11	REAL	ARRAY
10502	JFS2	REAL	ARRAY	10646	JFS22	REAL	ARRAY
11012	JFS3	REAL	ARRAY	11156	JFS33	REAL	ARRAY
11322	JFS4	REAL	ARRAY	11466	JFS44	REAL	ARRAY
11632	JFS5	REAL	ARRAY	11776	JFS55	REAL	ARRAY
12142	JFS6	REAL	ARRAY	12306	JFS66	REAL	ARRAY
12452	JFS7	REAL	ARRAY	12616	JFS77	REAL	ARRAY
7440	JG	REAL		7442	JGS	REAL	

BLOCK	ADDRESS	LENGTH	FILE	DATE	PROCSSR	VER LEVEL	HARDWARE	COMMENTS
SKFL.SQ	25572	51	SL-SYSIO	01/10/78				
SMLRM.7	25643	0	SL-SYSIO	01/14/79				
HAR.SQ	25643	303	SL-SYSIO	01/10/78				
WEOX.SQ	26146	150	SL-SYSIO	01/10/78				
Z.SQ	26316	110	SL-SYSIO	01/10/78				
/PLTPLL/	26426	2						
AXIS3	26430	1053	SL-FT4LIB	12/29/76	FTN	4.6	433	6464 I OPT=2
LINE	27503	262	SL-FT4LIB	12/29/76	FTN	4.6	433	6464 I OPT=2
/PLTPLM/	27765	67						
MESPLT	30054	750	SL-FT4LIB	12/14/76	FTN	4.6	433	6464 I OPT=2
NUMBER	31024	313	SL-FT4LIB	12/29/76	FTN	4.6	433	6464 I OPT=2
PLTPKG	31337	1473	SL-FT4LIB	04/15/77				
/PLT999/	33032	2						
SYMBOL	33034	1134	SL-FT4LIB	12/29/76	FTN	4.6	433	6464 I OPT=2
CPUMSG	34170	10	SL-SYSLIB	06/11/78	COMPASS	3.4	460	07/19/74 SEND MACE MESSAGE.
CPUSYS	34200	47	SL-SYSLIB	06/11/78	COMPASS	3.4	460	06/25/75 PROCESS SYSTEM REQUEST.
ENCODE=	34247	125	SL-FORTRAN	10/16/78	COMPASS	3.4	460	FORMATTED WRITE INTO CORE.
GOTOER=	34374	14	SL-FORTRAN	10/16/78	COMPASS	3.4	460	COMPUTED GO TO ERROR PROCESSOR.
REMARK	34410	3	SL-FORTRAN	10/16/78	COMPASS	3.4	460	ISSUE A MESSAGE TO THE DAYFILE.
SINCOS=	34413	66	SL-FORTRAN	10/16/78	COMPASS	3.4	460	TRIGONOMETRIC SINE OR COSINE OF X. OPT=ALL.
SYSTEM	34501	26	SL-FORTRAN	10/16/78	COMPASS	3.4	460	USER CALLABLE ERROR PROCESSOR.
XTOI.	34527	63	SL-FORTRAN	10/16/78	COMPASS	3.4	460	REAL TO INTEGER EXPONENTIATION.
EXP.MSG	34612	16	SL-FORTRAN	10/16/78	COMPASS	3.4	460	COMMON ERROR MESSAGES FOR EXPONENTIATION.
SYS=AID	34630	7	SL-FORTRAN	10/16/78	COMPASS	3.4	460	AUXILIARY MATH LIBRARY LINK FOR ERROPS.
(LWA+1)	34637	(34526)						

.734 CP SECONDS 526008 CM STORAGE USED 7 TABLE MOVES

15 hole

JG.M/S	JGS	JGSS	JF.M/S	JFS	JFSS	C
0.000	0.000	0.000	.608	3.720	.993	.993
0.000	0.000	0.000	.127	.774	.456	.456
5.004	1.057	.533	.127	.774	.456	.988
6.940	1.466	.627	.091	.554	.385	1.013
9.760	2.061	.744	.052	.316	.291	1.035
16.731	3.534	.974	0.000	0.000	0.000	.974
0.000	0.000	0.000	.190	1.161	.558	.558
7.775	1.642	.664	.085	.519	.373	1.037
5.035	1.074	.537	.141	.876	.485	1.022
6.435	1.372	.607	.122	.744	.447	1.054
5.655	1.194	.566	.150	.917	.496	1.062
11.372	2.402	.803	.024	.145	.199	1.001
3.010	0.000	0.000	.364	2.230	.774	.774
1.270	.631	.431	.216	1.319	.593	1.024
4.391	.927	.499	.182	1.114	.547	1.046
5.004	1.057	.533	.153	.933	.511	1.044
5.695	1.203	.578	.142	.869	.495	1.049

0.000	0.000	0.000	.189	1.154	.557	.557
1.184	.250	.259	.189	1.154	.557	.816
2.248	.475	.357	.189	1.154	.557	.914
3.025	.808	.466	.170	1.039	.528	.994
4.325	.914	.495	.159	.972	.511	1.006
3.698	.781	.458	.174	1.061	.534	.992
4.015	.848	.477	.169	1.032	.526	1.004
4.421	.934	.501	.158	.964	.509	1.010
5.326	1.125	.550	.141	.861	.481	1.030
6.304	1.331	.598	.136	.833	.473	1.071
7.802	1.648	.665	.108	.658	.420	1.085
8.469	1.789	.693	.080	.490	.363	1.056
9.264	1.944	.722	.064	.392	.324	1.047
10.024	2.117	.754	.053	.324	.295	1.049
10.384	2.193	.767	.048	.295	.282	1.049
11.162	2.358	.796	.038	.232	.250	1.045
12.899	2.724	.855	.023	.138	.193	1.048
17.633	3.724	1.000	0.000	0.000	0.000	1.000

9 hole

JG,M/S	JGS	JGS5	JF,M/S	JFS	JFS3	C
2.939	.621	.460	.103	.662	.475	.935
3.451	.729	.496	.100	.614	.457	.956
11.751	2.482	.919	0.000	0.000	0.000	.919
4.011	.847	.537	.084	.515	.419	.956
0.000	0.000	0.000	.551	3.370	1.071	1.071
1.743	.368	.354	.207	1.265	.656	1.010
1.347	.284	.311	.227	1.386	.647	.958
2.440	.515	.419	.137	.838	.534	.953
2.205	.466	.398	.147	.898	.553	.951
6.371	1.346	.677	.045	.275	.305	.983
10.382	2.193	.864	.016	.099	.184	1.048
8.353	1.764	.775	.017	.102	.187	.962
0.000	0.000	0.000	.358	[illegible]	[illegible]	[illegible]

1.610	.340	.340	.218	1.333	.674	1.014
2.694	.569	.440	.132	.810	.525	.965
2.145	.453	.393	.155	.946	.568	.960
3.004	.635	.465	.106	.651	.471	.936
3.611	.763	.510	.093	.571	.441	.951
4.559	.963	.573	.071	.435	.395	.957
6.177	1.305	.667	.035	.214	.270	.937
6.734	1.422	.696	.030	.181	.243	.944
10.535	2.225	.871	0.000	0.000	0.000	.871

5 hole

JG,M/S	JGS	JGS5	JF,M/S	JFS	JFS5	C
0.000	0.000	0.000	.734	4.489	1.316	1.316
3.007	.635	.495	.151	.925	.597	1.092
2.312	.488	.434	.191	1.170	.672	1.105
2.892	.611	.485	.155	.951	.606	1.091
3.785	.799	.555	.115	.706	.522	1.077
8.688	1.835	.841	0.000	0.000	0.000	.841
0.000	0.000	0.000	1.206	7.375	1.686	1.686
5.170	1.092	.649	.074	.453	.418	1.067
2.920	.617	.488	.158	.965	.610	1.097
2.287	.483	.432	.191	1.170	.672	1.103
6.444	1.361	.724	.035	.216	.289	1.013
8.989	1.899	.856	0.000	0.000	0.000	.856
0.000	0.000	0.000	.572	3.502	1.162	1.162
2.312	.488	.434	.196	1.193	.680	1.114
2.904	.613	.486	.151	.926	.597	1.084
3.878	.819	.562	.092	.561	.465	1.027
4.754	1.004	.622	.059	.363	.374	.996
12.063	2.548	.991	0.000	0.000	0.000	.991
0.000	0.000	0.000	.232	1.417	.739	.739
.387	.082	.177	.232	1.417	.739	.916
1.021	.216	.288	.232	1.417	.739	1.027
1.074	.227	.296	.228	1.394	.733	1.029
1.555	.329	.356	.213	[illegible]	.793	[illegible]

4.306	.909	.592	.101	.620	.489	1.081
3.798	.802	.556	.121	.739	.534	1.030
2.340	.503	.440	.161	.983	.616	1.056
3.225	.681	.512	.134	.818	.561	1.074

JG,M/S	JGS	JGS5	JF,M/S	JFS	JFS5	C

5A hole

0.000	0.000	0.000	.339	2.071	.894	.894
.567	.120	.215	.301	1.841	.842	1.057
.721	.152	.242	.231	1.783	.823	1.071
1.073	.227	.296	.213	1.302	.708	1.004
1.343	.284	.331	.167	1.020	.627	.958
1.702	.359	.372	.123	.763	.542	.915
1.945	.411	.398	.117	.718	.526	.924
2.246	.474	.428	.101	.616	.487	.915
2.588	.547	.459	.084	.513	.445	.904
2.962	.626	.491	.073	.449	.415	.907
4.076	.861	.576	.041	.250	.311	.887
.565	.119	.214	.265	1.623	.791	1.005
.736	.156	.245	.239	1.462	.751	.996
1.304	.275	.326	.169	1.033	.631	.957
1.936	.409	.397	.100	.609	.485	.882
1.325	.280	.328	.164	1.000	.621	.949
1.711	.361	.373	.128	.782	.549	.922
2.213	.467	.425	.102	.622	.490	.914
2.500	.528	.451	.082	.500	.439	.890
1.463	.309	.345	.140	.854	.576	.921
.946	.200	.278	.201	1.231	.683	.966

JG,M/S	JGS	JGS5	JF,M/S	JFS	JFS5	C

3 hole

0.000	0.000	0.000	1.122	6.862	1.671	1.671
.732	.135	.251	.271	1.659	.822	1.073
.391	.083	.183	.257	1.571	.800	.983
1.317	.278	.337	.223	1.403	.756	1.032
1.937	.409	.458	.147	.933	.[illegible]	1.013

2.374	.501	.452	.104	.637	.509	.361
0.000	0.000	0.000	.382	2.337	.975	.975
.475	.130	.202	.253	1.550	.794	.397
.623	.132	.231	.245	1.496	.781	1.012
.737	.160	.255	.233	1.451	.771	1.026
1.277	.270	.331	.192	1.176	.692	1.023
1.821	.385	.396	.143	.876	.597	.993
1.951	.412	.410	.106	.649	.514	.924
2.590	.547	.472	.091	.553	.477	.949
3.007	.635	.509	.084	.513	.457	.966
0.000	0.000	0.000	.647	3.955	1.269	1.269
.994	.210	.292	.218	1.336	.738	1.030
1.410	.298	.348	.192	1.176	.692	1.040
1.794	.379	.393	.124	.759	.556	.949
3.311	.699	.534	.068	.415	.411	.945
3.615	.764	.558	.058	.355	.380	.938
4.378	.925	.614	.030	.181	.271	.885

JG,M/S	JGS	JGSS	JF,M/S	JFS	JFSS	C
40 hole						
0.000	0.000	0.000	.347	2.124	.773	.773
1.550	.327	.306	.206	1.259	.600	.906
2.102	.444	.356	.182	1.114	.563	.921
2.736	.578	.407	.162	.994	.533	.940
3.553	.751	.463	.131	.803	.479	.942
2.519	.532	.390	.162	.994	.533	.923
2.920	.617	.420	.155	.951	.521	.942
3.790	.801	.479	.138	.846	.492	.970
3.334	.704	.449	.145	.885	.503	.952
4.216	.890	.505	.120	.733	.458	.962
4.749	1.003	.536	.107	.655	.433	.968
5.250	1.109	.563	.104	.639	.429	.991
5.871	1.240	.596	.091	.557	.393	.995
6.471	1.367	.625	.081	.496	.376	1.001

7.172	1.515	.658	.072	.440	.355	1.013
7.906	1.670	.691	.063	.386	.332	1.023
8.869	1.873	.732	.053	.323	.304	1.036
14.597	3.083	.939	0.000	0.000	0.000	.939
JG,M/S	JGS	JGS5	JF,M/S	JFS	JFS5	C
2 hole						
0.000	0.000	0.000	.212	1.293	.840	.840
.353	.074	.201	.212	1.293	.840	1.042
.595	.126	.261	.202	1.230	.820	1.082
.921	.195	.325	.148	.903	.701	1.026
1.251	.264	.379	.112	.686	.611	.990
1.085	.229	.353	.163	.996	.736	1.089
1.705	.360	.443	.111	.682	.609	1.051
2.311	.488	.515	.064	.394	.463	.978
2.965	.626	.584	.047	.286	.394	.978
3.592	.759	.642	.038	.229	.353	.995
4.873	1.029	.748	.025	.156	.291	1.039
0.000	0.000	0.000	.260	1.593	.931	.931
.205	.043	.153	.250	1.528	.912	1.065
.306	.065	.187	.243	1.485	.899	1.086
.460	.097	.230	.219	1.340	.854	1.083
.757	.160	.295	.162	.991	.734	1.029
1.069	.226	.350	.122	.749	.639	.989
1.504	.318	.416	.090	.548	.546	.961
1.214	.256	.373	.177	1.082	.767	1.140
2.149	.454	.497	.064	.390	.460	.957
2.629	.555	.549	.059	.364	.445	.994
3.730	.788	.654	.030	.184	.316	.971
0.000	0.000	0.000	.168	1.026	.747	.747
.959	.203	.332	.150	.920	.707	1.039
1.221	.258	.374	.139	.849	.679	1.054
1.726	.365	.445	.094	.578	.561	1.006
3.060	.650	.595	.045	.277	.399	.993
4.148	.876	.690	.025	.17	.304	[illegible]

15 hole

$h_{in} = 445\,mm$

JG,M/S	JGS	JGS5	JF,M/S	JFS	JFS5	C
[illegible]	[illegible]	[illegible]	[illegible]	0.000	0.000	1.000
0.000	0.000	0.000	.127	.777	.457	.457
2.362	.499	.366	.127	.777	.457	.823
8.409	1.776	.691	.076	.464	.353	1.043
6.844	1.446	.623	.110	.671	.425	1.047
9.128	1.928	.719	.058	.357	.310	1.029
9.937	2.099	.751	.048	.293	.280	1.031
11.656	2.462	.813	.020	.122	.181	.994
3.235	.683	.428	.181	1.105	.545	.973
3.554	.751	.449	.168	1.030	.526	.975
4.977	1.051	.531	.143	.872	.484	1.015
6.066	1.281	.586	.125	.763	.453	1.039
6.712	1.418	.617	.101	.618	.407	1.024
0.000	0.000	0.000	.283	1.734	.682	.682
1.626	.343	.304	.233	1.426	.619	.922
1.882	.397	.327	.218	1.336	.599	.926
2.437	.515	.372	.205	1.257	.581	.953
4.055	.856	.479	.152	.930	.500	.979
5.464	1.154	.557	.127	.774	.456	1.012
6.666	1.412	.616	.113	.693	.431	1.047
8.412	1.777	.691	.065	.395	.326	1.016
9.506	2.008	.734	.050	.306	.286	1.021
11.439	2.416	.805	.022	.133	.189	.994
JG,M/S	JGS	JGS5	JF,M/S	JFS	JFS5	C

Appendix II. Computer Program List and the Steam/Water Reduced Data.

The input of this program includes:

VTS steam venturi temperature reading(mV).
VPS steam venturi pressure reading(V).
VWS steam venturi pressure drop reading(V).
VTG steam temperature at the channel inlet(mV).
VPG steam pressure at the channel inlet(V).
WL reading of water rotameter 1(lbs/min).
VTL water inlet temperature reading(mV).
IP perforated plate no. defined in Appendix I.
RUN run no. in the form of XXXX.ZZ, where XXXX shows the test run no., and ZZ is the height of water inlet spray in inches.
VTLO water overflow temperature(mV).
VTP temperature reading 2 mm above the plate(mV).
WL1 reading of water rotameter 2(lbs/sec.).

The output of the program includes:

RUN run no.
PER perforation ratio.
WS, WL steam and water mass flow rate(kg/s).
VGH j_g(m/s).
VLH j_f(m/s).
EHG $W_s h_{fg}$(KW).
EHL $W_f C_p (T_{sat} - T_{f,in})$ (KW).
EHLO $W_f C_p (T_{out} - T_{f,in})$ (KW).
REH EHL/EHG
JGS H_g^*/C^2
JLS H_f^*/C^2
TSC,TLC,TLOC,TLPC temperature of steam inlet, water inlet water outlet, and two-phase mixture at 2 mm above the plate (^oC).

807.24	.254	.27E-01	.54E+00	63.85	.72	68.26	192.05	74.06	2.81	1.77	1.21	141.6	14.8	47.8	98.4
808.24	.254	.27E-01	.62E+00	64.89	.82	69.93	219.02	71.76	3.11	1.79	1.31	141.6	14.8	42.7	98.7
27.00	.141	.46E-02	.21E-01	19.72	.05	10.74	8.15	7.98	.76	1.05	.35	141.6	9.1	98.2	98.9
28.00	.141	.58E-02	.35E-01	24.98	.09	13.72	13.50	12.46	.98	1.18	.45	141.6	8.8	91.1	98.7
29.00	.141	.79E-02	.51E-01	34.19	.12	18.67	19.45	18.66	1.04	1.38	.54	141.6	8.1	96.3	97.7
30.00	.141	.12E-01	.82E-01	52.49	.20	28.79	31.62	29.52	1.10	1.71	.68	141.6	7.4	93.8	96.3
31.00	.141	.18E-01	.11E+00	78.77	.26	38.78	42.45	39.96	1.09	1.99	.79	141.6	7.4	94.6	98.2
32.00	.141	.21E-01	.14E+00	89.06	.33	48.88	53.21	49.55	1.09	2.23	.88	141.6	7.1	93.6	97.5
33.00	.141	.27E-01	.19E+00	117.01	.46	64.17	74.89	69.95	1.15	2.55	1.04	141.6	6.9	94.1	98.2
34.00	.141	.34E-01	.18E+00	104.75	.40	57.61	64.02	58.80	1.11	2.42	.97	141.6	6.9	92.4	98.2
59.00	.141	.59E-02	.35E-01	25.53	.09	13.91	13.32	12.94	.96	1.19	.45	141.6	10.1	97.5	96.3
60.00	.141	.96E-02	.66E-01	41.46	.16	22.77	25.12	23.28	1.10	1.52	.61	141.6	9.3	93.4	97.8
61.00	.141	.15E-01	.96E-01	62.51	.23	34.20	36.55	34.66	1.07	1.87	.76	141.6	8.8	95.3	97.9
62.00	.141	.19E-01	.12E+00	81.58	.30	44.66	47.54	44.97	1.06	2.13	.84	141.6	8.6	95.0	98.1
63.00	.141	.23E-01	.15E+00	97.90	.37	53.73	58.64	54.54	1.07	2.34	.93	141.6	8.6	93.6	83.7
64.00	.141	.27E-01	.20E+00	115.80	.48	64.18	76.02	68.12	1.18	2.54	1.06	141.6	8.4	88.1	84.0
830.00	.141	.36E-02	.21E-01	15.30	.05	8.32	7.99	7.47	.91	.92	.35	141.6	15.8	99.1	98.9
831.00	.141	.67E-02	.51E-01	28.84	.12	15.83	17.88	16.48	1.13	1.27	.54	141.6	15.5	93.4	98.2
832.00	.141	.11E-01	.83E-01	46.08	.20	25.32	29.26	26.79	1.16	1.60	.69	141.6	15.5	92.9	98.7
833.00	.141	.15E-01	.11E+00	63.09	.27	34.76	39.22	35.25	1.13	1.84	.79	141.6	15.3	91.4	98.9
834.00	.141	.17E-01	.14E+00	73.57	.33	40.69	48.68	42.53	1.20	2.01	.88	141.6	15.0	89.3	98.2
835.00	.141	.21E-01	.16E+00	83.99	.40	46.79	58.42	50.87	1.17	2.24	.97	141.6	15.0	89.0	98.7

836.00	.141	.24E-01	.19E+00	105.01	.47	58.25	69.13	59.02	1.19	2.42	1.05	141.6	15.0	87.6	98.2
837.00	.141	.26E-01	.22E+00	113.07	.53	62.90	77.83	64.95	1.24	2.51	1.12	141.6	15.0	85.3	98.4
838.00	.141	.27E-01	.25E+00	118.24	.59	65.84	87.88	72.83	1.33	2.57	1.18	141.6	14.8	85.3	98.4
839.00	.141	.28E-01	.25E+00	121.02	.59	67.38	87.88	72.83	1.30	2.60	1.18	141.6	14.8	85.4	98.4
840.00	.141	.33E-01	.27E+00	141.18	.66	78.34	97.64	83.13	1.25	2.81	1.25	141.6	14.8	87.3	98.2
841.00	.141	.38E-01	.32E+00	162.48	.77	90.15	114.43	95.81	1.27	3.01	1.35	141.6	14.8	86.1	98.2
842.00	.141	.41E-01	.36E+00	178.10	.86	99.29	126.57	103.82	1.27	3.15	1.42	141.6	14.8	84.7	97.7
843.00	.141	.48E-01	.40E+00	205.14	.96	114.31	142.48	117.28	1.25	3.38	1.51	141.6	14.8	84.9	96.3
844.00	.141	.51E-01	.43E+00	218.05	1.04	122.07	153.54	121.61	1.26	3.49	1.56	141.6	14.8	82.3	96.0
845.00	.141	.38E-01	.43E+00	165.63	1.04	94.78	153.54	98.59	1.62	3.04	1.56	141.6	14.8	69.5	93.4
846.00	.141	.17E-01	.43E+00	71.45	1.04	42.88	153.54	46.74	3.58	2.00	1.56	141.6	14.8	40.7	69.4
847.00	.141	.19E-01	.39E+00	80.00	.93	47.71	138.10	48.45	2.89	2.11	1.48	141.6	14.8	44.7	54.1
848.00	.141	.34E-01	.39E+00	145.08	.93	83.15	138.10	87.11	1.66	2.84	1.48	141.6	14.8	68.5	88.8
849.00	.141	.28E-01	.35E+00	113.80	.84	65.27	124.18	71.66	1.90	2.51	1.41	141.6	14.8	64.0	82.5
850.00	.141	.21E-01	.35E+00	88.94	.84	52.46	124.18	53.39	2.37	2.23	1.41	141.6	14.8	51.4	66.1
851.04	.141	.30E-02	.21E-01	12.72	.05	6.91	7.57	7.49	1.10	.84	.35	141.5	15.5	99.1	98.7
852.04	.141	.76E-02	.51E-01	32.65	.12	18.07	17.88	15.31	.93	1.35	.54	139.7	15.5	90.7	97.5
853.04	.141	.10E-01	.82E-01	44.66	.20	24.29	28.92	25.92	1.19	1.57	.68	141.6	15.3	91.2	98.4
854.04	.141	.13E-01	.11E+00	54.38	.27	30.29	39.33	32.47	1.30	1.74	.79	141.6	15.0	85.2	97.2
855.04	.141	.17E-01	.14E+00	71.87	.33	39.73	48.64	42.67	1.23	2.00	.88	141.6	15.0	89.5	98.4
856.00	.141	.19E-01	.16E+00	80.78	.40	45.24	58.42	46.06	1.29	2.17	.97	141.6	15.0	82.0	98.4
857.04	.141	.20E-01	.19E+00	88.17	.47	49.53	69.13	53.14	1.40	2.22	1.05	141.5	15.0	80.3	98.4

858.04	.141	.24E-01	.22E+00	103.58	.53	58.16	77.83	60.09	1.14	2.40	1.12	141.6	15.0	80.6	98.4
859.04	.141	.26E-01	.25E+00	111.37	.59	63.26	87.62	60.65	1.39	2.49	1.19	141.6	15.0	73.8	84.9
860.04	.141	.28E-01	.28E+00	121.20	.67	68.14	99.31	75.77	1.46	2.60	1.26	141.6	15.0	79.9	98.9
861.04	.141	.30E-01	.28E+00	127.94	.67	71.93	99.31	75.77	1.38	2.67	1.26	141.6	15.0	79.9	98.9
862.04	.141	.32E-01	.31E+00	138.05	.75	78.09	110.81	79.83	1.42	2.77	1.33	141.6	15.0	76.2	89.3
863.04	.141	.34E-01	.35E+00	144.84	.84	82.11	124.26	87.76	1.51	2.84	1.41	141.6	15.0	75.0	85.8
864.04	.141	.39E-01	.39E+00	169.17	.93	95.62	137.70	99.99	1.44	3.07	1.44	141.6	15.0	76.7	98.2
860.04	.141	.42E-01	.44E+00	178.72	1.05	101.72	155.50	105.56	1.53	3.16	1.57	141.6	14.8	72.6	89.0
1130.12	.141	.88E-02	.11E+00	37.91	.26	21.95	35.99	19.34	1.64	1.45	.78	141.6	19.0	62.5	89.3
1131.12	.141	.12E-01	.16E+00	51.12	.40	29.57	56.21	30.75	1.90	1.69	.97	141.6	18.2	61.0	97.3
1132.12	.141	.17E-01	.22E+00	73.80	.53	42.61	75.40	42.58	1.77	2.03	1.12	141.6	17.7	64.2	78.4
1133.12	.141	.21E-01	.28E+00	90.82	.67	52.76	96.13	51.47	1.82	2.25	1.26	140.4	17.7	61.8	95.1
1134.12	.141	.56E-02	.31E-01	23.45	.12	13.30	17.41	12.08	1.31	1.14	.54	141.6	17.7	74.8	97.0
1135.12	.141	.11E-01	.14E+00	46.91	.33	27.27	46.38	25.09	1.72	1.62	.88	139.9	18.0	61.8	91.7
1136.12	.141	.14E-01	.19E+00	59.32	.48	34.21	65.77	30.02	1.92	1.82	1.04	141.2	18.0	65.4	87.1
1137.12	.141	.24E-01	.34E+00	102.98	.82	59.84	116.51	60.33	1.95	2.40	1.38	141.6	17.7	60.3	81.1
1138.12	.141	.24E-01	.43E+00	104.85	1.04	62.12	148.58	55.79	2.39	2.42	1.57	141.6	17.7	48.6	95.0
1139.12	.141	.24E-01	.51E+00	104.85	1.23	63.01	176.12	47.08	2.79	2.42	1.71	141.6	17.7	38.7	84.8
1140.12	.141	.25E-01	.59E+00	108.01	1.41	64.11	201.21	73.13	3.14	2.45	1.82	141.6	17.7	47.6	75.8
1141.12	.141	.27E-01	.68E+00	114.23	1.58	69.22	228.26	48.11	3.27	2.52	1.91	141.6	17.5	35.0	73.6
35.12	.141	.43E-02	.23E-01	18.36	.05	10.09	8.83	8.14	.87	1.01	.36	141.6	5.1	92.6	93.8
36.12	.141	.53E-02	.35E-01	22.75	.09	12.62	13.54	11.41	1.07	1.13	.48	141.6	8.6	84.1	93.1

37.12	.141	.66E-02	.51E-01	28.43	.12	16.06	19.87	14.99	1.24	1.26	.54	141.6	8.1	77.0	96.1
38.12	.141	.82E-02	.82E-01	35.35	.20	20.39	31.28	19.23	1.53	1.40	.69	141.6	8.4	64.7	88.1
39.12	.141	.12E-01	.11E+00	50.79	.28	29.31	42.00	23.70	1.43	1.68	.79	141.6	8.4	64.6	91.0
40.12	.141	.18E-01	.16E+00	79.54	.40	47.59	63.00	23.81	1.32	2.11	.97	141.6	8.4	42.7	72.4
41.12	.141	.20E-01	.19E+00	87.44	.46	52.31	73.50	27.55	1.41	2.21	1.04	141.6	8.4	42.7	72.4
42.12	.141	.23E-01	.22E+00	98.76	.53	59.09	84.00	31.48	1.42	2.35	1.12	141.6	8.4	42.7	72.4
43.12	.141	.25E-01	.25E+00	105.86	.59	63.33	94.50	35.42	1.49	2.43	1.18	141.6	8.4	42.7	72.4
44.12	.141	.27E-01	.27E+00	114.11	.66	68.27	105.00	39.35	1.54	2.52	1.25	141.6	8.4	42.7	72.4
65.12	.141	.53E-02	.35E-01	22.86	.09	12.76	13.28	10.91	1.04	1.13	.45	141.6	10.3	84.0	95.0
66.12	.141	.76E-02	.67E-01	32.74	.16	18.55	25.36	18.44	1.37	1.35	.62	141.6	9.3	75.3	96.7
67.12	.141	.11E-01	.96E-01	45.48	.23	25.85	36.55	25.87	1.41	1.59	.74	141.6	8.8	73.4	95.0
68.12	.141	.14E-01	.12E+00	58.18	.30	32.90	47.12	35.00	1.43	1.80	.84	141.6	8.6	78.5	96.0
69.12	.141	.18E-01	.16E+00	79.05	.40	44.70	62.83	46.67	1.41	2.10	.97	141.6	8.6	76.5	96.0
70.12	.141	.23E-01	.22E+00	98.29	.54	56.31	85.05	58.07	1.51	2.34	1.12	141.6	8.4	68.8	85.8
90.00	.141	.44E-02	.21E-01	19.07	.05	10.37	7.62	7.50	.73	1.03	.35	141.6	15.0	98.7	97.7
91.00	.141	.69E-02	.51E-01	29.73	.12	16.33	18.61	17.16	1.14	1.29	.54	141.6	12.1	93.1	91.9
92.00	.141	.12E-01	.82E-01	50.66	.20	27.76	30.58	28.71	1.10	1.68	.68	141.6	11.1	94.6	89.0
93.00	.141	.15E-01	.11E+00	66.84	.27	36.65	41.39	37.87	1.11	1.93	.79	141.6	10.6	92.4	92.9
94.00	.141	.21E-01	.14E+00	88.79	.33	48.65	51.23	48.12	1.05	2.23	.88	141.6	10.6	94.6	91.9
95.00	.141	.24E-01	.18E+00	103.33	.40	56.81	61.47	56.41	1.08	2.40	.97	141.6	10.6	93.6	92.9
96.00	.141	.28E-01	.19E+00	112.39	.46	62.40	71.92	61.57	1.15	2.50	1.04	141.6	10.3	87.1	92.8
97.12	.141	.44E-02	.21E-01	13.03	.05	10.3	7.75	7.63	.75	1.03	.35	141.6	13.5	98.7	97.7

98.12	.141	.58E-02	.51E-01	24.97	.12	14.01	18.56	14.55	1.32	1.18	.54	141.6	12.3	81.1	96.4
99.12	.141	.83E-02	.82E-01	35.68	.20	20.33	30.36	20.77	1.49	1.41	.68	141.6	11.1	71.9	98.7
100.12	.141	.11E-01	.11E+00	45.60	.26	26.20	40.87	25.79	1.56	1.59	.79	141.6	10.8	67.1	99.6
101.12	.141	.14E-01	.14E+00	56.12	.33	33.27	51.09	33.47	1.54	1.80	.88	141.6	10.8	70.3	98.7
102.12	.141	.16E-01	.16E+00	69.57	.40	39.68	61.30	41.66	1.55	1.97	.97	141.6	10.8	71.4	97.9
103.12	.141	.18E-01	.19E+00	78.31	.46	44.96	72.12	46.11	1.60	2.09	1.04	141.6	10.1	67.6	98.9
104.12	.141	.21E-01	.22E+00	89.95	.53	52.00	82.19	48.71	1.58	2.24	1.12	141.6	10.3	63.5	98.7
105.12	.141	.24E-01	.25E+00	101.73	.59	58.14	92.47	61.76	1.59	2.38	1.18	141.6	10.3	70.2	98.6
106.12	.141	.25E-01	.27E+00	105.59	.66	60.35	102.74	60.62	1.70	2.43	1.25	141.6	10.3	70.2	98.4
119.00	.085	.38E-02	.21E-01	27.15	.09	8.95	7.62	7.17	.85	1.25	.46	141.6	15.0	35.0	93.4
120.00	.085	.74E-02	.51E-01	52.91	.20	17.53	18.51	17.00	1.06	1.77	.71	141.6	12.6	92.9	82.5
121.00	.085	.11E-01	.82E-01	81.91	.33	27.16	30.44	27.85	1.12	2.20	.90	141.6	10.8	32.4	92.6
122.00	.085	.16E-01	.11E+00	114.42	.44	37.79	41.74	39.22	1.10	2.60	1.05	141.6	9.8	94.6	83.2
123.00	.085	.20E-01	.14E+00	145.05	.55	48.07	51.94	47.72	1.08	2.92	1.17	141.6	9.3	32.6	86.1
124.00	.085	.23E-01	.17E+00	165.63	.68	55.13	63.87	56.93	1.16	3.12	1.30	141.6	10.1	90.2	90.5
125.00	.085	.23E-01	.19E+00	165.30	.78	55.04	73.15	65.00	1.33	3.13	1.39	141.6	10.1	90.0	77.7
126.00	.085	.27E-01	.19E+00	193.02	.78	64.27	73.15	65.00	1.14	3.37	1.39	141.6	10.1	90.0	77.7
127.00	.085	.22E-01	.22E+00	159.98	.88	54.63	83.32	60.23	1.52	3.07	1.48	141.6	9.1	74.8	73.6
128.00	.085	.27E-01	.22E+00	195.84	.88	66.98	83.32	60.23	1.24	3.40	1.48	141.6	9.1	74.8	73.6
129.00	.085	.16E-01	.25E+00	113.78	.99	40.54	93.23	41.79	2.30	2.59	1.57	141.6	9.6	50.1	96.4
130.00	.085	.11E-01	.28E+00	81.40	1.12	29.66	105.66	31.19	3.56	2.13	1.67	141.6	9.6	36.3	94.4
163.00	.085	.40E-02	.24E-01	28.26	.10	9.41	8.61	7.65	.92	1.25	.60	141.6	13.8	89.7	91.9

164.00	.085	.71E-02	.44E-01	90.34	.10	16.00	18.23	14.83	.97	1.72	.67	141.5	12.5	92.0	79.9
165.00	.085	.90E-02	.63E-01	63.92	.25	21.12	22.99	21.50	1.09	1.94	.73	141.6	12.1	94.1	79.6
166.00	.085	.14E-01	.96E-01	97.10	.38	32.11	35.66	33.19	1.11	2.39	.98	141.6	11.1	93.8	92.9
167.00	.085	.19E-01	.13E+00	134.61	.50	44.52	47.00	43.76	1.06	2.82	1.12	141.6	10.8	93.8	84.7
168.00	.085	.20E-01	.15E+00	142.36	.58	47.56	53.95	46.30	1.13	2.90	1.20	141.6	11.8	88.1	83.7
169.00	.085	.22E-01	.15E+00	154.55	.60	51.35	55.93	50.35	1.09	3.02	1.23	141.6	11.6	91.2	74.8
170.00	.085	.24E-01	.17E+00	170.88	.69	57.07	63.83	55.39	1.12	3.17	1.31	141.6	11.6	88.3	74.8
171.00	.085	.28E-01	.21E+00	183.60	.85	62.22	78.25	61.26	1.27	3.29	1.46	141.6	11.3	79.9	74.1
172.00	.085	.13E-01	.24E+00	89.91	.96	32.56	89.41	29.15	2.75	2.30	1.55	141.6	11.3	40.2	23.2
173.00	.085	.13E-01	.25E+00	89.91	1.01	32.56	93.48	30.47	2.87	2.30	1.58	141.6	11.3	40.2	23.2
174.00	.085	.13E-01	.26E+00	89.91	1.05	32.56	97.54	31.80	3.00	2.30	1.62	141.6	11.3	40.2	23.2
175.00	.085	.13E-01	.27E+00	89.91	1.07	32.56	99.57	32.46	3.06	2.30	1.64	141.6	11.3	40.2	23.2
176.00	.085	.13E-01	.22E+00	89.91	.88	32.56	81.29	26.50	2.50	2.30	1.48	141.6	11.3	40.2	23.2
1115.12	.085	.93E-02	.11E+00	66.14	.45	22.76	38.18	24.53	1.68	1.97	1.06	141.6	18.7	70.9	92.5
1116.12	.085	.11E-01	.17E+00	76.21	.67	26.53	56.96	32.01	2.15	2.12	1.29	141.6	18.2	64.2	90.0
1117.12	.085	.16E-01	.22E+00	116.30	.88	40.63	75.17	40.36	1.85	2.62	1.48	141.6	18.0	62.0	83.4
1118.12	.085	.19E-01	.27E+00	135.16	1.10	47.83	93.96	43.55	1.96	2.82	1.65	133.9	18.0	56.0	81.3
1119.12	.085	.93E-02	.13E+00	66.51	.54	23.37	46.04	23.37	1.97	1.98	1.16	140.7	18.0	59.6	89.2
1120.12	.085	.15E-01	.19E+00	106.77	.77	37.10	65.77	37.83	1.77	2.51	1.38	141.6	18.0	65.2	86.1
1121.12	.085	.54E-02	.51E-01	38.86	.20	13.24	17.36	12.43	1.31	1.51	.71	141.5	18.0	76.7	92.2
1122.12	.085	.17E-01	.34E+00	124.73	1.38	44.48	118.40	47.43	2.67	2.71	1.85	141.6	17.7	50.7	87.1
1123.12	.085	.19E-01	.43E+00	133.31	1.72	48.02	148.20	46.30	3.03	2.30	2.07	141.5	17.7	43.4	90.5

1124.12	.085	.19E-01	.52E+00	133.44	2.08	47.80	178.72	63.35	3.74	2.80	2.27	141.6	17.7	46.9	83.1
1125.12	.085	.19E-01	.50E+00	137.33	2.31	49.87	198.39	50.06	3.94	2.84	2.40	141.6	17.7	38.5	82.8
1126.12	.085	.19E-01	.47E+00	133.39	1.87	48.20	161.68	46.97	3.35	2.80	2.16	141.6	17.5	41.5	79.6
1127.12	.085	.18E-01	.39E+00	125.09	1.56	44.85	134.84	44.78	3.00	2.71	1.97	141.6	17.5	44.9	85.6
1128.12	.085	.19E-01	.65E+00	136.22	2.59	49.96	223.07	53.44	4.50	2.83	2.54	141.6	17.5	37.3	84.4
131.12	.085	.29E-02	.21E-01	20.99	.09	6.93	7.79	7.54	1.13	1.11	.46	141.6	13.0	97.3	97.2
132.12	.085	.51E-02	.49E-01	36.37	.20	12.48	18.31	12.56	1.47	1.46	.70	141.5	11.3	72.6	94.1
133.12	.085	.85E-02	.83E-01	50.44	.33	20.80	31.24	21.14	1.50	1.89	.91	141.5	10.3	70.9	94.6
134.12	.085	.11E-01	.11E+00	76.61	.44	26.40	41.21	27.56	1.55	2.12	1.04	141.5	10.1	70.2	92.2
135.12	.085	.14E-01	.14E+00	99.43	.55	34.34	51.65	33.76	1.50	2.42	1.17	141.5	9.8	68.8	93.6
136.12	.085	.15E-01	.17E+00	109.90	.67	37.34	63.02	47.93	1.69	2.54	1.29	141.6	9.8	78.4	77.0
137.12	.085	.18E-01	.19E+00	116.90	.77	40.62	72.51	62.25	1.78	2.62	1.38	141.6	9.6	82.3	83.4
138.12	.085	.18E-01	.22E+00	130.15	.88	45.91	83.29	42.97	1.81	2.77	1.48	141.6	9.6	56.2	86.4
139.12	.085	.20E-01	.25E+00	140.15	.99	49.10	93.44	52.45	1.90	2.87	1.57	141.6	9.6	60.3	91.4
140.12	.085	.21E-01	.27E+00	146.71	1.10	51.40	103.59	58.15	2.02	2.94	1.65	141.6	9.6	60.3	93.4
141.12	.085	.24E-02	.34E-02	17.03	.01	5.75	1.28	1.04	.22	1.00	.18	141.6	11.1	80.4	99.2
177.24	.085	.38E-02	.21E-01	26.94	.09	9.01	7.57	5.46	.86	1.26	.46	141.6	15.5	87.6	96.5
178.24	.085	.38E-02	.34E-02	26.93	.01	8.89	1.19	1.12	.13	1.26	.18	141.6	15.8	95.3	99.6
179.24	.085	.55E-02	.51E-01	39.00	.20	13.40	18.46	12.46	1.38	1.52	.71	141.6	12.8	71.7	94.1
180.24	.085	.71E-02	.83E-01	51.05	.33	17.72	30.76	18.36	1.74	1.73	.91	141.6	11.8	66.9	95.0
181.24	.085	.96E-02	.11E+00	68.62	.44	23.66	40.53	26.65	1.71	2.01	1.04	141.6	11.6	69.7	95.0
182.24	.085	.13E-01	.14E+00	89.70	.55	31.11	50.60	31.26	1.63	2.30	1.17	141.6	11.3	65.9	96.5

183.24	.085	.16E-01	.16E+00	115.17	.66	39.73	61.13	40.17	1.54	2.60	1.28	141.6	11.1	69.5	95.9
184.24	.085	.18E-01	.19E+00	130.20	.77	44.51	71.32	51.11	1.60	2.77	1.38	141.6	11.1	74.8	95.5
185.24	.085	.19E-01	.22E+00	138.22	.88	47.94	81.96	51.13	1.71	2.85	1.48	141.6	10.6	66.4	97.0
186.24	.085	.21E-01	.24E+00	143.31	.98	51.76	91.44	58.12	1.77	2.97	1.56	141.6	10.3	67.3	87.1
187.24	.085	.23E-01	.27E+00	165.56	1.10	57.77	101.83	59.21	1.76	3.12	1.65	141.6	11.1	62.7	95.3
188.00	.085	.34E-02	.21E-01	24.12	.09	8.02	7.81	8.96	.97	1.19	.46	141.6	12.8	90.5	97.9
189.00	.085	.70E-02	.51E-01	49.64	.20	16.41	18.82	17.57	1.15	1.71	.71	141.6	11.1	94.1	84.2
190.00	.085	.11E-01	.82E-01	79.06	.33	26.17	29.65	27.42	1.13	2.16	.90	141.5	13.0	93.4	86.9
191.00	.085	.14E-01	.11E+00	103.28	.44	34.30	40.19	36.26	1.17	2.47	1.04	141.6	12.3	91.4	88.8
192.00	.085	.19E-01	.14E+00	132.89	.55	44.21	50.38	44.92	1.14	2.30	1.17	141.6	12.1	90.5	70.0
193.00	.085	.13E-01	.16E+00	95.87	.66	33.46	60.62	34.85	1.81	2.38	1.28	141.6	11.8	62.5	35.3
194.00	.085	.21E-01	.18E+00	153.17	.66	51.46	60.79	50.43	1.18	3.00	1.28	141.6	11.6	84.3	81.5
195.00	.085	.14E-01	.19E+00	102.23	.77	35.99	70.93	36.80	1.97	2.45	1.38	141.6	11.6	57.4	31.1
196.00	.085	.22E-01	.19E+00	158.51	.77	53.74	71.32	54.98	1.33	3.06	1.38	141.6	11.1	79.6	49.4
197.00	.085	.14E-01	.22E+00	103.43	.88	36.76	82.19	37.88	2.24	2.47	1.48	141.6	10.3	51.7	29.4
198.00	.085	.15E-01	.25E+00	103.69	.99	37.05	92.21	38.98	2.49	2.47	1.57	141.6	10.6	48.4	29.8
199.00	.085	.15E-01	.27E+00	103.85	1.10	37.92	103.02	27.18	2.72	2.47	1.65	141.6	10.1	33.8	29.1
200.12	.085	.21E-02	.34E-02	14.88	.01	5.07	1.25	.92	.25	.94	.18	141.6	11.3	76.2	99.4
201.12	.085	.32E-02	.21E-01	22.70	.09	7.70	7.79	5.94	1.01	1.16	.46	141.6	13.0	79.4	95.0
202.12	.085	.58E-02	.31E-01	41.19	.20	14.07	18.61	13.38	1.32	1.56	.71	141.6	12.1	75.4	87.3
203.12	.085	.84E-02	.83E-01	60.16	.33	20.74	30.71	20.32	1.48	1.88	.91	141.6	11.3	70.0	83.7
204.12	.085	.10E-01	.11E+00	71.82	.43	25.00	39.32	23.40	1.60	2.02	1.04	141.6	11.3	64.7	88.3

205.12	.085	.12E-01	.13E+00	83.59	.54	29.25	49.99	28.04	1.71	2.22	1.16	141.6	11.3	61.1	85.4
206.12	.085	.13E-01	.16E+00	93.18	.66	32.64	60.96	33.70	1.87	2.34	1.29	141.6	11.3	60.1	84.9
207.12	.085	.14E-01	.19E+00	97.96	.77	34.50	71.72	37.40	2.08	2.40	1.38	141.6	10.6	57.2	81.3
208.12	.085	.14E-01	.22E+00	101.88	.88	35.72	81.51	44.72	2.28	2.45	1.48	141.6	11.1	59.9	84.4
209.12	.085	.15E-01	.25E+00	107.81	.99	38.38	91.70	40.86	2.39	2.52	1.57	141.6	11.1	58.7	80.1
210.12	.085	.15E-01	.27E+00	107.81	1.10	38.38	101.89	45.40	2.66	2.52	1.65	141.6	11.1	58.7	80.1
211.24	.085	.27E-02	.34E-02	19.20	.01	6.56	1.19	.84	.18	1.06	.18	141.6	15.8	75.0	98.4
212.24	.085	.33E-02	.21E-01	23.37	.09	7.33	7.42	5.55	.94	1.17	.46	141.6	17.2	79.1	93.8
213.24	.085	.52E-02	.49E-01	37.39	.20	12.78	17.43	12.34	1.37	1.48	.70	141.6	15.3	75.0	93.4
214.24	.085	.78E-02	.83E-01	55.63	.33	20.18	29.77	8.64	1.48	1.81	.91	141.6	14.0	39.0	50.1
215.24	.085	.98E-02	.11E+00	70.27	.43	24.47	39.25	23.03	1.60	2.03	1.04	141.6	12.8	64.0	17.2
216.24	.085	.12E-01	.14E+00	85.44	.55	29.81	50.52	28.18	1.69	2.24	1.17	141.6	11.8	62.7	96.2
217.24	.085	.13E-01	.16E+00	93.19	.66	32.84	60.62	30.87	1.85	2.34	1.28	141.6	11.8	56.7	97.9
218.24	.085	.15E-01	.19E+00	104.91	.77	37.00	71.32	36.23	1.93	2.49	1.38	141.6	11.1	56.2	97.9
219.24	.085	.16E-01	.22E+00	111.69	.88	39.46	81.06	40.06	2.05	2.56	1.48	141.6	11.6	55.3	97.5
220.24	.085	.18E-01	.25E+00	115.51	.99	41.15	91.45	48.11	2.22	2.61	1.57	141.6	11.1	58.2	95.6

Subroutine PHIS2

a) General Description: To estimate the specific volumn, enthalpy, and entropy of saturated and/or superheated steam.

b) Computational Procedure : The equations and constants used in this subroutine are described in ASME Steam Tables, 3rd edition.

c) Usage

1) Calling Sequence : CALL PHIS2(T,P,ID,V,S,H)

2) Arguments :

ID =	1 (SI Unit)	2 (English Unit)
T	K	^{o}F
P	kPa	psi
V	m^3/kg	ft^3/lb_m
S	kJ/kg.K	$Btu/lb_m\ ^{o}R$
H	kJ/kg	Btu/lbm

d) Required Subroutines & Storage & Tapes : None

```
      PROGRAM WEE2       74/4    OPT=1 TRACE                FTN 4.6+460        10/03/79  19.41.47       PAGE     1

 1                PROGRAM WEE2(INPUT,OUTPUT,TAPE 99)
                  DIMENSION AI(4),PER(10)
                  DIMENSION AS(10),ALS(10)
                  REAL JX0(300),JY0(300),JX12(100),JY12(100),JX24(100),JY24(100)
 5                DIMENSION EX0(300),EY0(300),EX12(100),EY12(100),EX24(100),
                 AEY24(100)
                  DIMENSION VX0(300),VY0(300),VX12(100),VY12(100),VX24(100),
                 AVY24(100)
                  DIMENSION EX27(90),EY27(90),EX28(90),EY28(90),EX29(90),EY29(90)
10                DIMENSION VX27(90),VY27(90),VX28(90),VY28(90),VX29(90),VY29(90)
                  REAL JGS,JLS,JGA,JLA,JGM,JGSC
                  REAL JX27(90),JY27(90),JX28(90),JY28(90),JX29(90),JY29(90)
                  DATA DH,DT/.0094,.176/
                  DATA(PER(I),I=1,5)/.423,.254,.141,.085,.000/
15                DATA (A(I),I=1,4)/.013607,.0063684,.0046692,.0027961/
                  DATA(AS(I),I=1,6)/.413,.413,.413,.413,.187,.125/
                  DATA (ALS(I),I=1,6)/101.6,108.7,60.3,36.1,146.4,65.9/
                  N1=0
                  N2=0
20                N3=0
                1 I=0
                  PRINT 6
                6 FORMAT(/4X,*RUN   PER   HS,KG/S  WL,KG/S  VGH,M/S  VLH,M/S  *,
                 A,*EHG,KW      EHL,KW      EHLO      REH       JGS       JLS       TSC *,
25               B*  TLC    TLOC   TLPC*)
                  KQ=3
                  KQ=1
                2 READ*,VIS,VPS,VHS,VIG,VPG,WL,VTL,IP,RUN,VTLO,VTP,WLL
                  IF(VIS.GE.10.) GO TO 2
30                IF(VIS.LE.0.) GO TO 2
                  IF(VIS.LE.0.) GO TO 800
                  IF(VIS.GE.100.) GO TO 890
                  RX=.4110*.0361*WL-.1042E-2*WL*WL
                  IF(WL.GE.20.) RX=.724
35                IF(RX.GE.0.724) RX=.724
                  WL=(RX*WL+WLL)760.
                  I=I+1
                  IF(VIS.GE.60.) GO TO 21
                  IF(VIS.GE.50.) GO TO 21
40                IF(VIS.GE.45.) GO TO 19
                  IF(VIS.GE.35.) GO TO 17
                  IF(VIS.GE.24.) GO TO 15
                  IF(VIS.GE.12.) GO TO 10
                  GO TO 20
45             10 KQ=2
                  KS=1
                  I2=I+1
                  EX0(I)=0.
                  EY0(I)=0.
50                EX0(I2)=20.
                  EY0(I2)=20.
                  VX0(I)=0.
                  VY0(I)=0.
                  VX0(I2)=0.2
55                VY0(I2)=40.
                  JX0(I)=0.
                  JY0(I)=0.
                  JX0(I2)=1.
                  JX0(I2)=.25
60                JX0(I2)=0.125
                  JY0(I2)=.5
                  JY0(I2)=1.
                  JY0(I2)=.25
                  N1=I-1
65                I=0
                  GO TO 2
               15 KQ=3
                  KS=2
                  I2=I+1
70                EX12(I)=0.
                  EY12(I)=0.
                  EX12(I2)=20.
                  EY12(I2)=20.
                  VX12(I)=0.
75                VY12(I)=0.
                  VX12(I2)=0.2
                  VY12(I2)=40.
                  JX12(I)=0.
                  JY12(I)=0.
```

```
      JX12(I2)=1.
      JX12(I2)=.25
      JX12(I2)=0.125
      JY12(I2)=.5
      JY12(I2)=1.
      JY12(I2)=.25
      N2=I-1
      I=0
      GO TO 2
   17 I2=I+1
      EX24(I)=0.
      EY24(I)=0.
      EX24(I2)=20.
      EY24(I2)=20.
      VY24(I)=0.
      VX24(I)=0.
      VX24(I2)=0.2
      VY24(I2)=40.
      JX24(I)=0.
      JY24(I)=0.
      JX24(I2)=0.125
      JX24(I2)=1.
      JX24(I2)=0.5
      JX24(I2)=.25
      JY24(I2)=2.0
      JY24(I2)=1.
      JY24(I2)=.5
      JY24(I2)=.25
      KS=3
      NJ=I-1
      KQ=4
      I=0
      GO TO 2
   19 KQ=5
      KS=4
      I2=I+1
      EX27(I)=0.
      EY27(I)=0.
      EX27(I2)=20.
      EY27(I2)=20.
      VX27(I)=0.
      VY27(I)=0.
      VX27(I2)=0.2
      VY27(I2)=40.
      JX27(I)=0.
      JY27(I)=0.
      JX27(I2)=0.125
      JX27(I2)=1.
      JX27(I2)=0.5
      JX27(I2)=0.25
      JY27(I2)=2.
      JY27(I2)=1.
      JY27(I2)=.5
      JY27(I2)=.25
      N4=I-1
      I=0
      GO TO 2
   21 KQ=6
      KS=5
      I2=I+1
      EX20(I)=0.
      EY20(I)=0.
      EX20(I2)=20.
      EY20(I2)=20.
      VX20(I)=0.
      VY20(I)=0.
      VX20(I2)=0.2
      VY20(I2)=40.
      JX20(I)=0.
      JY20(I)=0.
      JX20(I2)=0.125
      JX20(I2)=1.
      JX20(I2)=0.5
      JX20(I2)=0.25
      JY20(I2)=2.
      JY20(I2)=1.
      JY20(I2)=.5
      JY20(I2)=.25
      N5=I-1
```

223.00	.423	.35E-01	.34E+00	50.73	.27	86.02	122.54	86.62	1.41	1.40	.67	141.4	12.8	74.6	92.
224.00	.423	.37E-01	.37E+00	53.48	.29	90.86	133.40	90.92	1.47	1.44	.69	145.1	12.6	72.1	92.6
225.00	.423	.39E-01	.39E+00	55.85	.31	95.35	142.11	92.15	1.49	1.47	.72	145.1	12.6	69.3	91.0
226.00	.423	.34E-01	.41E+00	48.94	.33	84.89	150.01	82.38	1.77	1.38	.74	144.3	12.6	60.8	80.1
227.00	.423	.33E-01	.43E+00	47.44	.35	82.76	158.31	79.53	1.91	1.35	.76	145.1	12.6	56.5	76.8
229.00	.423	.33E-01	.50E+00	47.10	.40	81.72	183.22	78.60	2.25	1.35	.81	145.1	12.6	53.6	74.8
230.00	.423	.29E-01	.54E+00	42.36	.43	75.23	197.06	72.39	2.62	1.28	.84	145.3	12.6	44.7	56.7
231.00	.423	.33E-01	.58E+00	47.14	.47	83.70	212.50	80.83	2.54	1.35	.87	145.1	12.3	45.7	60.1
232.00	.423	.36E-01	.62E+00	51.80	.49	92.08	225.37	83.82	2.45	1.42	.90	145.1	12.3	44.9	57.9
233.00	.423	.36E-01	.65E+00	51.50	.52	91.48	237.90	88.98	2.60	1.41	.93	145.1	12.8	45.4	58.4
601.00	.423	.19E-01	.21E-01	27.89	.02	45.45	7.77	7.72	.17	1.04	.17	141.6	13.3	99.4	99.1
602.00	.423	.21E-01	.40E-01	29.67	.03	48.32	14.39	14.29	.30	1.07	.21	141.9	13.0	99.4	99.1
608.00	.423	.35E-01	.27E+00	50.48	.22	84.04	98.19	83.97	1.17	1.40	.60	141.6	12.6	87.3	95.3
609.00	.423	.32E-01	.25E+00	45.88	.20	76.29	90.17	77.86	1.18	1.33	.57	141.6	12.6	88.1	94.6
610.00	.423	.25E-01	.19E+00	36.03	.15	59.75	68.93	62.18	1.15	1.18	.50	139.7	12.6	91.4	92.9
611.00	.423	.22E-01	.14E+00	31.26	.11	50.84	50.10	49.47	.99	1.10	.43	143.4	12.6	98.9	97.5
612.00	.423	.21E-01	.82E-01	30.58	.07	49.69	29.85	23.48	.60	1.09	.33	143.3	12.6	98.9	98.7
613.00	.423	.27E-01	.22E+00	38.76	.17	64.58	78.15	67.25	1.21	1.23	.53	141.6	12.6	88.9	94.1
614.00	.423	.22E-01	.15E+00	31.80	.12	52.07	55.11	53.05	1.06	1.11	.45	141.6	12.6	96.7	95.8
615.00	.423	.24E-01	.18E+00	34.41	.13	56.17	68.11	56.88	1.07	1.15	.47	145.1	12.6	95.3	96.6
616.00	.423	.23E-01	.11E+00	33.20	.09	53.87	40.08	39.69	.74	1.13	.38	144.5	12.6	99.1	98.9
617.00	.423	.22E-01	.51E-01	31.67	.04	51.47	18.51	18.33	.36	1.11	.28	145.6	12.6	99.1	99.1

644.00	.423	.52E-01	.44E+00	75.28	.35	127.60	159.37	117.39	1.25	1.71	.76	141.6	12.6	77.0	97.7
645.00	.423	.55E-01	.48E+00	78.33	.38	132.69	174.21	129.29	1.31	1.74	.79	141.6	12.6	77.5	98.7
646.00	.423	.40E-01	.51E+00	57.78	.41	101.33	187.04	94.47	1.85	1.50	.82	141.6	12.6	56.7	77.8
653.00	.423	.42E-01	.60E+00	59.70	.48	105.34	219.73	101.90	2.09	1.57	.49	141.6	12.6	53.1	85.6
652.00	.423	.44E-01	.66E+00	63.05	.53	111.79	240.58	103.33	2.15	1.50	.93	141.6	12.6	50.1	59.1
648.00	.423	.58E-01	.51E+00	82.58	.41	139.83	187.04	138.81	1.34	1.73	.82	141.6	12.6	77.5	96.3
650.00	.423	.63E-01	.56E+00	90.40	.45	153.10	204.99	152.14	1.34	1.37	.86	141.6	12.6	77.5	96.3
651.00	.423	.83E-01	.80E+00	90.40	.48	148.77	219.73	205.47	1.48	1.87	.89	141.2	12.8	94.3	73.6
690.00	.423	.33E-01	.27E+00	46.73	.22	77.93	93.34	83.73	1.27	1.35	.60	141.6	13.3	86.4	95.3
691.00	.423	.42E-01	.35E+00	59.65	.28	99.92	126.78	102.98	1.27	1.52	.68	141.6	13.3	84.7	97.3
692.00	.423	.44E-01	.39E+00	63.11	.31	106.53	140.11	106.69	1.32	1.57	.72	141.6	13.5	79.4	95.8
693.00	.423	.45E-01	.43E+00	64.11	.35	110.20	155.85	98.85	1.41	1.58	.75	141.6	13.3	68.3	86.1
694.00	.423	.41E-01	.52E+00	58.49	.41	101.60	186.48	105.61	1.84	1.51	.82	141.6	13.5	62.5	74.6
695.00	.423	.29E-01	.84E+00	41.58	.52	73.71	232.13	95.54	3.15	1.27	.92	141.6	13.5	43.1	56.5
696.00	.423	.29E-01	.98E+00	41.01	.46	73.42	208.52	73.89	2.84	1.26	.87	141.6	13.5	44.2	57.0
697.00	.423	.29E-01	.47E+00	41.01	.38	72.61	171.93	74.19	2.36	1.25	.79	141.6	13.5	50.9	61.1
698.00	.423	.45E-01	.43E+00	65.27	.35	110.85	156.39	112.55	1.41	1.59	.76	141.6	13.5	75.8	93.8
699.00	.423	.45E-01	.38E+00	64.65	.31	108.44	137.99	110.77	1.27	1.58	.71	141.6	13.5	83.0	95.5
256.04	.423	.25E-01	.14E+00	35.87	.11	58.49	49.81	48.77	.85	1.10	.43	142.6	13.0	93.2	98.9
257.04	.423	.26E-01	.17E+00	37.00	.13	60.43	60.77	58.83	1.01	1.20	.47	142.6	13.0	97.2	98.9
258.04	.423	.27E-01	.19E+00	36.37	.16	63.21	70.14	64.20	1.11	1.22	.50	142.6	13.0	92.6	98.9
259.04	.423	.26E-01	.22E+00	37.77	.18	62.61	79.70	71.41	1.27	1.21	.54	142.6	13.0	91.0	98.9

260.04	.423	.26E-01	.25E+00	37.79	.20	63.45	90.66	72.93	1.43	1.21	.57	141.2	13.8	83.9	98.7
901.04	.423	.16E-01	.27E-01	23.28	.02	37.95	9.56	9.47	.25	.35	.19	141.6	14.8	99.1	98.9
902.04	.423	.21E-01	.44E-01	29.90	.04	48.75	15.84	15.68	.32	1.08	.24	141.6	14.8	99.1	98.9
903.04	.423	.22E-01	.63E-01	31.06	.05	50.61	22.43	22.27	.44	1.10	.29	141.6	15.0	99.4	99.4
904.04	.423	.23E-01	.82E-01	32.76	.07	53.38	29.01	28.80	.54	1.13	.33	141.6	15.0	99.4	99.4
905.04	.423	.23E-01	.10E+00	33.59	.08	54.84	35.88	35.20	.67	1.14	.37	141.6	15.0	98.4	99.1
906.04	.423	.25E-01	.19E+00	35.62	.15	59.38	68.15	57.41	1.15	1.18	.50	141.6	15.0	86.6	98.9
907.04	.423	.27E-01	.25E+00	39.06	.20	65.41	88.60	71.87	1.35	1.23	.57	141.6	15.0	84.0	98.9
908.04	.423	.23E-01	.13E+00	33.07	.10	53.96	46.34	45.62	.86	1.13	.41	141.6	15.0	98.7	98.7
910.04	.423	.27E-01	.22E+00	38.79	.18	64.47	78.08	67.33	1.21	1.23	.54	141.6	15.0	98.7	98.9
911.04	.423	.23E-01	.16E+00	32.62	.13	53.44	56.47	54.14	1.06	1.13	.46	141.6	15.0	96.5	99.1
912.04	.423	.27E-01	.28E+00	38.62	.22	65.03	99.60	77.19	1.53	1.22	.61	141.6	14.8	80.8	98.9
913.04	.423	.31E-01	.35E+00	44.71	.28	76.12	123.87	86.54	1.63	1.32	.68	141.6	14.8	74.3	98.9
914.04	.423	.34E-01	.39E+00	48.34	.31	82.64	138.68	92.83	1.68	1.37	.72	141.6	15.0	71.9	98.9
915.04	.423	.36E-01	.43E+00	51.02	.34	87.69	151.15	95.61	1.72	1.41	.75	141.6	15.0	69.8	98.7
916.04	.423	.35E-01	.47E+00	49.97	.37	86.73	165.74	93.55	1.91	1.39	.78	141.6	15.0	63.0	98.7
917.04	.423	.35E-01	.50E+00	50.50	.40	88.00	177.07	94.93	2.01	1.40	.81	141.6	15.0	60.5	98.9
918.04	.423	.35E-01	.54E+00	50.40	.43	88.44	191.43	93.42	2.17	1.40	.84	141.6	15.0	56.5	98.7
919.04	.423	.36E-01	.58E+00	51.05	.46	89.76	204.94	97.08	2.28	1.41	.87	141.6	15.0	55.3	98.9
920.04	.423	.36E-01	.62E+00	51.08	.49	89.98	219.02	100.38	2.43	1.41	.90	141.6	14.8	54.1	98.9
921.04	.423	.37E-01	.66E+00	53.10	.53	94.02	235.73	99.62	2.51	1.44	.94	141.6	15.0	50.9	98.9
7.12	.423	.24E-01	.22E+00	34.48	.18	59.71	85.59	60.75	1.48	1.17	.54	141.6	6.6	72.9	99.1

8.12	.423	.21E-01	.16E+00	30.62	.13	51.27	64.19	53.17	1.25	1.09	.47	141.6	6.6	84.0	99.1
9.12	.423	.21E-01	.11E+00	30.53	.09	49.78	42.68	42.29	.86	1.09	.38	141.6	6.9	99.1	99.4
10.12	.423	.20E-01	.82E-01	28.68	.07	46.77	31.71	31.33	.68	1.06	.33	141.6	7.1	98.9	99.1
11.12	.423	.19E-01	.51E-01	27.81	.04	45.04	19.55	19.32	.43	1.04	.26	141.6	7.6	98.9	118.4
73.12	.423	.17E-01	.34E-02	24.37	.00	39.73	1.23	1.21	.03	.97	.07	141.6	13.3	99.1	.2
74.12	.423	.18E-01	.21E-01	25.53	.02	41.62	7.77	7.60	.19	1.00	.17	141.6	13.3	99.1	.2
75.12	.423	.18E-01	.33E-01	25.51	.03	41.61	12.02	11.87	.29	1.00	.21	141.6	11.6	98.9	.2
77.12	.423	.22E-01	.93E-01	30.92	.07	50.47	35.03	34.41	.69	1.10	.35	141.6	10.1	98.4	.2
76.12	.423	.20E-01	.63E-01	29.22	.05	47.68	23.48	23.12	.49	1.07	.29	141.6	11.1	98.7	.2
78.12	.423	.23E-01	.12E+00	33.45	.10	54.62	45.45	44.54	.83	1.14	.40	141.6	9.8	98.2	.2
79.12	.423	.23E-01	.16E+00	33.70	.13	55.27	58.68	55.93	1.06	1.14	.45	141.6	9.8	95.8	.2
80.12	.423	.25E-01	.20E+00	35.48	.16	59.53	75.20	68.58	1.26	1.17	.51	141.6	9.3	87.1	.2
81.12	.423	.26E-01	.23E+00	36.67	.18	62.30	87.49	83.93	1.40	1.19	.55	141.6	9.1	79.5	.2
82.12	.423	.27E-01	.27E+00	38.54	.22	65.73	103.74	73.33	1.58	1.22	.60	141.6	9.1	73.4	.2
249.12	.423	.17E-01	.21E-01	24.70	.02	40.24	7.77	7.67	.19	.98	.17	142.4	13.3	98.9	99.4
250.12	.423	.18E-01	.34E-01	26.58	.03	43.18	12.24	12.09	.28	1.01	.21	144.1	13.0	98.9	99.1
259.12	.423	.27E-01	.19E+00	38.36	.15	64.35	69.94	54.17	1.09	1.22	.50	144.1	12.8	80.3	98.9
260.12	.423	.27E-01	.22E+00	38.36	.18	65.62	78.93	64.78	1.23	1.23	.54	144.4	12.8	83.5	99.1
261.12	.423	.27E-01	.25E+00	38.58	.20	65.44	89.92	62.60	1.37	1.22	.57	144.6	12.8	73.6	99.1
262.12	.423	.26E-01	.27E+00	38.21	.22	65.46	99.91	62.75	1.53	1.22	.60	144.4	12.8	67.6	99.1
263.12	.423	.27E-01	.27E+00	38.91	.22	66.58	98.51	63.48	1.48	1.23	.60	144.1	13.0	69.0	99.1
264.12	.423	.27E-01	.31E+00	39.24	.25	68.15	111.34	60.09	1.66	1.24	.64	144.1	13.0	93.1	98.9

265.12	.423	.28E-01	.35E+00	39.80	.28	69.38	127.15	84.21	1.83	1.24	.69	146.1	13.0	97.0	99.9
266.12	.423	.28E-01	.39E+00	40.15	.31	70.71	140.91	61.01	1.99	1.25	.72	145.1	13.0	90.7	98.9
680.12	.423	.26E-01	.27E+00	37.48	.22	64.87	98.78	58.86	1.52	1.21	.60	141.2	13.8	85.2	99.1
681.12	.423	.28E-01	.35E+00	39.87	.28	69.17	126.97	70.14	1.84	1.24	.68	143.6	13.5	81.3	98.9
682.12	.423	.27E-01	.48E+00	38.95	.38	68.94	172.05	70.12	2.50	1.23	.79	144.1	13.3	48.6	99.1
683.12	.423	.27E-01	.64E+00	39.08	.52	70.57	231.73	60.94	3.28	1.23	.92	144.1	13.5	38.3	99.1
684.12	.423	.27E-01	.59E+00	38.91	.47	70.00	212.09	62.25	3.03	1.23	.88	143.9	13.3	38.7	99.1
685.12	.423	.27E-01	.54E+00	38.72	.43	69.49	193.31	59.11	2.78	1.22	.84	144.1	13.5	40.8	99.1
686.12	.423	.27E-01	.50E+00	38.88	.40	69.63	181.67	59.54	2.61	1.23	.81	143.8	13.3	41.7	98.9
687.12	.423	.27E-01	.43E+00	38.50	.35	68.36	155.87	61.47	2.24	1.22	.75	143.1	13.5	47.6	98.9
688.12	.423	.27E-01	.39E+00	39.07	.31	68.60	140.11	64.50	2.04	1.23	.72	144.3	13.5	51.3	99.1
689.12	.423	.29E-01	.31E+00	41.59	.25	72.10	113.05	64.80	1.57	1.27	.64	142.4	13.3	63.0	99.1
675.12	.423	.23E-01	.16E+00	32.90	.13	56.68	59.44	50.40	1.09	1.13	.47	143.1	13.5	86.9	99.1
674.12	.423	.24E-01	.15E+00	34.33	.12	58.34	53.53	49.09	.95	1.15	.44	144.3	13.5	92.9	99.1
673.12	.423	.27E-01	.22E+00	38.85	.18	65.01	80.24	65.80	1.23	1.23	.54	141.6	13.5	84.4	99.1
672.12	.423	.21E-01	.11E+00	30.84	.09	50.41	38.92	37.34	.77	1.04	.38	142.9	13.5	96.5	99.1
660.12	.423	.17E-01	.21E-01	24.80	.02	40.48	7.84	7.70	.19	.98	.17	141.6	12.6	98.4	98.7
661.12	.423	.23E-01	.11E+00	33.31	.09	54.45	40.08	39.02	.74	1.14	.38	141.6	12.6	97.7	99.1
662.12	.423	.19E-01	.51E-01	26.79	.04	43.73	18.51	18.17	.43	1.02	.25	141.6	12.6	98.4	98.7
663.12	.423	.18E-01	.35E-01	25.57	.03	41.71	12.99	12.83	.31	1.00	.22	141.6	12.3	98.9	99.1
664.12	.423	.20E-01	.66E-01	28.28	.05	46.14	24.30	23.93	.53	1.05	.30	141.6	12.3	98.7	99.1
665.12	.423	.22E-01	.93E-01	31.38	.07	51.29	34.15	33.77	.77	1.10	.35	141.6	12.3	97.7	98.9

666.12	.423	.28E-01	.19E+00	39.49	.15	65.26	70.33	63.46	1.08	1.24	.56	141.6	12.3	96.3	98.9
667.12	.423	.20E-01	.78E-01	28.43	.06	46.60	28.61	27.38	.61	1.05	.32	141.6	12.3	96.3	98.9
668.12	.423	.24E-01	.14E+00	33.81	.11	55.43	50.24	47.56	.91	1.15	.43	141.6	12.3	95.3	98.9
669.12	.423	.26E-01	.16E+00	37.67	.13	61.83	60.28	57.05	.97	1.21	.47	141.6	12.3	95.3	98.9
767.12	.423	.18E-01	.21E-01	25.64	.02	41.92	6.57	6.52	.16	1.00	.17	133.7	26.6	99.4	99.4
768.12	.423	.21E-01	.51E-01	30.49	.04	49.73	14.74	14.61	.30	1.09	.26	141.6	30.3	94.9	99.4
769.12	.423	.22E-01	.82E-01	30.88	.07	50.41	23.95	23.41	.47	1.10	.33	141.6	29.8	98.4	99.6
770.12	.423	.22E-01	.11E+00	31.27	.09	51.00	31.27	30.78	.61	1.10	.37	141.6	29.8	98.9	99.4
771.12	.423	.22E-01	.14E+00	31.94	.11	52.27	40.19	38.46	.77	1.11	.43	141.6	29.8	97.0	99.4
772.12	.423	.22E-01	.16E+00	31.56	.13	52.20	48.39	42.17	.93	1.11	.47	141.6	29.6	91.0	98.7
773.12	.423	.23E-01	.19E+00	33.24	.15	54.68	55.74	51.03	1.02	1.14	.50	141.6	30.1	94.1	99.1
774.12	.423	.24E-01	.22E+00	34.97	.18	57.98	64.30	55.56	1.11	1.17	.54	141.6	29.8	90.5	98.9
775.12	.423	.25E-01	.25E+00	35.49	.20	59.63	73.08	54.42	1.23	1.17	.57	141.6	29.6	82.0	98.9
776.12	.423	.27E-01	.28E+00	38.53	.22	64.89	81.30	61.11	1.26	1.22	.60	141.6	29.6	82.5	99.1
777.12	.423	.28E-01	.35E+00	39.88	.28	67.85	103.75	66.61	1.53	1.24	.68	141.6	29.6	74.8	98.9
779.12	.423	.27E-01	.41E+00	39.04	.33	67.16	120.13	66.03	1.73	1.23	.73	141.6	29.6	68.3	98.9
780.12	.423	.28E-01	.48E+00	39.80	.38	69.12	140.45	66.13	2.03	1.24	.79	141.6	29.6	62.7	99.1
781.12	.423	.28E-01	.55E+00	40.29	.44	70.25	160.13	69.62	2.28	1.25	.85	141.6	29.8	60.3	99.1
782.12	.423	.28E-01	.62E+00	40.74	.50	71.54	182.77	68.53	2.53	1.26	.91	141.6	29.6	56.0	99.1
784.12	.423	.24E-01	.28E+00	34.74	.22	57.84	61.21	46.61	1.06	1.16	.60	141.6	46.3	87.1	98.3
785.12	.423	.22E-01	.24E+00	31.81	.20	52.68	53.90	45.41	1.02	1.11	.57	140.2	47.1	91.7	98.9
786.12	.423	.22E-01	.22E+00	32.24	.18	52.64	47.77	44.55	.91	1.12	.54	141.6	47.9	96.5	98.9

787.12	.423	.22E-01	.19E+00	31.63	.16	51.82	42.63	37.67	.82	1.11	.60	144.1	47.1	93.3	99.4
788.12	.423	.23E-01	.16E+00	32.70	.13	53.19	34.24	33.05	.64	1.13	.45	144.1	47.4	98.2	99.6
789.12	.423	.21E-01	.12E+00	30.78	.10	50.08	27.11	26.07	.54	1.09	.40	144.1	47.1	97.9	99.5
790.12	.423	.21E-01	.85E-01	29.77	.07	48.35	19.05	18.66	.39	1.07	.33	144.1	46.9	98.3	99.1
791.12	.423	.18E-01	.41E-01	26.02	.03	42.20	8.93	8.73	.21	1.00	.23	144.1	47.6	99.1	99.4
792.12	.423	.25E-01	.35E+00	36.34	.28	60.66	75.52	55.07	1.25	1.13	.68	141.6	47.9	85.3	99.1
793.12	.423	.25E-01	.42E+00	35.84	.34	60.75	94.72	54.02	1.56	1.18	.75	141.6	46.4	77.0	99.6
794.12	.423	.27E-01	.51E+00	38.13	.41	64.92	113.65	56.43	1.75	1.22	.82	141.6	47.1	74.3	99.1
795.12	.423	.26E-01	.56E+00	38.00	.45	65.09	124.44	55.46	1.91	1.21	.86	141.6	47.1	70.7	99.1
796.12	.423	.25E-01	.44E+00	35.26	.35	58.97	73.26	51.21	1.34	1.17	.76	141.6	56.7	84.7	99.1
797.12	.423	.25E-01	.36E+00	35.18	.29	58.84	64.20	52.80	1.11	1.17	.69	141.6	57.2	92.4	98.7
798.12	.423	.24E-01	.32E+00	34.26	.26	56.56	57.98	47.41	1.03	1.15	.65	141.6	57.0	92.7	98.7
799.12	.423	.21E-01	.26E+00	30.59	.21	50.51	46.93	38.26	.93	1.09	.58	141.6	56.2	91.9	98.9
670.12	.423	.21E-01	.22E+00	29.57	.18	48.57	39.67	35.13	.82	1.07	.54	141.5	56.7	95.0	99.4
671.12	.423	.20E-01	.17E+00	29.07	.14	47.48	30.79	29.51	.65	1.06	.47	141.6	56.2	98.2	99.4
672.12	.423	.20E-01	.11E+00	28.28	.09	46.11	19.83	19.33	.43	1.05	.38	141.6	56.7	98.9	99.4
673.12	.423	.20E-01	.51E-01	28.54	.04	46.56	9.01	8.72	.19	1.05	.26	141.6	57.4	98.7	99.4
674.12	.423	.19E-01	.63E-01	27.18	.05	44.30	7.54	7.36	.17	1.03	.22	141.6	71.4	99.4	99.4
675.12	.423	.20E-01	.11E+00	28.27	.09	46.11	12.65	12.15	.27	1.05	.38	141.6	72.4	99.0	99.4
676.12	.423	.19E-01	.18E+00	27.40	.13	44.73	17.82	16.74	.40	1.03	.47	141.6	74.1	98.4	99.4
677.12	.423	.20E-01	.22E+00	28.43	.18	46.43	24.81	23.10	.53	1.05	.54	141.6	73.6	98.2	99.4
678.12	.423	.20E-01	.28E+00	28.44	.22	46.33	30.58	27.04	.66	1.05	.61	141.6	73.8	97.8	99.4

679.12	.423	.19E-01	.31E+00	27.47	.25	45.09	35.06	28.92	.78	1.03	.64	141.6	73.1	95.3	99.1
83.24	.423	.17E-01	.21E-01	23.83	.02	38.90	7.95	7.81	.20	.96	.17	141.6	11.3	98.4	.2
84.24	.423	.18E-01	.51E-01	25.85	.04	42.17	18.82	18.59	.45	1.00	.26	141.6	11.1	98.9	.2
85.24	.423	.19E-01	.82E-01	27.75	.07	45.24	30.52	30.07	.67	1.04	.33	141.6	10.8	98.7	.2
86.24	.423	.20E-01	.11E+00	28.97	.09	47.29	41.21	40.49	.87	1.06	.39	141.6	10.1	98.6	.2
87.24	.423	.22E-01	.14E+00	32.24	.11	52.65	51.65	50.61	.98	1.12	.43	141.6	9.8	98.5	.3
88.24	.423	.25E-01	.16E+00	36.50	.13	59.61	61.98	60.73	1.04	1.19	.47	141.6	9.8	98.2	.2
89.24	.423	.27E-01	.19E+00	38.62	.15	63.03	72.31	68.34	1.14	1.22	.50	141.6	9.8	95.6	.3
922.24	.423	.26E-01	.27E+00	37.88	.22	65.00	97.64	62.97	1.50	1.21	.60	141.6	14.8	69.7	98.7
923.24	.423	.27E-01	.32E+00	38.94	.26	67.51	113.83	65.36	1.69	1.23	.65	141.6	14.8	63.7	98.9
924.24	.423	.27E-01	.37E+00	38.96	.29	68.15	130.01	56.19	1.91	1.23	.69	141.6	14.8	58.2	98.9
925.24	.423	.27E-01	.41E+00	38.63	.33	68.04	146.20	67.40	2.15	1.22	.74	141.6	14.8	54.1	98.9
926.24	.423	.28E-01	.46E+00	40.72	.37	71.73	162.38	74.87	2.26	1.26	.78	141.6	14.8	54.1	98.9
927.24	.423	.29E-01	.50E+00	41.86	.40	74.03	178.56	77.28	2.41	1.28	.81	141.6	14.8	51.7	98.9
928.24	.423	.28E-01	.53E+00	40.37	.43	72.02	189.35	70.27	2.63	1.25	.84	141.6	14.8	46.4	98.7
929.24	.423	.29E-01	.58E+00	41.49	.46	74.04	205.54	75.68	2.78	1.27	.87	141.6	14.8	46.2	98.7
930.24	.423	.30E-01	.66E+00	43.71	.53	78.32	235.44	79.87	3.01	1.30	.93	141.6	14.8	43.7	98.9
931.24	.423	.26E-01	.21E+00	37.58	.17	82.67	74.60	82.67	1.19	1.21	.33	141.6	14.8	86.4	98.7
932.24	.423	.22E-01	.14E+00	32.17	.11	52.66	48.82	47.09	.93	1.12	.43	141.6	14.8	97.0	98.7
930.00	.254	.83E-02	.51E-01	19.88	.07	19.47	17.84	17.76	.92	.98	.18	141.6	15.5	99.1	98.9
931.00	.254	.86E-02	.76E-01	20.46	.10	20.54	26.77	22.01	1.30	1.00	.46	141.6	15.3	84.9	94.6
932.00	.254	.18E-01	.14E+00	37.37	.18	37.69	48.68	46.58	1.29	1.16	.69	141.6	15.0	82.3	97.0

933.00	.254	.12E-01	.10E+00	26.98	.14	29.03	36.04	30.34	1.27	1.40	.54	141.6	15.0	84.3	96.7
934.00	.254	.17E-01	.15E+00	40.54	.20	40.90	52.57	41.46	1.23	1.41	.64	141.6	15.0	82.0	95.5
935.00	.254	.21E-01	.18E+00	50.83	.25	51.10	65.23	52.55	1.28	1.58	.72	141.6	15.0	81.5	97.5
936.00	.254	.25E-01	.21E+00	59.48	.29	59.73	75.94	62.25	1.27	1.71	.77	141.6	15.0	84.7	98.2
937.00	.254	.27E-01	.25E+00	64.70	.33	65.19	88.01	70.15	1.35	1.79	.83	141.6	15.0	82.8	98.2
20.00	.254	.86E-02	.21E-01	20.63	.03	20.19	7.73	7.65	.38	1.01	.24	141.6	13.8	99.1	99.1
21.00	.254	.12E-01	.51E-01	29.59	.07	28.95	18.87	18.74	.65	1.21	.38	141.6	10.8	99.4	99.4
22.00	.254	.13E-01	.82E-01	31.03	.11	30.83	31.28	29.43	1.02	1.26	.48	141.6	8.4	94.6	98.4
23.00	.254	.16E-01	.11E+00	38.80	.15	38.33	42.23	39.52	1.10	1.38	.55	141.6	7.9	96.1	98.9
24.00	.254	.20E-01	.14E+00	46.99	.18	46.71	52.64	47.18	1.13	1.52	.62	141.6	8.1	90.5	94.3
25.00	.254	.24E-01	.16E+00	57.02	.22	56.40	63.85	59.29	1.13	1.68	.68	141.6	7.1	93.4	98.7
940.00	.254	.24E-01	.21E+00	57.19	.29	57.75	75.94	59.88	1.32	1.68	.77	141.2	15.0	82.3	97.2
941.00	.254	.26E-01	.25E+00	61.35	.33	62.31	87.62	65.87	1.41	1.74	.83	140.9	15.0	78.9	97.0
942.00	.254	.27E-01	.25E+00	64.86	.33	65.87	87.62	65.87	1.33	1.79	.83	140.9	15.0	78.9	97.0
943.00	.254	.29E-01	.27E+00	70.36	.37	71.55	97.36	71.53	1.36	1.86	.87	141.6	15.0	77.5	95.8
944.00	.254	.33E-01	.32E+00	78.99	.43	80.32	113.13	83.11	1.41	1.97	.94	141.6	15.0	77.5	95.0
945.00	.254	.36E-01	.34E+00	85.14	.48	86.56	120.96	89.21	1.40	2.05	.97	141.6	15.0	77.7	94.3
946.00	.254	.41E-01	.39E+00	98.40	.52	100.07	137.29	100.97	1.37	2.20	1.04	141.6	14.8	77.5	95.3
947.00	.254	.29E-01	.41E+00	69.25	.55	72.93	147.14	71.58	2.02	1.85	1.07	141.6	14.8	96.2	82.7
948.00	.254	.29E-01	.47E+00	69.70	.63	74.00	167.23	75.21	2.26	1.96	1.14	140.4	14.8	91.1	81.5
949.00	.254	.28E-01	.51E+00	67.71	.68	72.30	181.80	72.74	2.51	1.83	1.19	141.2	14.8	98.9	84.2
950.00	.254	.30E-01	.54E+00	70.71	.72	75.13	192.05	93.57	2.56	1.97	1.23	141.6	14.8	91.1	74.0

951.00	.254	.21E-01	.58E+00	49.94	.77	54.60	205.54	45.89	3.76	1.57	1.27	141.6	14.8	33.8	47.1
952.00	.254	.20E-01	.62E+00	48.09	.82	52.66	219.02	46.36	4.15	1.54	1.31	141.6	14.8	32.8	47.4
952.00	.254	.18E-01	.62E+00	42.67	.82	46.72	219.02	46.36	4.69	1.45	1.31	141.6	14.8	32.8	47.4
954.00	.254	.45E-01	.43E+00	107.22	.57	109.08	151.59	111.05	1.39	2.30	1.09	141.6	14.8	77.2	95.3
955.00	.254	.50E-01	.46E+00	120.08	.62	121.76	165.08	124.67	1.36	2.43	1.14	141.6	14.8	79.1	95.5
956.00	.254	.55E-01	.51E+00	131.44	.68	133.11	181.26	138.43	1.36	2.54	1.19	141.6	14.8	79.9	96.5
957.00	.254	.59E-01	.54E+00	140.15	.72	142.05	192.49	145.92	1.36	2.63	1.23	141.6	14.8	79.4	97.2
958.00	.254	.60E-01	.58E+00	142.72	.77	145.37	205.54	148.83	1.41	2.65	1.27	141.6	14.8	76.5	91.1
930.00	.254	.83E-02	.51E-01	19.88	.07	19.47	17.88	17.70	.92	.99	.38	141.6	15.5	99.1	98.9
931.00	.254	.86E-02	.76E-01	20.46	.10	20.54	26.77	22.01	1.30	1.00	.46	141.6	15.3	84.3	94.6
932.00	.254	.16E-01	.14E+00	37.37	.18	37.69	48.68	38.53	1.29	1.36	.62	141.6	15.0	82.3	97.0
933.00	.254	.12E-01	.10E+00	28.98	.14	29.09	36.88	30.34	1.27	1.20	.54	141.5	15.0	84.0	96.7
934.00	.254	.17E-01	.15E+00	40.54	.20	40.90	52.57	41.46	1.29	1.41	.64	141.5	15.0	82.0	95.5
935.00	.254	.21E-01	.18E+00	50.83	.25	51.15	65.23	52.55	1.28	1.58	.72	141.6	15.0	81.5	97.5
936.00	.254	.25E-01	.21E+00	59.48	.29	59.73	75.94	62.25	1.27	1.71	.77	141.6	15.0	84.7	98.2
937.00	.254	.27E-01	.25E+00	64.70	.33	65.15	88.01	70.15	1.35	1.79	.83	141.6	15.0	82.8	98.2
20.00	.254	.86E-02	.21E-01	20.63	.03	20.19	7.73	7.65	.38	1.01	.24	141.6	13.8	99.1	99.1
21.00	.254	.12E-01	.51E-01	29.59	.07	28.96	18.87	18.74	.65	1.21	.38	141.6	10.8	93.4	98.4
22.00	.254	.13E-01	.82E-01	31.03	.11	30.63	31.28	29.43	1.02	1.24	.48	141.6	8.4	94.6	98.4
23.00	.254	.16E-01	.11E+00	38.80	.15	38.33	42.24	39.52	1.10	1.38	.55	141.6	7.9	94.1	98.9
24.00	.254	.20E-01	.14E+00	46.99	.18	46.71	52.64	47.18	1.13	1.52	.62	141.6	8.1	90.5	96.1
25.00	.254	.24E-01	.16E+00	57.02	.22	56.40	63.85	58.24	1.13	1.68	.69	141.6	7.1	91.4	98.7

940.00	.254	.24E-01	.21E+00	57.19	.29	57.75	75.94	59.08	1.32	1.60	.77	141.2	15.0	82.0	97.2
941.00	.254	.26E-01	.25E+00	61.35	.33	62.31	87.62	65.87	1.41	1.74	.83	140.3	15.0	78.9	97.0
942.00	.254	.27E-01	.25E+00	64.86	.33	65.87	87.62	65.87	1.33	1.79	.83	140.3	15.0	78.9	97.0
943.00	.254	.29E-01	.27E+00	70.36	.37	71.55	97.36	71.53	1.36	1.86	.87	141.6	15.0	77.5	95.8
944.00	.254	.33E-01	.32E+00	78.99	.43	80.32	113.13	83.11	1.41	1.97	.95	141.6	15.0	77.5	95.0
945.00	.254	.36E-01	.34E+00	85.14	.46	86.54	120.96	89.21	1.40	2.05	.97	141.6	15.0	77.7	94.3
946.00	.254	.41E-01	.39E+00	98.40	.52	100.07	137.23	100.97	1.37	2.20	1.06	141.6	14.8	77.5	95.1
947.00	.254	.29E-01	.41E+00	69.25	.55	72.09	147.14	71.58	2.02	1.85	1.07	141.6	14.8	56.2	52.7
948.00	.254	.29E-01	.47E+00	69.70	.63	74.00	167.23	75.21	2.26	1.85	1.14	140.4	14.8	53.1	61.5
949.00	.254	.28E-01	.51E+00	67.71	.68	72.30	181.80	72.74	2.51	1.83	1.19	141.2	14.8	48.9	64.2
950.00	.254	.30E-01	.54E+00	70.71	.72	75.13	192.05	82.57	2.56	1.87	1.23	141.6	14.8	51.4	66.0
951.00	.254	.21E-01	.58E+00	49.94	.77	54.60	205.54	45.83	3.76	1.57	1.27	141.6	14.8	33.8	67.1
952.00	.254	.20E-01	.62E+00	48.09	.82	52.66	219.02	46.36	4.16	1.54	1.31	141.6	14.8	32.8	67.4
953.00	.254	.18E-01	.62E+00	42.67	.82	46.72	219.02	46.35	4.69	1.45	1.31	141.6	14.8	32.8	67.4
954.00	.254	.45E-01	.43E+00	107.22	.57	109.08	151.59	111.05	1.39	2.30	1.09	141.6	14.8	77.2	95.3
955.00	.254	.50E-01	.46E+00	120.08	.62	121.76	165.04	124.67	1.36	2.43	1.14	141.6	14.8	79.1	95.5
956.00	.254	.55E-01	.51E+00	131.44	.68	133.11	181.26	138.43	1.36	2.54	1.19	141.6	14.8	79.9	96.5
957.00	.254	.59E-01	.54E+00	140.15	.72	142.05	192.49	145.32	1.36	2.63	1.23	141.6	14.8	79.4	97.2
958.00	.254	.60E-01	.58E+00	142.72	.77	145.37	205.54	148.83	1.41	2.65	1.27	141.6	14.8	76.5	93.1
959.04	.254	.80E-02	.21E-01	19.13	.03	18.74	7.62	7.32	.41	.37	.24	141.5	15.0	98.9	98.7
960.04	.254	.10E-01	.51E-01	23.97	.07	23.48	17.94	17.75	.77	1.09	.38	141.5	15.0	98.9	98.4
961.04	.254	.11E-01	.80E-01	23.46	.11	25.11	28.37	26.71	1.11	1.12	.47	141.6	15.0	95.0	97.3

962.04	.254	.13E-01	.11E+00	31.10	.15	31.24	40.23	32.89	1.29	1.24	.56	141.6	14.8	84.4	98.4
963.04	.254	.15E-01	.14E+00	35.11	.18	36.78	48.82	35.35	1.33	1.33	.62	141.6	14.8	76.5	98.4
964.04	.254	.18E-01	.16E+00	42.88	.22	43.42	58.53	44.74	1.35	1.45	.68	141.6	14.8	79.9	98.7
965.04	.254	.20E-01	.19E+00	48.39	.26	49.27	68.35	49.69	1.39	1.54	.73	141.6	14.8	78.7	98.7
966.04	.254	.21E-01	.22E+00	49.76	.29	50.85	78.11	54.80	1.54	1.57	.78	141.6	14.8	74.6	98.7
967.04	.254	.25E-01	.25E+00	58.81	.34	60.18	88.83	62.25	1.43	1.70	.84	141.6	14.8	73.3	98.4
968.04	.254	.28E-01	.32E+00	65.96	.42	67.91	112.50	73.19	1.66	1.80	.94	141.6	14.8	70.2	99.4
969.04	.254	.30E-01	.32E+00	70.69	.42	72.78	112.50	73.19	1.55	1.87	.94	141.6	14.8	70.2	97.9
970.04	.254	.32E-01	.35E+00	77.23	.47	79.68	125.22	79.69	1.57	1.95	.99	141.6	14.8	69.0	98.4
971.04	.254	.35E-01	.39E+00	83.12	.52	85.90	138.10	86.33	1.61	2.02	1.04	141.6	14.8	68.1	98.7
972.04	.254	.36E-01	.43E+00	86.42	.57	89.78	151.59	89.19	1.69	2.06	1.09	141.6	14.8	64.9	98.2
973.04	.254	.40E-01	.47E+00	96.14	.63	99.42	167.82	104.02	1.69	2.18	1.14	141.6	14.5	67.6	98.4
974.04	.254	.43E-01	.51E+00	102.84	.69	106.57	183.20	110.89	1.72	2.25	1.20	141.6	14.8	66.4	97.9
975.04	.254	.47E-01	.57E+00	111.87	.77	116.50	204.19	116.67	1.75	2.35	1.26	141.6	14.8	63.5	97.9
976.12	.254	.73E-02	.21E-01	17.34	.03	16.99	7.64	7.50	.45	.92	.24	141.6	14.8	98.4	98.9
977.12	.254	.81E-02	.51E-01	19.34	.07	19.04	18.04	17.19	.95	.98	.38	141.6	14.8	96.8	98.7
978.12	.254	.96E-02	.85E-01	22.98	.11	23.13	30.13	24.22	1.30	1.06	.49	141.6	14.8	83.2	98.7
979.12	.254	.10E-01	.11E+00	24.17	.14	24.77	38.13	26.14	1.54	1.09	.56	141.6	14.8	73.1	98.2
980.12	.254	.12E-01	.14E+00	28.81	.18	29.70	48.77	31.36	1.64	1.19	.62	141.6	14.5	69.5	97.7
981.12	.254	.14E-01	.16E+00	32.27	.22	33.36	58.76	36.63	1.76	1.26	.68	141.6	14.5	67.8	98.2
982.12	.254	.16E-01	.20E+00	34.33	.26	35.80	70.51	39.74	1.97	1.30	.74	141.6	14.5	62.7	98.2
983.12	.254	.15E-01	.22E+00	36.57	.29	38.55	78.14	43.23	2.11	1.34	.79	141.6	14.5	56.7	98.4

984.12	.254	.16E-01	.24E+00	39.17	.33	41.22	87.15	43.51	2.11	1.19		\5	14.5	57.2	98.4
985.12	.254	.17E-01	.28E+00	41.26	.37	43.89	98.91	41.85	2.23	1.43	.88	141.6	14.5	50.7	98.4
986.12	.254	.18E-01	.31E+00	42.30	.42	44.59	111.45	54.39	2.50	1.44	.93	141.6	14.5	56.2	98.2
987.12	.254	.19E-01	.36E+00	44.93	.48	48.14	127.92	47.33	2.66	1.49	1.00	141.6	14.5	46.2	98.2
988.12	.254	.22E-01	.39E+00	53.75	.52	57.35	139.87	56.21	2.44	1.53	1.04	141.6	14.5	48.9	97.9
989.12	.254	.23E-01	.43E+00	54.84	.57	58.69	152.03	57.58	2.59	1.64	1.09	141.6	14.5	46.9	98.2
990.12	.254	.24E-01	.47E+00	56.15	.63	60.00	165.91	65.14	2.78	1.66	1.16	141.6	14.5	47.0	98.4
991.12	.254	.28E-01	.52E+00	61.41	.70	66.83	187.43	52.66	2.81	1.74	1.21	141.6	14.5	38.5	98.4
992.12	.254	.26E-01	.58E+00	61.75	.78	66.97	208.09	58.96	3.11	1.74	1.27	141.6	14.5	38.7	98.2
993.12	.254	.28E-01	.65E+00	66.25	.87	71.89	232.44	65.18	3.23	1.81	1.35	141.6	14.5	38.5	97.7
994.24	.254	.73E-02	.21E-01	17.33	.03	16.99	7.57	7.43	.45	.92	.24	141.6	15.5	98.4	98.9
995.24	.254	.77E-02	.32E-01	18.50	.07	18.13	18.32	17.98	1.01	.95	.38	141.6	15.5	98.4	98.7
996.24	.254	.92E-02	.85E-01	22.08	.11	22.04	29.89	25.66	1.36	1.04	.49	141.6	15.5	88.1	98.7
997.24	.254	.11E-01	.11E+00	25.53	.15	26.00	38.83	28.06	1.49	1.12	.55	141.6	15.3	76.5	98.7
998.24	.254	.12E-01	.14E+00	28.24	.18	29.01	47.96	31.92	1.65	1.18	.61	141.6	15.3	71.7	98.6
999.24	.254	.13E-01	.17E+00	30.49	.22	31.66	57.61	33.50	1.82	1.23	.68	141.6	15.8	65.2	98.7
001.24	.254	.15E-01	.20E+00	36.59	.26	37.98	69.52	41.21	1.83	1.34	.74	141.6	15.0	65.4	98.4
002.24	.254	.17E-01	.23E+00	40.14	.31	41.87	81.78	45.70	1.95	1.41	.80	141.6	15.0	62.5	98.4
003.24	.254	.19E-01	.28E+00	46.03	.37	48.54	98.62	47.70	2.01	1.51	.88	141.6	14.8	56.0	98.7
004.24	.254	.20E-01	.31E+00	46.97	.42	51.75	111.11	51.87	2.19	1.56	.93	141.6	14.8	54.6	98.7
005.24	.254	.22E-01	.38E+00	51.44	.51	54.91	138.33	53.75	2.49	1.59	1.03	141.6	14.8	48.4	98.7
006.24	.254	.24E-01	.46E+00	56.86	.61	61.40	163.71	51.13	2.66	1.67	1.13	141.6	14.9	41.5	98.5

618.00	.423	.25E-01	.18E+00	35.57	.14	58.25	64.12	59.25	1.10	1.17	.48	145.1	12.6	93.4	97.0
619.00	.423	.35E-01	.32E+00	50.80	.26	85.25	116.03	94.43	1.36	1.41	.65	141.6	12.6	83.7	93.1
620.00	.423	.40E-01	.36E+00	58.10	.29	98.33	131.88	97.87	1.34	1.50	.69	141.6	12.6	77.5	91.7
621.00	.423	.48E-01	.44E+00	69.58	.35	117.98	159.56	117.09	1.35	1.54	.76	141.6	12.6	76.7	91.2
623.00	.423	.31E-01	.43E+00	45.08	.35	79.26	157.99	78.28	1.99	1.32	.75	141.2	12.3	55.8	83.5
622.00	.423	.26E-01	.51E+00	37.66	.41	67.37	185.75	68.56	2.76	1.31	.82	141.6	12.3	44.7	84.4
624.00	.423	.54E-01	.51E+00	76.85	.41	137.49	185.75	68.56	1.35	1.73	.82	141.6	12.3	44.7	84.4
624.00	.423	.27E-01	.58E+00	39.14	.47	70.39	213.51	73.39	3.01	1.23	.88	140.7	12.3	42.5	88.4
630.00	.423	.19E-01	.21E-01	26.63	.02	43.40	7.79	7.74	.18	1.02	.17	141.6	13.0	99.4	99.1
631.00	.423	.20E-01	.34E-01	28.59	.03	46.68	12.24	12.16	.26	1.05	.21	140.4	13.0	99.4	99.1
632.00	.423	.21E-01	.51E-01	30.72	.04	49.99	18.40	18.27	.37	1.09	.26	142.6	13.0	99.4	99.1
633.00	.423	.22E-01	.99E-01	31.85	.08	52.03	35.97	35.71	.69	1.11	.36	140.2	12.8	99.4	99.4
634.00	.423	.23E-01	.12E+00	33.66	.09	54.75	41.96	41.44	.77	1.14	.39	143.4	12.8	98.3	98.9
635.00	.423	.24E-01	.15E+00	33.75	.12	55.00	52.95	52.58	.96	1.14	.44	141.3	12.8	99.4	97.7
636.00	.423	.25E-01	.16E+00	35.58	.13	58.34	59.94	55.71	1.03	1.17	.47	143.8	12.4	93.8	94.6
637.00	.423	.26E-01	.19E+00	38.09	.15	63.33	68.34	53.59	1.10	1.22	.50	142.4	12.8	87.1	97.2
638.00	.423	.29E-01	.22E+00	40.89	.18	67.99	79.03	68.98	1.14	1.26	.54	141.6	12.8	88.1	98.2
639.00	.423	.32E-01	.25E+00	46.63	.20	77.12	90.92	79.97	1.18	1.35	.57	141.6	12.8	89.5	98.2
640.00	.423	.38E-01	.29E+00	54.70	.23	90.93	105.01	90.36	1.15	1.46	.62	141.6	12.6	87.3	97.2
641.00	.423	.41E-01	.33E+00	59.49	.26	99.50	119.85	98.86	1.20	1.52	.66	141.6	12.6	84.7	98.2
642.00	.423	.45E-01	.38E+00	65.06	.29	109.40	132.69	104.63	1.21	1.59	.69	141.6	12.6	81.5	97.7
643.00	.423	.49E-01	.40E+00	70.96	.32	119.03	146.53	114.04	1.23	1.66	.73	141.6	12.6	83.3	98.2

BLOCK	ADDRESS	LENGTH	FILE	DATE	PROCSSR	VER LEVEL	HARDWARE	COMMENTS
PUT.SQ	34302	1500	SL-SYSIO	01/10/78				
/REW.FO/	36002	7						
REW.SQ	36011	42	SL-SYSIO	01/10/78				
/PUT.RT/	36053	11						
RLEQ.RM	36064	43	SL-SYSIO	01/10/78				
/SKFL.FO/	36127	7						
SKFL.SQ	36136	51	SL-SYSIO	01/10/78				
SHLRM.Z	36207	0	SL-SYSIO	01/14/78				
WAR.SQ	36207	303	SL-SYSIO	01/10/78				
WEOX.SQ	36512	150	SL-SYSIO	01/10/78				
Z.SQ	36662	110	SL-SYSIO	01/10/78				
/PLTPLL/	36772	2						
AXIS3	36774	1053	SL-FT4LIB	12/29/76	FTN	4.6 433	6464 I	OPT=2
LINE	40047	262	SL-FT4LIB	12/29/76	FTN	4.6 433	6464 I	OPT=2
/PLTPLM/	40331	67						
MESPLT	40420	750	SL-FT4LIB	12/14/76	FTN	4.6 433	6464 I	OPT=2
NUMBER	41370	313	SL-FT4LIB	12/29/76	FTN	4.6 433	6464 I	OPT=2
PLTPKG	41703	1473	SL-FT4LIB	04/15/77				
/PLT999/	43376	2						
SYMBOL	43400	1134	SL-FT4LIB	12/29/76	FTN	4.6 433	6464 I	OPT=2
CPUMSG	44534	10	SL-SYSLIB	06/11/78	COMPASS	3.4 460		07/19/74 SEND MACE MESSAGE.
CPUSYS	44544	47	SL-SYSLIB	06/11/78	COMPASS	3.4 460		06/25/75 PROCESS SYSTEM REQUEST.
ENCODE=	44613	125	SL-FORTRAN	10/16/78	COMPASS	3.4 460		FORMATTED WRITE INTO CORE.
GOTOER=	44740	14	SL-FORTRAN	10/16/78	COMPASS	3.4 460		COMPUTED GO TO ERROR PROCESSOR.
REMARK	44754	3	SL-FORTRAN	10/16/78	COMPASS	3.4 460		ISSUE A MESSAGE TO THE DAYFILE.
SINCOS=	44757	66	SL-FORTRAN	10/16/78	COMPASS	3.4 460		TRIGONOMETRIC SINE OR COSINE OF X. OPT=ALL.
SYSTEM	45045	26	SL-FORTRAN	10/16/78	COMPASS	3.4 460		USER CALLABLE ERROR PROCESSOR.
(LWA+1)	45073	(44762)						

.904 CP SECONDS   63200B CM STORAGE USED   47 TABLE MOVES

RUN	PER	WS,KG/S	WL,KG/S	VGH,M/S	VLH,M/S	EHG,KW	EHL,KW	EHLO	REH	JGS	JLS	TSC	TLC	TLOC	TLPC
1.00	.423	.19E-01	.21E-01	26.65	.02	43.45	7.28	7.21	.17	1.02	.17	141.6	18.7	99.1	99.4
2.00	.423	.19E-01	.51E-01	27.87	.04	45.45	19.79	19.56	.45	1.04	.26	141.6	7.6	98.9	99.1
3.00	.423	.20E-01	.83E-01	28.97	.07	47.27	32.17	31.71	.68	1.06	.33	141.6	7.1	98.7	99.4
4.00	.423	.23E-01	.11E+00	32.44	.09	52.35	42.00	41.28	.79	1.12	.38	141.6	8.4	98.4	99.1
5.00	.423	.25E-01	.16E+00	35.56	.13	58.74	65.04	59.32	1.11	1.18	.47	141.6	5.4	91.7	98.4
6.00	.423	.28E-01	.22E+00	40.23	.18	67.00	82.42	70.59	1.23	1.25	.54	141.6	10.1	87.1	98.7
50.00	.423	.25E-01	.13E+00	35.33	.10	57.65	47.52	46.82	.82	1.17	.41	141.6	3.8	94.7	.2
51.00	.423	.24E-01	.18E+00	34.52	.14	57.13	66.30	59.44	1.16	1.16	.48	141.6	9.6	90.7	.2
52.00	.423	.27E-01	.21E+00	38.59	.17	64.15	80.80	70.13	1.26	1.22	.53	141.6	9.6	89.1	.2
222.00	.423	.34E-01	.31E+00	49.31	.25	81.31	113.71	83.68	1.16	1.38	.64	143.6	12.8	77.0	92.6

```
      WS=WS/2.2
      WL=WL/2.2
240   VGH=.30480*VGH
      VLH=.30480*VLH
      TSC=(TG-32.)/1.8
      TLC=(TL-32.)/1.8
      TLOC=(TLO-32.)/1.8
245   TLPC=(TLP-32.)/1.8
      PRINT 7,RUN,PER(IP),WS,WL,VGH,VLH,ENG,ENL,ENLO,REN,JGS,JLS,TSC,TLC
     A,TLOC,TLPC
    7 FORMAT(/2X,F7.2,F5.3,2E9.2,8F9.2,4F6.1,/)
      GO TO 2
250   IF(KQ.EQ.1) GO TO 25
      IF(KQ.EQ.2) GO TO 26
      IF(KQ.EQ.3) GO TO 27
      IF(KQ.EQ.4) GO TO 28
      IF(KQ.EQ.5) GO TO 29
255   GO TO 30
   25 EX0(I)=ENL
      EY0(I)=ENG
      VX0(I)=VLH
      VY0(I)=VGH
260   JX0(I)=JLS
      JY0(I)=JGS
      GO TO 2
   26 EX12(I)=ENL
      EY12(I)=ENG
265   VX12(I)=VLH
      VY12(I)=VGH
      JX12(I)=JLS
      JY12(I)=JGS
      GO TO 2
270   27 EX24(I)=ENL
      EY24(I)=ENG
      VX24(I)=VLH
      VY24(I)=VGH
      JX24(I)=JLS
275   JY24(I)=JGS
      GO TO 2
      28 EX27(I)=ENL
      EY27(I)=ENG
      VX27(I)=VLH
280   VY27(I)=VGH
      JX27(I)=JLS
      JY27(I)=JGS
      GO TO 2
   29 EX28(I)=ENL
285   EY28(I)=ENG
      VX28(I)=VLH
      VY28(I)=VGH
      JX28(I)=JLS
      JY28(I)=JGS
290   GO TO 2
   30 EX29(I)=ENL
      EY29(I)=ENG
      VX29(I)=VLH
      VY29(I)=VGH
295   JX29(I)=JLS
      JY29(I)=JGS
      GO TO 2
  800 CONTINUE
      CALL NAMPLT
300   CALL PLOT(00.0,1.5,-3)
  800 CALL PLOT(10.0,0.0,-3)
      CALL AXIS(0.,0.,14H    WG,HFG, KW,14,7.,30.,0.0,20.,20.)
      CALL AXIS(0.,0.,20H   WL,(TSAT-TIN), KW,-20,14.,0.,0.,20.,20.)
      IF(N1.LE.0) GO TO 811
305   CALL LINE(EX0,EY0,N1,1,-1,1)
      CALL SYMBOL(1.0,6.8,.12,37HDH = 10.5 MM, HIN =   5 MM
     A0.,37)
      CALL SYMBOL(1.,6.56,.12,1,0.,-1)
      CALL SYMBOL(1.5,5.5,.12,14H15 HOLE   42.3,0.0,14)
310   CALL SYMBOL(1.5,5.26,.12,2,0.,-1)
      CALL SYMBOL(1.5,6.2,.12,14H 9 HOLE   23.4,0.0,14)
      IF(KS.EQ.1) GO TO 805
  811 IF(N2.LE.0) GO TO 812
      CALL LINE(EX12,EY12,N2,1,-1,2)
315   IF(KS.EQ.2) GO TO 805
  812 IF(N3.LE.0) GO TO 813
```

```
      I=0
      GO TO 2
   23 KQ=7
      KS=6
      I2=I+1
      EX29(I)=0.
      EY29(I)=0.
      EX29(I2)=20.
      EY29(I2)=20.
      VX29(I)=0.
      VY29(I)=0.
      VX29(I2)=0.2
      VY29(I2)=40.
      JX29(I)=0.
      JY29(I)=0.
      JX29(I2)=0.125
      JX29(I2)=1.
      JX29(I2)=0.5
      JX29(I2)=0.25
      JY29(I2)=2.
      JY29(I2)=1.
      JY29(I2)=.5
      JY29(I2)=.25
      N6=I-1
      I=0
      GO TO 2
C     CALC. THE STEAM FLOW RATE,WS(LB/S).
C
   20 TS=TEMF(VTS)
      PS=30.*VPS
      CALL PHIS2(TS,PS,2,VS,SS,HS)
      IF(IP.GE.10) GO TO 205
      WS=.051*SQRT(VWS/VS)
      GO TO 221
  205 IP=IP-10
      WS=.35*SQRT(VWS/VS)
C
C     CALC. THE STEAM VELOCITY IN TEST COLUMN(VGC) AND THROUGH HOLES(VGH).
C
  221 TLO=TEMF(VTLO)
      TLP=TEMF(VTP)
      TL=TEMF(VTL)
      IF(VTG.LE.5.7) VTG=5.8
      TG=TEMF(VTG)
      PG=1.428*VPG/27.68+14.696
      CALL PHIS2(TG,PG,2,VG,SG,HG)
      VGC=30.288*WS*VG
      VGH=VGC/PER(IP)
      VL=.016719
      VLC=30.288*WL*VL
      VLH=VLC/PER(IP)
      EHG=WS*(HG-180.17)*1.055+WS*(212.-TLO)*1.055
      EHL=WL*(212.-TL)*1.055
      EHLO=WL*(TLO-TL)*1.055
      REH=EHL/EHG
      DA=DT*PER(IP)**0.5
      DG=1./VG
      DL=1./VL
      JGS=VGH*(DG/(32.2*DH*(DL-DG)))**.5
      JLS=VLH*(DL/(32.2*DH*(DL-DG)))**.5
      FCON=0.28
       FCON=0.24
      FCON=0.49
      FCON=0.42
      JGSC=FCON*JLS*(212.-TL)/((HG-180.17)+(212.-TLO))*SQRT(DL/DG)
       W1=AS(IP)/.787*6.2832*A(IP)/.03302
      ALF=TANH(W1)
      CK=(AS(IP)/(2./DH)**((1.-ALF)/4.)
      CS=CK*(1.97+4.33E-3*ALS(IP))
      JGSC=JGSC/CS**2.
      IF(IP.EQ.1) GO TO 251
      IF(JGSC.GE.2.22) JGSC=2.22
      GO TO 252
  251 IF(JGSC.GE.0.50) JGSC=0.50
  252 JGS=JGS/CS**2.
      IF(JGS.LE.0.1) JGS=0.1
      JLS=JLS/CS**2.
      JGS=SQRT(JGS)
      JLS=SQRT(JLS)
```

```
                CALL LINE(EX24,EY24,N3,1,-1,3)
                CALL SYMBOL(1.,5.96,.12,3,0.,-1)
                CALL SYMBOL(1.,5.9,.12,14H 5 HOLE   14.1,0.0,14)
     320        CALL SYMBOL(1.,5.66,.12,4,0.,-1)
                CALL SYMBOL(1.,5.6,.12,14H5A HOLE   14.1,0.,14)
                CALL SYMBOL(1.,5.36,.12,5,0.,-1)
                CALL SYMBOL(1.,5.3,.12,14H 3 HOLE    8.5,0.,14)
                CALL SYMBOL(1.,5.06,.12,0,0.,-1)
     325        CALL SYMBOL(1.,5.,.12,14H3A HOLE     8.5,0.,14)
                IF(KS.EQ.3) GO TO 805
            813 IF(N4.LE.0) GO TO 814
                CALL LINE(EX27,EY27,N4,1,-1,4)
                IF(KS.EQ.4) GO TO 805
     330    814 IF(N5.LE.0) GO TO 815
                CALL LINE(EX28,EY28,N5,1,-1,5)
                IF(KS.EQ.5) GO TO 805
            815 IF(N6.LE.0) GO TO 805
                CALL LINE(EX29,EY29,N6,1,-1,0)
     335        IF(KS.EQ.6) GO TO 805
            805 CALL PLOT(7.0,0.,-3)
                CALL AXIS(0.,0.,20H    WL.(TSAT-TIN), KW,-20,14.,0.,0.,20.,20.)
                CALL AXIS(0.,0.,14HVAP. VEL., M/S,14,9.,90.,0.,40.,20.)
                IF(N1.LE.0) GO TO 821
     340        CALL LINE(EX0,VY0,N1,1,-1,1)
                CALL SYMBOL(1.0,6.8,.12,37HDH = 10.5 MM, HIN =   5 MM
               A0,.37)
                CALL SYMBOL(1.,6.56,.12,1,0.,-1)
                CALL SYMBOL(1.5,6.5,.12,14H15 HOLE   42.3,0.0,14T
     345        CALL SYMBOL(1.,6.26,.12,2,0.,-1)
                CALL SYMBOL(1.5,6.2,.12,14H 9 HOLE   25.4,0.0,14)
                IF(KS.EQ.1) GO TO 805
            821 IF(N2.LE.0) GO TO 822
                CALL LINE(EX12,VY12,N2,1,-1,2)
     350        IF(KS.EQ.2) GO TO 806
            822 IF(N3.LE.0) GO TO 823
                CALL LINE(EX24,VY24,N3,1,-1,3)
                CALL SYMBOL(1.,5.96,.12,3,0.,-1)
                CALL SYMBOL(1.5,5.9,.12,14H 5 HOLE   14.1,0.0,14)
     355        CALL SYMBOL(1.,5.66,.12,4,0.,-1)
                CALL SYMBOL(1.5,5.6,.12,14H5A HOLE   14.1,0.,14)
                CALL SYMBOL(1.,5.36,.12,5,0.,-1)
                CALL SYMBOL(1.5,5.3,.12,14H 3 HOLE    8.5,0.,14)
                CALL SYMBOL(1.,5.06,.12,0,0.,-1)
     360        CALL SYMBOL(1.5,5.,.12,14H3A HOLE    8.5,0.,14)
                IF(KS.EQ.3) GO TO 806
            823 IF(N4.LE.0) GO TO 824
                CALL LINE(EX27,VY27,N4,1,-1,4)
                IF(KS.EQ.4) GO TO 806
     365    824 IF(N5.LE.0) GO TO 825
                CALL LINE(EX28,VY28,N5,1,-1,5)
                IF(KS.EQ.5) GO TO 806
            825 IF(N6.LE.0) GO TO 806
                CALL LINE(EX29,VY29,N6,1,-1,0)
     370        IF(KS.EQ.6) GO TO 806
            806 CALL PLOT(20.,0.,-3)
                CALL AXIS(0.,0.,12HSQRT(RLIN)/G,-12,12.,0.,0.,.125,20.)
                CALL AXIS(0.,0.,20HSQRT(KG-F*LM*RLIN)/C,20,8.,90.,0.,.25,20.)
                IF(N1.LE.0) GO TO 831
     375        CALL LINE(JX0,JY0,N1,1,-1,1)
                CALL SYMBOL(1.,6.56,.12,1,0.,-1)
                CALL SYMBOL(1.0,6.8,.12,37HDH = 10.5 MM, HIN =   5 MM
               A0,.37)
                CALL SYMBOL(1.,6.56,.12,1,0.,-1)
     380        CALL SYMBOL(1.5,6.5,.12,14H15 HOLE   42.3,0.0,14)
                CALL SYMBOL(1.,6.26,.12,2,0.,-1)
                CALL SYMBOL(1.5,6.2,.12,14H 9 HOLE   25.4,0.0,14)
                IF(KS.EQ.1) GO TO 890
            831 IF(N2.LE.0) GO TO 832
     385        CALL LINE(JX12,JY12,N2,1,-1,2)
                IF(KS.EQ.2) GO TO 890
            832 IF(N3.LE.0) GO TO 833
                CALL LINE(JX24,JY24,N3,1,-1,3)
                CALL SYMBOL(1.,5.96,.12,3,0.,-1)
     390        CALL SYMBOL(1.5,5.9,.12,14H 5 HOLE   14.1,0.0,14)
                CALL SYMBOL(1.,5.66,.12,4,0.,-1)
                CALL SYMBOL(1.5,5.6,.12,14H5A HOLE   14.1,0.,14)
                CALL SYMBOL(1.,5.36,.12,5,0.,-1)
                CALL SYMBOL(1.5,5.3,.12,14H 3 HOLE    8.5,0.,14)
     395        CALL SYMBOL(1.,5.06,.12,0,0.,-1)
```

```
                      CALL SYMBOL(1.5,5.,.12,14HJA HOLE    0.5,0.,14)
                      IF(KS.EQ.3) GO TO 890
                  833 IF(N4.LE.0) GO TO 834
                      CALL LINE(JX27,JY27,N4,1,-1,4)
      400             IF(KS.EQ.4) GO TO 890
                  834 IF(N5.LE.0) GO TO 835
                      CALL LINE(JX28,JY28,N5,1,-1,5)
                      IF(KS.EQ.5) GO TO 890
                  835 IF(N6.LE.0) GO TO 890
      405             CALL LINE(JX29,JY29,N6,1,-1,6)
                      IF(KS.EQ.6) GO TO 890
                  890 GO TO 1
                  898 CALL ENDPLT
                      STOP
      410             END
```

CARD NR. SEVERITY DETAILS DIAGNOSIS OF PROBLEM

250	I		THERE IS NO PATH TO THIS STATEMENT.
335	I	885	THIS IF DEGENERATES INTO A SIMPLE TRANSFER TO THE LABEL INDICATED.
370	I	886	THIS IF DEGENERATES INTO A SIMPLE TRANSFER TO THE LABEL INDICATED.
406	I	890	THIS IF DEGENERATES INTO A SIMPLE TRANSFER TO THE LABEL INDICATED.

SYMBOLIC REFERENCE MAP (R=1)

ENTRY POINTS
6211 WEE2

VARIABLES	SN	TYPE	RELOCATION				
10523	A	REAL	ARRAY	10514	ALF	REAL	
10557	ALS	REAL	ARRAY	10541	AS	REAL	ARRAY
10515	CK	REAL		10516	CS	REAL	
10507	DA	REAL		10510	DG	REAL	
10201	DH	REAL		10511	DL	REAL	
10202	DT	REAL		10503	EHG	REAL	
10504	EHL	REAL		10505	EHLO	REAL	
12535	EX0	REAL	ARRAY	13665	EX12	REAL	ARRAY
14175	EX24	REAL	ARRAY	16455	EX27	REAL	ARRAY
16741	EX28	REAL	ARRAY	17225	EX29	REAL	ARRAY
13211	EY0	REAL	ARRAY	14031	EY12	REAL	ARRAY
14341	EY24	REAL	ARRAY	16607	EY27	REAL	ARRAY
17073	EY28	REAL	ARRAY	17357	EY29	REAL	ARRAY
10512	FCON	REAL		10475	HG	REAL	
10464	HS	REAL		10434	I	INTEGER	
10445	IP	INTEGER		10456	I2	INTEGER	
10425	JGA	REAL	*UNDEF	10427	JGM	REAL	*UNDEF
10423	JGS	REAL		10430	JGSC	REAL	
10426	JLA	REAL	*UNDEF	10424	JLS	REAL	
10565	JX0	REAL	ARRAY	11715	JX12	REAL	ARRAY
12255	JX24	REAL	ARRAY	20542	JX27	REAL	ARRAY
21031	JX28	REAL	ARRAY	21315	JX29	REAL	ARRAY
11341	JY0	REAL	ARRAY	12061	JY12	REAL	ARRAY
12371	JY24	REAL	ARRAY	20677	JY27	REAL	ARRAY
21163	JY28	REAL	ARRAY	21447	JY29	REAL	ARRAY
10435	KQ	INTEGER		10453	KS	INTEGER	
10431	N1	INTEGER		10432	N2	INTEGER	
10433	N3	INTEGER		10455	N4	INTEGER	
10456	N5	INTEGER		10457	N6	INTEGER	
10527	PER	REAL	ARRAY	10472	PG	REAL	
10461	PS	REAL		10506	REM	REAL	
10446	RUN	REAL		10452	RX	REAL	
10474	SG	REAL		10463	SS	REAL	
10471	TG	REAL		10470	TL	REAL	
10520	TLG	REAL		10466	TLO	REAL	
10521	TLOG	REAL		10467	TLP	REAL	
10522	TLPG	REAL		10460	TS	REAL	
10517	TSG	REAL		10473	VG	REAL	
10476	VGG	REAL		10477	VGH	REAL	
10500	VL	REAL		10501	VLG	REAL	
10502	VLH	REAL		10442	VPG	REAL	
10437	VPS	REAL		10462	VS	REAL	
10441	VTG	REAL		10444	VTL	REAL	

```
      FUNCTION TEMF(V)
      IF(V.GT.2.022) GO TO 1
      TC=24.70926*V+.19772
      GO TO 5
    1 IF(V. GT.4.095) GO TO 2
      TC=24.10577*V+1.27761
      GO TO 5
    2 IF(V.GT.6.137) GO TO 3
      TC=24.50284*V-.47449
      GO TO 5
    3 TC=25.0174*V-3.57737
    5 TEMF=1.8*TC+32.
      RETURN
      END
```

```
          SYMBOLIC REFERENCE MAP (R=1)

 ENTRY POINTS
     4   TEMF

 VARIABLES     SN  TYPE          RELOCATION
    52   TC        REAL                                51   TEMF       REAL
     0   V         REAL              F.P.

 STATEMENT LABELS
    13   1                                 20   2                                 25   3
    30   5

 STATISTICS
   PROGRAM LENGTH                  53B        43
        57400B CM USED
```

```
      SUBROUTINE PHIS2(T,P,ID,V,S,H)
      DIMENSION N(8),IZ(8,3),L(8),IX(8,2),B(10,7),BB(8,2),RL(3),BBB(7)
      DATA TC1,PC1/647.3,3208.234759/
      DATA (N(I),I=1,8)/2,3,2,2,3,3*2/
      DATA (IZ(I,1),I=1,8)/13,2*18,25,32,12,2*24/
      DATA(IZ(I,2),I=1,8)/3,2,10,14,28,11,18,14/
      DATA (IZ(I,3),I=2,5)/1,0,0,24/
      DATA (L(I),I=6,8)/1,1,2/
      DATA (IX(I,1),I=6,8)/14,19,54/
      DATA IX(8,2)/27/
      DATA (BBB(I),I=1,5),BS/2.856067796E1,-5.438923329E1,
     A4.330662834E-1,-6.547711697E-1,8.565182058E-2,1.683599274E1/
      DATA (B(1,I),I=1,2)/6.670375918E-2,1.388983801/
      DATA (B(2,I),I=1,3),(B(3,I),I=1,2)/8.390104328E-2,2.614670893E-2,
     A-3.373439453E-2,4.520918904E-1,1.069036614E-1/
      DATA (B(4,I),I=1,2),(B(5,I),I=1,3)/-5.975336707E-1,-8.847535804E-2
     A,5.958051609E-1,-5.159303373E-1,2.075021122E-1/
      DATA (B(6,I),I=1,2),(B(7,I),I=1,2),(B(8,I),I=1,2)/1.190610271E-1,
     A-9.867174132E-2,1.683998803E-1,-5.809438001E-2,6.552390126E-3,
     B5.710218649E-4/
      DATA (B(9,I),I=1,7)/1.936587558E2,-1.388522425E3,4.126607219E3,
     A-6.508211677E3,5.745984054E3,-2.693088365E3,5.235718623E2/
      DATA BA,BB(6,1),BB(7,1),BB(8,1),BB(8,2)/7.633333333E-1,
     A4.006073948E-1,8.636081627E-2,-8.532322921E-1,3.460208861E-1/
      DATA (RL(I),I=1,3),RI/1.574373327E1,-3.417061978E1,1.931380707E1,
     A4.260321148/
      IF(ID.EQ.2) GO TO 3
      PR=P/22120.
      TR=T/647.3
      GO TO 5
    3 PR=P/PC1
      TR=((T+459.67)/1.8)/TC1
    5 BTL=RL(1)+RL(2)*TR+RL(3)*TR**2
      DBL=RL(2)+2.*RL(3)*TR
      X=EXP(BA*(1.-TR))
      V2=0.
      DO 15 MU=1,5
      V1=0.
      KKK=N(MU)
      DO 10 MV=1,KKK
   10 V1=V1+B(MU,MV)*X**IZ(MU,MV)
   15 V2=V1*MU*PR**(MU-1)+V2
      V8=0.
      DO 20 MU=6,8
      V4=0.
      KKK=N(MU)
      DO 25 MV=1,KKK
   25 V4=V4+B(MU,MV)*X**IZ(MU,MV)
      V5=(MU-2)/PR**(MU-1)*V4
      V6=0.
      KKS=L(MU)
      DO 30 LH=1,KKS
   30 V6=V6+BB(MU,LH)*X**IX(MU,LH)
      V7=V6+1./(PR**(MU-2))
   20 V8=V8+V5/V7**2
      V9=0.
      DO 35 K=1,7
   35 V9=V9+B(9,K)*X**(K-1)
      V9=11.*(PR/BTL)**10*V9
      VR=RI*TR/PR-V2-V8+V9
C
C     CALC. THE REDUCED ENTROPY, SR.
C
      S1=0.
      DO 101 MV=1,5
  101 S1=S1+(MV-1)*BBB(MV)*TR**(MV-2)
      S1=-S1-RI*ALOG(PR)+BS*ALOG(TR)
      S3=0.
      DO 102 MU=1,5
      S2=0.
      KKK=N(MU)
      DO 103 MV=1,KKK
  103 S2=S2+IZ(MU,MV)*B(MU,MV)*X**IZ(MU,MV)
  102 S3=PR**MU*S2+S3
      S3=BA*S3
      S4=0.
      DO 104 MV=1,7
  104 S4=(10.*DBL/BTL+(MV-1)*BA)*B(9,MV)*X**(MV-1)+S4
      S4=S4*PR*(PR/BTL)**10
```

```
      S10=0.
      DO 105 MU=6,8
      S9=0.
      KKK=N(MU)
      DO 106 MV=1,KKK
      S6=0.
      KKS=L(MU)
      DO 107 LM=1,KKS
  107 S6=S6+IX(MU,LM)*BB(MU,LM)*X**IX(MU,LM)
      S7=0.
      KKS=L(MU)
      DO 108 LM=1,KKS
  108 S7=S7+BB(MU,LM)*X**IX(MU,LM)
      S7=S7*PR**(2-MU)
      S8=(IZ(MU,MV)-S6/S7)*B(MU,MV)*X**IZ(MU,MV)
  106 S9=S9+S8
  105 S10=S9/S7+S10
      S10=BA*S10
      SR=S1-S10-S3+S4
      H1=0.
      DO 201 MV=1,5
  201 H1=H1+DDD(MV)*(MV-2)*TR**(MV-1)
      H1=-H1+BS*TR
      H3=0.
      DO 202 MU=1,5
      H2=0.
      KKK=N(MU)
      DO 204 MV=1,KKK
  204 H2=H2+B(MU,MV)*(1.+IZ(MU,MV)*BA*TR)*X**IZ(MU,MV)
  202 H3=H3+PR**MU*H2
      H4=0.
      DO 203 MV=1,7
  203 H4=H4+(1.+TR*(10.*DBL/BTL+(MV-1)*BA))*B(9,MV)*X**(MV-1)
      H4=PR*(PR/BTL)**10*H4
      H8=0.
      DO 209 MU=6,8
      H6=0.
      KKS=L(MU)
      DO 207 LM=1,KKS
  207 H6=H6+BB(MU,LM)*X**IX(MU,LM)
      H6=H6*PR**(2-MU)
      KKK=N(MU)
      DO 205 MV=1,KKK
      H5=0.
      KKS=L(MU)
      DO 206 LM=1,KKS
  206 H5=H5+IX(MU,LM)*BB(MU,LM)*X**IX(MU,LM)
      H5=H5*BA*TR
      H7=1.+IZ(MU,MV)*BA*TR-H5/H6
  205 H7=H7*B(MU,MV)*X**IZ(MU,MV)
  209 H8=H7/H6+H8
      HR=H1-H3-H8+H4
      IF(IO.EQ.2) GO TO 300
      H=HR*70.1204
      V=VR*.00317
      S=SR*.108327514
      GO TO 302
  300 H=HR*30.14634566
      V=VR*0.05079948
      S=SR*0.025873582
  302 RETURN
      END
```

SYMBOLIC REFERENCE MAP (R=1)

ENTRY POINTS
3 PHIS2

VARIABLES	SN	TYPE	RELOCATION					
1035 B		REAL	ARRAY	653	BA	REAL		
1143 BB		REAL	ARRAY	1165	DDD	REAL	ARRAY	
652 BS		REAL		700	BTL	REAL		
701 DBL		REAL		0	H	REAL		F.P.
744 HR		REAL		734	H1	REAL		
736 H2		REAL		735	H3	REAL		

NRC FORM 335 (7-77)

U.S. NUCLEAR REGULATORY COMMISSION

BIBLIOGRAPHIC DATA SHEET

1. REPORT NUMBER (Assigned by DDC)
NUREG/CR-1808

4. TITLE AND SUBTITLE (Add Volume No., if appropriate)
Countercurrent Air/Water and Steam/Water Flow above a Perforated Plate

2. (Leave blank)

3. RECIPIENT'S ACCESSION NO.

7. AUTHOR(S)
Chang-Li Hsieh, S. G. Bankoff, R. S. Tankin, M. C. Yuen

5. DATE REPORT COMPLETED
MONTH October YEAR 1979

9. PERFORMING ORGANIZATION NAME AND MAILING ADDRESS (Include Zip Code)
Department of Chemical Engineering
Northwestern University
Evanston, Illinois 60201

DATE REPORT ISSUED
MONTH November YEAR 1980

6. (Leave blank)

8. (Leave blank)

12. SPONSORING ORGANIZATION NAME AND MAILING ADDRESS (Include Zip Code)
U.S. Nuclear Regulatory Commission
Office of Nuclear Regulatory Research
Washington, D. C. 20555

10. PROJECT/TASK/WORK UNIT NO.

11. CONTRACT NO
FIN No. B6188

13. TYPE OF REPORT
Topical

PERIOD COVERED (Inclusive dates)
October 1978-October 1979

15. SUPPLEMENTARY NOTES

14. (Leave blank)

16. ABSTRACT (200 words or less)

The perforated plate weeping phenomena have been studied in both air/water and steam/cold water systems. The air/water experiment is designed to investigate the effect of geometric factors of the perforated plate on the rate of weeping. A new dimensionless flow rate in the form of H* is suggested. The data obtained are successfully correlated by this H* scaling in the conventional flooding equation.

The steam/cold water experiment is concentrated on locating the boundary between weeping and no weeping. The effects of water subcooling, water inlet flow rate, and position of water spray are investigated. Depending on the combination of these factors, several types of weeping were observed. The data obtained at high water spray position can be related to the air/water flooding correlation by replacing the steam flow rate to an effective steam flow rate, which is determined by the mixing efficiency above the plate.

17. KEY WORDS AND DOCUMENT ANALYSIS

17a. DESCRIPTORS

Perforated Plate Weeping Phenomena
Flooding Phenomena
Hydrodynamics

17b. IDENTIFIERS/OPEN-ENDED TERMS

18. AVAILABILITY STATEMENT
Unlimited

19. SECURITY CLASS (This report)
Unclassified

21. NO. OF PAGES

20. SECURITY CLASS (This page)
Unclassified

22. PRICE
$

NRC FORM 335 (7-77)

UNITED STATES
NUCLEAR REGULATORY COMMISSION
WASHINGTON, D. C. 20555

OFFICIAL BUSINESS
PENALTY FOR PRIVATE USE, $300

POSTAGE AND FEES PAID
U.S. NUCLEAR REGULATORY
COMMISSION

U.S. MAIL

120555003908 1 R1R2R4
US NRC
ASLBP
CHAIRMAN
EW450
WASHINGTON DC 20555